REPUBLIC OF TURKEY

YILDIZ TECHNICAL UNIVERSITY

GRADUATE SCHOOL OF NATURAL AND APPLIED SCIENCES

USE OF CARBON FIBER LAYERS AND STEEL PLATES TO REPAIR FATIGUE DAMAGE AT THE RIB-TO-RIB BUTT-WELDED CONNECTIONS OF ORTHOTROPIC STEEL DECK UNDER FATIGUE LOADING

Saifaldien SHAKIR

DOCTOR OF PHILOSOPHY THESIS

Department of Civil Engineering

Civil Engineering (English) Program

Advisor

Assist. Prof. Dr.Fatih ALEMDAR

July, 2020

REPUBLIC OF TURKEY

YILDIZ TECHNICAL UNIVERSITY

GRADUATE SCHOOL OF NATURAL AND APPLIED SCIENCES

USE OF CARBON FIBER LAYERS AND STEEL PLATES TO REPAIR FATIGUE DAMAGE AT THE RIB-TO-RIB BUTT-WELDED CONNECTIONS OF ORTHOTROPIC STEEL DECK UNDER FATIGUE LOADING

A thesis submitted by Saifaldien SHAKIR in partial fulfillment of the requirements for the degree of DOCTOR OF PHILOSOPHY is approved by the committee on 13.07.2020 in Department of Civil Engineering, Civil Engineering (English) Program.

Assist. Prof. Dr. Fatih ALEMDAR

Yıldız Technical University

Advisor

Approved By the Examining Committee

Assist. Prof. Dr. Fatih ALEMDAR, Advisor
Yıldız Technical University _____

Assoc. Prof. Dr. Serkan BEKİROĞLU, Member
Yıldız Technical University _____

Assoc. Prof. Dr. Murat KIRÇIL, Member
Yıldız Technical University _____

Assist. Prof. Dr. Serkan SAĞIROĞLU, Member
Uludağ University _____

Prof. Dr. Bülent AKBAŞ, Member
Gebze Technical University _____

I hereby declare that I have obtained the required legal permissions during data collection and exploitation procedures, that I have made the in-text citations and cited the references properly, that I haven't falsified and/or fabricated research data and results of the study and that I have abided by the principles of the scientific research and ethics during my thesis study under the title of Use of Carbon Fiber Layers and Steel Plates to Repair Fatigue Damage at the Rib-To-Rib Butt-Welded Connections of Orthotropic Steel Deck under Fatigue Loading. In the case of a discovery of false statement, I am to acknowledge any legal consequence.

Saifaldien SHAKIR

Signature

All of the tests were performed using an Instron machine, which was provided by project number TR10/15/YNK/0034 from the Istanbul Development Agency under the project name “Sönümleyici Mesnet Test Merkezi.”

Dedicated to my family

and my best friend

ACKNOWLEDGEMENTS

Yildiz Technical University is one of the seven government universities situated in Istanbul besides being the 3rd oldest university of Turkey with its history dating back to 1911. It is regarded as one of the best universities in the country as well. I am happy and proud as a student of such renowned university.

I would like to articulate my profound gratitude and indebtedness to my supervisor Assist. Prof. Dr. Fatih ALEMDAR, he has always been a motivating and supporting person throughout the study period and in my life stations. It has been a great honor for me to work under his guidance and conduct my studies.

I would then like to express my gratitude for my country, the Republic of Iraq. It has always been a source of inspiration for me, may Allah give it peace and prosperity again.

I want to thank my family for their continuous encouragement. I am especially thankful to my wife for her help, support, patience, and encouragement to complete this study.

Finally, I would like to thank my fellow postgraduate students and the people who have been involved directly or indirectly in my endeavor.

Saifaldien SHAKIR

TABLE OF CONTENTS

LIST OF SYMBOLS

a	Crack Length
Δ_p	Change in Applied Load per Fatigue Cycle
Δ_y	Change in Deflection per Fatigue Cycle
t_d	Deck Thickness
a_{DW}	Down Crack
E	Modulus of Elasticity
N	Number of Cycle
t_r	Rib Thickness
SIF	Stress Intensity Factor
J Value	Strain Energy Release Rate Value
S-N	Stress-Number of Cycle
K	Stiffness
ΔK	Stress Intensity Factor Range
a_{UP}	Up Crack
σ_u	Ultimate Stress
σ_y	Yield Stress

LIST OF ABBREVIATIONS

AFRP	Aramid Fiber Reinforced Polymer
BSP	Bolted Steel Plates
CP	Connection Plate
CFRP	Carbon Fiber Reinforcement Polymer
CJP	Complete Joint Penetration
GFRP	Glass Fiber Reinforced Polymer
GMAW	Gas Metal Arc Welding
HSM	Hot-Spot Stress Method
LEFM	Linear Elastic Fracture Mechanics
NR	No Repairment
OSDs	Orthotropic Steel Decks
PJP	Partial Joint Penetration
RRBW	Rib-to-Rib Butt Welded
RD	Rib-to-Deck Joint
RR	Rib-to-Rib
SP	Steel Plates
SPS	Sandwich Plate System
SMAW	Shielded Metal Arc Welding
SHSS	Structural Hot-Spot Stresses
SAW	Submerged Arc Welding
UHPC	Ultra-High Performance Concrete
VCCT	Virtual Crack Closure Technique
WMT	Weld Melt Through

LIST OF FIGURES

LIST OF TABLES

ABSTRACT

Use of Carbon Fiber Layers and Steel Plates to Repair Fatigue Damage at the Rib-To-Rib Butt-Welded Connections of Orthotropic Steel Deck under Fatigue Loading

Saifaldien SHAKIR

Department of Civil Engineering

Doctor of Philosophy Thesis

Advisor: Assist.Prof. Dr. Fatih ALEMDAR

Orthotropic steel decks (OSDs) are one of the most chosen solutions when the dead-weight is the primary concern. Due to their light construction style and low rigidity fatigue have been observed as cracks running through especially in the connections because of concentrated and residual stresses at welded details. Studies concerning the cases which use (RR) butt-welded connections are limited in the literature. In this study, a set of cyclic loading experiments is carried out for the investigation of the fatigue life and crack propagation characteristics of full-scale rib-to-rib (RR) butt-welded connections with trapezoidal cross-sections. Two repairment methods based on bonded carbon fiber reinforced polymer layers (CFRP) and bolted steel plates (BSP) for the failed specimens are utilized and fatigue life improvements are tested. The cyclic test rig is first verified under static loading with strain gage readings which are compared to finite element simulations. Crack growth characteristics are observed as provided by dye-penetrant and dynamic stiffness crack detection methods. Crack lengths against the number of cycles were recorded for construction of the fatigue strength (S-N) Curves as given in AASHTO (2007). The test revealed that as long as the bond quality of the CFRP layers the steel plates

were maintained, the decrease in stress demand was enough to extend the fatigue life from AASHTO fatigue-design Category E' for the unrepaired configuration to the infinite fatigue life range. Test results also showed that the dynamic stiffness curve was drastically improved for the repaired specimens. To better understand the experimental results a numerical study based on finite element simulations is undertaken as well. The results indicate a remarkable decrease in stress levels in fatigue sensitive details after the application of proposed repair methods. Overall, the performance of these two lightweight methods for repairing movable OSD proved to be efficient and durable.

Keywords: Fatigue; CFRP layers; steel plates; repair; orthotropic steel deck.

ÖZET

Yorulma tipi yuklemeye maruz orthotropik celik tabliyelerin uc uca kaynakli boyuna kirislerindeki yorulma hasarlarinin karbon fiber takabakalar ve celik levhalarla tamiri

Saifaldien SHAKIR

İnşaat Mühendisliği Bölümü

Doktora Tezi

Danışman: Dr. Öğretim Üyesi Fatih ALEMDAR

Orthotropik çelik köprü tabliyeleri ölü ağırlığın önemli bir faktör olduğu büyük açıklıklı köprülerde sıklıkla kullanımaktadır. Son bir kaç on sene zarfında bu tip tabliyelerde özellikle kaynak bölgelerinde çatlaklarla sıklıkla karşılaşılmaya başlanmıştır. Çatlak gelişiminin en büyük nedenlerinden birisinin ağır taşıt yükleri altında tabliyenin yeterli rijitliğe sahip olmaması dolayısıyla özellikle kaynak bölgelerindeki gerilme yığılmaları olduğu düşünülmektedir. Literatürde bu yapıların bu tip hasarları üzerindeki çalışmalar sınırlıdır. Bu çalışma kapsamında trapezoidal kesitli körü kirişleri üzerindeki enine birleşim kaynaklarının tekrarlı yükler altında ilerlemesi hem deneysel hem de nümerik olarak çalışılmış ve bunların tamiri için iki yöntem önerilmiştir. Yöntemlerin ilki karbon fiberle güçlendirilmiş polimer (CFRP) esaslı olup diğeri ise kiriş gövdesine açılan delikler vasıtasıyla ekstra çelik levhaların kirişse bulonlanarak eklenmesine dayanmaktadır. Uygulanan tamir tekniklerinin temel amacı özellikle varolan çatlaklar çevresindeki gerilme değerlerini düşürmek ve dolayısıyla servis ömrünü artırmaktır. Öncelikle test düzeneği statik yükleme aldında alınan strain gage okumaları ve karşılıklı sonlu

eleman analizleri ile doğrulanmıştır. Daha sonra trapezoidal kesit bir ilk çatlak oluşacak şekilde kesilmiş ve tekrarlı yüklere maruz bırakılmıştır. Bu deneylerde numune tamamen güç tükenmesine ulaşana kadar dinamik rijitliği ve toplam çatlak uzunluğu karşılık gelen tekrar sayısıyla kayıt altına alınmıştır. Boyama tekniği ve dinamik rijitlik ölçümleri ile çatlağın ilerlemesi izlenmiştir. CFRP ve çelik levha teknikleri ayrı ayrı numunelere uygulanarak tekrarlı testlere devam edilmiştir. Bunlar sonucunda tamir edilmiş numunelerin AASHTO kategorisinde sonsuz servis ömrü seviyesine geçtiği gözlemlenmiştir. Deneysel sonuçları daha iyi anlamak için detaylı sonlu eleman modelleri kurulmuştur. Bunlar ile çatlak civarındaki gerilme dağılımlarının tamirden önce ve sonraki durumları ile çatlak ilerlemesinde önemli bir faktör olan enerji salınım oranları hesaplanmıştır. Bu sonuçların deneylerle uyumlu olduğu gözlemlenmiştir. Buna göre tamiratlar sonucunda gerilme değerleri büyük oranda düşmektedir bu da numunelerin ömrünü arttırmaktadır. Genel olarak bu iki tip hafif onarım metodunun başarılı olduğunu gösteren ve orthotropik tabliyelerin tamiri için önemli dizayn verilerinin derlendiği bir çalışma ortaya konmuştur.

Anahtar Kelimeler: Yorulma; karbon fiber polimer güçlendirme; çelik plakalar; tamirat; ortotropik çelik tabliyeler.

1
INTRODUCTION

1.1 Literature Review

Bridge deck plates which are stiffened orthotopically via transfer diaphragms and longitudinal ribs are shortly called orthotropic steel decks (OSDs). Such items are extensively employed in various bridge applications due to their advantages such as lightweight, increased load-bearing capacity, and practical construction. Construction practices have seen a great number of improvements during the last several decades and engineers have achieved all manner of improvement regarding design, fabrication, inspection, and maintenance of such bridge decks. Moreover, structural performance has consequently been enhanced to a great degree. Nevertheless the nature of the fatigue resistance continuing to be quite a conspicuous issue especially for OSDs, as these are under cyclic loading by the tires of motor vehicles and are under the effect of ever-changing dynamic loading regimes. Another negative effect of OSD fatigue performance is that numerous welds between steel plates cause local stress concentrations near the toes and roots of weldments, including residual stresses that result from the welding and stress ranges induced by live loads that accumulate to high levels because of the structural discontinuities. This is generally viewed as a major reason behind material fractures after high cyclic loads. After the initial report of OSD fatigue cracks in the Severn Bridge (Great Britain) in 1971, it was discovered that a concerning level of fatigue cracking had been occurring in OSD structures around the world. In China, fatigue cracks were found in several OSD bridges. In total, over 1,000 cracks were discovered on the Hu Meng Bridge in Guangdong Province (1997). They were first discovered at around 2003. In order to mitigate effects rehabilitation technologies which include high ductility concrete and sandwich plate systems have been used. During a regular inspection of the Jiang Yin Bridge in Jiangsu Province in 1997, more than 100 fatigue cracks were discovered and identified. The Jiang Yin Bridge is a

steel box girder suspension bridge with its first crack having been found in 2011. Furthermore, as illustrated in Fig. (1.1), several fatigue cracks were found in the Fatih Sultan Mehmet Bridge in Istanbul (FSM), Turkey [1], the main goal of this research coming out of this finding. Fatigue cracks have been discovered and identified, and have gradually increased in OSDs, generally originating from and occur due to repeated out-of-plane bending owing to repeated wheel loads. These fatigue cracks generally initiate at welded joints that exist between connection plate and trough rib and subsequently propagate to the rib wall. Such fatigue damage may cause a sudden decrease in the longitudinal rib stiffness. Out-of-plane bending results in high local flexural stresses in the welded joints between the connection plate and trough rib, because the plate and trough rib thicknesses are relatively small.

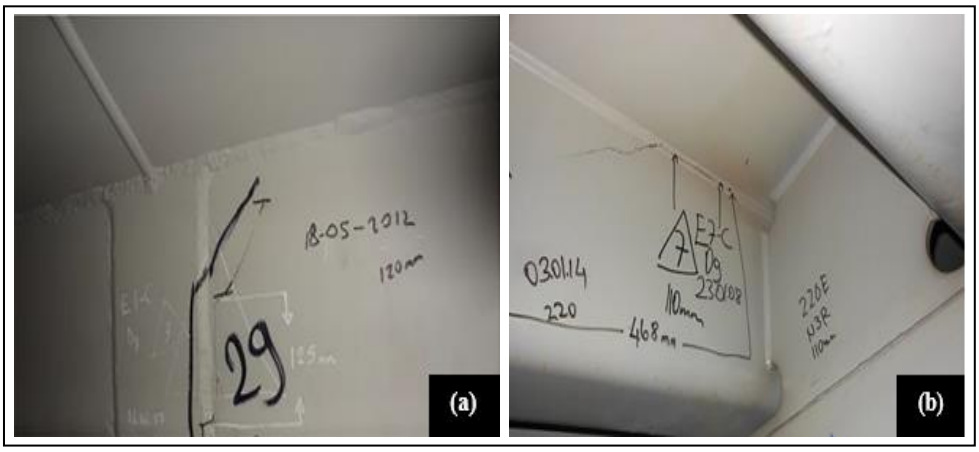

Figure 1.1 Fatigue cracks in a trapezoidal longitudinal rib (a) initiated at the welded joint , and (b) propagating to the rib wall [1]

The topic of fatigue resistance of OSDs, ever since the phenomenon of fatigue resistance first appeared in bridges [2, 3], has been deeply and rigorously investigated. OSDs mainly involve rib-to-deck weldings where most of the fatigue-related problems arise due to heavy wheel loads. Thus it has gathered a lot of attention from researchers.

Sim, Uang, and Sikorsky [4] studied how weld melt-through process and measures are taken to control distortion affected the fatigue performance of the welded joints, through the use of six orthotropic deck specimens that were full-sized. They determined that, where the weld roots were fully penetrated, no crack could be identified, while pre cambering appeared to be an advantage for fatigue resistance.

Sim and Uang [5], in their ongoing work, continued in their effective notch stress approach to carry out finite-element analyses for the test specimens. The results demonstrated that an increase in deck plate thickness helped in the reduction of stresses. However, there was little to no effect when reducing the rib wall thickness. Xiao et al. [6], using finite element (FE) software, performed local stress and fatigue analyses of rib-to-deck connections while wheel loads were being applied. It was shown that the surface stress in the deck plate far exceeded the stress in the rib wall which had a weld penetration of 75% into the wall of the rib. Ya, Yamada and Ishikawa [7] showed that when fatigue tests were performed on rib-to-deck specimens for fatigue, particularly on specimens with partial joint penetration (PJP) and weld melt-through (WMT) together, as well as 80% PJP and WMT separately, the WMT specimens seemed to show a smaller amount of reduction of fatigue strengths than the 80% of the PJP specimens. However, this discrepancy may have been due to a normal scattering of test data such that there were comparable fatigue strengths in both details. Liu et al. [8] created refined FE models by taking a multi-sub-model approach in order to analyze the structural hotspot stresses in rib-deck welded joints. Also, the researchers explored the effects of the radius of the weld toe, the mesh size, and the weld profile. Pfeil, Battista, and Mergulhão [9] studied numerically the stress concentrations at the rib-to-deck welded connection of trapezoidal closed ribs OSDs that were under heavy traffic load. In addition to these connections, the rib-to-floor beam connections, holes in diaphragms, and other connections were studied. Connor [10] investigated how, in OSDs, cutout geometry would affect stress endemic to rib-to-diaphragm welded joints, and a more advanced geometry inspired by an FE parametric study was proposed. By employing a real size laboratory test, Connor and Fisher [11] put forward a procedure to determine the values of the stresses found in rib-to-diaphragm connections, which is in accordance with AASHTO (2012) [12]. In addition to the efficacy of repairing cracks using stop-holes in an orthotropic steel bridge, Choi and Kim [13] determined the stress properties and behavior of the fatigue crack of longitudinal rib-to-crossbeam joints. Oh et al. [14], in their analytical and experimental research, proposed optimal height, thickness, and cross-beam shear area parameters as well as the efficiency and shapes of bulkhead plates with the aim

of countering fatigue cracks. Xiao et al. [15] studied the reasons for fatigue cracks that had been identified in longitudinal ribs of the Kinuura Bridge in Japan. The researchers determined, as a result of their experimental and theoretical study, that a lack of penetration zones would cause out of demand stress levels for butt-welded joints. Yokozeki and Miki [16] carried out experimental and analytical work to determine the fatigue performance of connections between longitudinal U-ribs and transverse ribs both containing and not containing a slit on the transverse rib web. Fatigue test results for the slit connections evaluated by the structural hot-spot stress (SHSS) method showed agreement with previous fatigue data of similar connection details. No fatigue crack was initiated on the connection without the slit after 4.6 million cycles compared to fatigue failure of the slit connection at 0.7 million cycles. Liu et al. [17] established the fatigue crack propagation numerical simulation method for U-rib butt weld of orthotropic steel bridge deck based on the theory of probabilistic fracture mechanics. The results showed that by the established numerical simulation method, a relatively accurate crack propagation process can be simulated, which provides a theoretical tool for its fatigue life estimation. Cheng et al. [18] investigated experimentally fatigue of rib-to-deck welded connections in OSDs by investigating hot-spot stresses (SHSS) at weld toes. The research includes the evaluation of the fatigue cracking process with S-N curves. They also proposed a simplified formula of crack growth rate to determine the fatigue threshold of rib-to-deck welded connections including 16 mm thick deck plates (with 80% PJP welds). Kainuma et al. [19], in their experimental study, investigated the fatigue response of rib-to-deck welded joints in OSDs for different structural parameters. The results demonstrated that fatigue cracks did not occur where the stresses were purely compressive and increasing the penetration rate had the beneficial effect of preventing root cracking. Increasing the deck plate thickness from 12 mm to 16 mm showed a significant improvement in fatigue durability. Finally, they came up with some important conclusions in welded joints such as grinding the weld toe could avoid crack at the toe but might lead to a deeper root crack, and the press straightening could be an effective treatment for preventing root cracks which are propagating in depth. Wei and Jiang [20] carried out fatigue life evaluations using the finite element method (FEM) in order to

explore the fatigue performance of U-shaped rib-to-deck welded connections of OSDs under cyclic loading, based on linear elastic fracture mechanics (LEFM). Results show that fatigue life calculated with LEFM is greater than the value in Eurocode 3, and fatigue life of the welded joint will be considerably longer when the deck plate thickness is 16-18 mm and initial crack length is less than 0.1 mm. Zhang, Liu, et al. [21] based on finite element numerical analysis, explained the fatigue performance improvements of composite bridge deck with a large longitudinal rib which is under the effect of typical fatigue prone stress range. The results indicate that the stress levels of rib-to-deck plate joints and longitudinal-to-diaphragm welding joints can be significantly reduced with composite bridge decks. Also, the opening of the diaphragm is an important structural detail for the control of the fatigue performance of the steel bridge deck. Zhang, Zhang, et al. [22] utilized a new type of steel and ultra-high performance concrete (UHPC) orthotropic composite bridge deck with the large longitudinal U ribs to understand the improvement on the mechanical behavior over the traditional orthotropic steel bridge deck. The results indicate that the composite bridge deck has good applicability to the continuous girder bridges of medium spans and the fatigue behavior of the composite bridge deck is significantly superior to the traditional one. Also, the increase of the opening width of the U ribs can cause an increase in the stress levels of the welded joints connecting the U ribs and the top plates. Zhu et al. [23] conducted static bending and fatigue tests on a full-scale orthotropic steel deck (OSD) specimen to study the effect of the inner bulkhead set inside the U-rib. Results of the tests and corresponding FE analysis of the specimen showed that inner bulkheads can be used to improve the fatigue life of the OSD and the bulkhead shape affects the stress levels of the weld toe of the rib-to-floor beam connection weld significantly. Fu et al. [24] studied the fatigue performance of a roof U-rib weld on orthotropic steel bridge decks by fatigue experiments on 40 specimens. They considered the influences of amplitude, penetration rate, loading position, and steel strength. The study shows that the increase in penetration rate can decrease the crack propagation rate and extend failure fatigue life. A greater steel strength can increase fatigue strength with respect to crack initiation. They also concluded that

under the same loading conditions, the fatigue life up to crack initiation is about half of the ultimate failure of life.

Ming Li; Yasuo Suzuki; Kunitaro Hashimoto; and Kunitomo Sugiura [25] studied the fatigue of the rib-to-deck joint in an OSD for two groups of RD joint specimens with weld-penetration ratios of 15 and 75% to assess the influence of the penetration ratio on the fatigue-crack type and its fatigue resistance. Fatigue test results suggested that the fatigue resistance of the RD joint specimens with 75 and 15% penetration ratios were approximately Class B and between Class C and Class D, respectively, per Japanese standards. Furthermore, results show that increasing the weld-penetration ratio can prevent root-to-throat fatigue cracks and enhance the fatigue resistance of RD joints. Cui et al. [26] worked on a method based on strain energy for the determination of the fatigue life is weldments of OSDs under heavy traffic. They also studied residual stresses as well. Their results indicated that their model which includes residual stresses is better in predicting fatigue life than the conventional approach. Yang, Kainuma and Jeong [27] investigated the effect of rib fractures on the structural response by carrying out the field tests at an actual bridge with artificial cracks by gas-cut and the results showed that once the fatigue cracks occurred at butt weld of ribs, the longitudinal stress is carried by the stiffener would be transferred to the localized deck plate and adjacent ribs. Kainuma et al. [28], in their experimental and numerical study, investigated the structural behavior of an orthotropic steel deck with bulb ribs. The behavior of the deck was examined, particularly the warped deformations of the developed fatigue cracks and the uniform stress distributions against moving loads attributed to the deck's asymmetric bulb ribs. An artificial fatigue crack serving as an authentic model of a fatigue crack was developed in the longitudinal bulb rib of an orthotropic steel deck in actual service. The loading tests were conducted on the orthotropic steel deck with artificial fatigue cracks. The test results were evaluated based on the artificial fatigue crack length on the longitudinal bulb ribs and compared with a nonlinear full finite-element analysis model considering the nonlinear contact behavior of artificial fatigue cracks. Alencar et al. [29], in their numerical work, used the hot-spot stress method (HSM) to evaluate the fatigue life of a welded joint subjected to distortion induced-fatigue, considering the vehicle speeds and a progressive

deterioration model for the road pavement. The welded joint was modeled by solid elements and was integrated with a 3D dynamic bridge model using the sub modeling technique. Besides the importance of considering the bridge-vehicle dynamic interactions with the pavement road-roughness, the dynamic amplification effects on local stresses and the relatively high scatter found in the fatigue lives considering global and local approaches show that a detailed local stress definition is fundamental to evaluate the fatigue performance of existing roadway bridges. The effects of the annual traffic increase rate on fatigue life are also discussed. Aygül et al. [30] studied the welded joints on orthotropic steel decks with cut-out holes by utilizing hot spot stress techniques on full-size specimens. In the theoretical part of their study, they incorporated various shell and solid elements as well as different weld modeling techniques. Analytical results were compared with different methods such as Batelle's approach and the experimental results. Results indicated that shell-based models produced unrealistically high stresses when welds were not considered. Another important finding was the substantial influence of the weld modeling technique on the hot-spot stresses. The study provided great insight into the modeling of the details and usage of the finite element method in order to address the stress states of the details in a realistic fashion. Again Mustafa Aygül et al. [31] utilized linear elastic fracture mechanics on the analysis of the distortion induced fatigue cracks in an existing bridge. A fatigue propagation analysis is conducted based on realistic load levels on the bridge which were obtained via strain measurements. It is found that cracks showed remarkably different characteristics of the propagation rate in different directions. It is seen that in the thickness direction crack propagates with a decelerating rate and finally arrested halfway through the rib wall as it gets longer whereas in the longitudinal direction crack continues propagation with a constant rate. Another important finding is that despite multi-mode (I, II and III) loading caused by the distortion-induced cracking, crack propagation was still dominated with Mode I. Other modes (II and III) contributed minimally depending on the location of the crack front and geometry of the cross-section of the beam. M. Aygül et al. [32], in an ongoing study, analyzed distortion-induced cracks of welded details in Söderström Bridge. They performed 3D crack simulations with variable amplitude load histories. For the sake of realistic

results on the fatigue life predictions, load histories were based on field measurements. Different rates and direction criteria were considered during the analysis and results were compared with the constant amplitude results of one of their previous studies [31]. It is seen that variable amplitude loading was better suited with respect to the real observations and indeed different growth rates were expected for different propagation directions. The most effective ingredients were found to be loading and geometrical configuration of the studied detail. This is because of the number of cycles and load levels associated with the variable amplitude definitions which were considerably different from a constant amplitude definition. Also, it is seen that the variable amplitude approach resulted in conservative predictions. Finally, it is indicated that albeit great differences basically similar crack formation and growth rates in character were observed in both approaches. As indicated previously fatigue life span of the OSD mainly depends on the welded details [33, 34] and the reason was the low stiffness levels of the deck and rib plates under heavy loads due to traffic [35–38]. Thus especially with increasing rate studies on the fatigue phenomena and strengthening methods have been conducted which are focusing on the stiffening of the OSDs such that fatigue life is extended [39-44]. A common method is to replace the existing cover with a stiffer overlay. This type of approach is especially well suited for fixed bridges where dead-weight is not a concern. One of the most popular solutions utilizing the replacement approach is installing a reinforced concrete overlay instead of the existing asphalt layer [39, 45]. In some studies, compact reinforced reactive powder concrete (CRRPC) was suggested for the replacement of the asphalte layer in order to strengthen the OSD [46]. Finite element simulations showed that it is possible to reduce the stress levels by 34–83% relatively when a 50-mm CRRPC layer is used instead of an 80-mm asphalt overlay. This would drastically improve fatigue life and moreover in situ hot-steam treatment of CRRPC would prevent shrinkage cracks. The stress reduction effect of the CRRPC is also verified with field measurements. Finally, it is stated that CRRPC can be considered a feasible and safe retrofitting and strengthening method for fixed OSD bridges. However as indicated above, for movable OSD bridges, additional weight is of great concern. Thus the most important parameter becomes reinforcement's dead-weight. The study presented

in this thesis is focused on two lightweight methods for repairing movable OSD: the bolted steel plates method and the bonded carbon fiber reinforced polymer layers (CFRP) method. Both repairment methods were used to stiffen (RR) butt-welded connections over cracks. In the bolted steel plates method, the steel plates with 10 mm thickness are bolted to the existing damaged longitudinal ribs by bolts. Recently, this method has been executed by Nunteknik Construction Company to repair the orthotropic fatigue cracks at the (RR) butt-welded connections in the Fatih Sultan Mehmet (FSM) Bridge in Istanbul [47], as illustrated in Fig. (1.2).

Figure 1.2 Faith sultan mehmet (FSM) bridge orthotropic crack repairs[47]

In the bonded CFRP layers method, the five layers of CFRP with total thickness 3 mm were bonded to the existing damaged longitudinal ribs with an epoxy resin layers and considered one of the new repairment methods to repair the damage caused by fatigue cracks at the (RR) butt-welded connections of OBD. Each repairment method was applied to the damaged ribs in the longitudinal direction allows for increasing the bending stiffness of the repair. The bolted steel plate method has been initially developed by Lightweight Structures B.V. [48] and the first trial of this method to strengthen a movable OSD bridge was completed on the Scharsterrijn Bridge in the Netherlands [49]. This method also showed great promise in repairment of reinforced concrete (RC) beams with severe shear damage. Alam et al. [50] found that the original shear capacity of (RC) beams can be obtained with steel plates and adhesive connectors.

Another study carried out by Teixeira de Freitas, Kolstein and Bijlaard [51] took into account two lightweight solutions (bonded and sandwich systems) for strengthening a movable OSD. The main target is to reduce the stress levels and hence extend the fatigue life. Both methods of repairment include the addition of a second plate. They observed that the main cause of the fatigue failure of the repairments for both systems was shear. In the case of bonded plates, adhesive joints and in case of sandwich system face-core interface were vulnerable to the developing shear stresses. Alemdar, Nagati, et al. [52] proposed a new repair method by adding steel angles that connect the transverse connection plate to the girder web which is also stiffened with a steel plate on the opposite side. They tested setup under cyclic loading and results showed that application was successful in preventing horseshoe-shaped cracks of the connection plate and cracks along the flange-to-web welds. The repaired specimens exceeded the infinite fatigue life for AASHTO Fatigue Category A in the number of cycles without any detectable crack growth. Other than steel enhancements CFRP polymer enhancements were also studied for the improvement of the fatigue performance of the weld details of OSD's [53-56]. It is seen that CFRP layers are effective in stress reduction and improvement of the fatigue life of welded connections drastically even tested under high-stress ranges. The most sensitive part in terms of strength is the bond between CFRP and steel which is closely related to the resin's composition and thickness. When an optimal composition is used for the bond it is deemed possible to extend the life of the welded connections from Category E to run out at high-stress ranges with CFRP overlays. Alemdar, Gangel, et al. [57] implemented fatigue damage repairment in steel plates which are under tension by using CFRP overlays. They concluded that an increase of the axial stiffness ratio to 0.4 tenfold increase in fatigue life can be observed. Moreover, infinite fatigue life can be obtained with an optimal axial stiffness ratio. The CFRP plate repairment methods used steel plates with a center hole under tension loading were also applied by Alemdar et al. [58], a very good relation fatigue life of the steel plate. These repair methods extended the specimen fatigue life about eight times compared to the non-reinforced specimen. Experimental tests by Schubbe and Mall [59] were conducted on aluminum plates which were repaired with bonded composite patches. Both for thick and thin plates

fatigue life was improved with an increasing axial stiffness ratio. They performed experiments with ratios of 1.0 and 1.3 and recommended 1.0 for aerospace structures. Using CFRP for the repair and strengthening of existing structures has gained momentum in the past twenty years. Haghani and Al-Emrani [60] stated that CFRP showed great promise for the repair of corroded steel beams by improving the fatigue life considerably. The design of adhesive joints which are used in the bonds is a major issue in this type of strengthening technique in steel structures. Nilsson and Al-Emrani [61] suggested steel sandwich bridge decks based on corrugated core steel sandwich plate instead of conventional steel bridge decks. They made extensive comparisons and found various advantages over conventional designs. Stiffness to weight ratio is improved, load distribution is more even, production and construction processes are more simplified and industrialized. In a study considering the effects of weld joint configuration on the fatigue performance and transverse shear stiffness, it is found that by replacing conventional orthotropic decks with steel sandwich plates weight savings up to 44% is possible. The popularity of the polymer-based reinforcement materials in the construction sector requires appropriate joining techniques, especially for field joints. One common method is bolted joints for fiber-reinforced polymer structures. Despite being detachable bolted joints have some shortcomings. Hole clearances which are important for appropriate field applications reduce the stiffness and effectiveness. Also, pre-tensioning is not possible due to the creep deformations of the composite material which results in considerable drops in bolt tension. Mara, Haghani, and Al-Emrani [62] proposed metallic inserts in the hole in order to overcome these problems. In a series of tests, they studied the relaxation of the bolt-tension and the stiffness and load-bearing characteristics of the joints. The study also includes finite element simulations. Several benefits mentioned were: minimization of bolt tension losses, the possibility of activating load transfer via friction under service loads, joint effectiveness is improved in terms of strength and stiffness. Although short term performance of FRPs bonded to steel members has been established fairly well subject of durability over the long term is still poorly understood. Heshmati, Haghani, and Al-Emrani [63] worked on the effect of identified experimental factors on the Carbon-FRP/steel joints. In their experiments, both the bonded specimens

and bulk material were tested under several aging scenarios. Results revealed the detrimental effects of de-icing salts. The interlaminar shear strength of FRP joints is significantly reduced by these elements. In another study, Haghani and Al-Emrani [64] searched the effects of moisture, temperature, and de-icing salts on CFRP-steel joints. In experiments, for 18 months, forty (40) CFRP/steel double lap-shear specimens were exposed to a de-icing salt solution with deionized water at 20°C and 45°C. Results showed a remarkable change in failure. Instead of cohesive failure interfacial or interlaminar failure dominated. Although for the first six months load capacity of the joints was observed to increase, afterward, specimens exposed to higher temperatures experienced a decline in the failure load. In another study, Heshmati, Haghani, and Al-Emrani [65] worked on the combined effects of moisture and thermal cycles on the CFRP joint performance. Considering cyclic environmental scenarios, they proposed experimental setups considering the role of moisture combined with freeze-thaw cycles. They investigate the possibility of a modeling platform in order to predict the remaining residual strength of the aged joints. Tests showed a strong reduction of 11% and 47% as a result of the wet-dry cycle in distilled and salty water respectively. These values are significantly larger than the scenarios based on wet exposure only. Additionally, no adverse effects of freeze-thaw cycles were found on the strength of the joints for 125 and 250 cycles.

1.2 Objective of the Thesis

From the literature, it is understood that investigations of the characteristic fatigue life, propagation of fatigue cracking, the mechanics of the failure, and repairing the damage under cyclic loading are severely limited (RR) butt-welded connections. The main objective of the thesis is to demonstrate the efficiency of the proposed repair methods by thoroughly testing and modeling the underlying mechanics. The main objective of this thesis divided into two parts. In Part I, the work was directed to address these issues experimentally for trapezoidal longitudinal ribs on orthotropic bridge decks in a controlled fashion for (RR) butt-welded connections. A static finite element model was carried out in order to assess the validity of the experimental setup. At the beginning of the tests, strain values under static loading were compared and checked with the numerical results for each specimen. Experiments were performed on six trapezoidal rib specimens, including five specimens with initial cracks which were created at the transverse butt-welded connections located at the bottom of the existing ribs. The last specimen was considered as a control specimen. The acentric cyclic load was considered as the simulation of tire loading on the deck with a maximum/minimum load of 100/10 kN with load ratio R=0.1 at 2 Hertz. Crack propagation characteristics were observed for the cracked specimens. a-N (crack length vs the number of cycles) and S-N (stress vs the number of cycles) diagrams for each case were produced which are potentially useful for the evaluation of fatigue life of cracked members. Also, dynamic stiffness readings are obtained in order to better evaluate stiffness degradation characteristics. Based on the results, conclusions regarding the fatigue life and failure mechanism of cracked (RR) butt-welded connections were drawn. In Part II, the work switched to investigate the performance of repairing orthotropic steel decks (OSDs) by adding steel plates and CFRP layers to the existing damaged longitudinal ribs. The repair methods aim to stiffen the existing rib plates, reducing the stresses at the welds of the rib hence increase the life of OSDs. Two repairments are subject to research, bolted steel plates method, and bonded CFRP polymer layers method. In the bolted steel plates method, the steel plates were bolted to the existing damaged longitudinal ribs of OSD by bolts. In the bonded CFRP method, the five layers of CFRP

were bonded to the existing damaged longitudinal ribs with an epoxy resin layer. Both repairments are considered lightweight methods to repair existing fatigue damage at the rib-to-rib (RR) butt-welded connections of OSD under cyclic fatigue loading and to restore the damaged trapezoidal longitudinal rib to its original strength. The significance of these newly repair methods is that it is simpler to implement and more cost-effective than existing retrofit measures. These methods of repairing were investigated because it is commonly used in steel bridges. Again a-N and S-N curves are obtained and conclusions regarding the fatigue life and failure mechanism of cracked (RR) butt-welded connections were drawn for the repaired sections. Dynamic stiffness readings are obtained for the evaluation of the different characteristics of the stiffness degradation of these different repairment methods. Moreover in order to better understand the mechanics of the fatigue failure extensive finite element modeling is carried out. Models with cracks were developed and the stress-reducing effect of the repairments is demonstrated for the repaired cases. Stress fields around the cracks for various crack lengths are compared for unrepaired specimens and specimens repaired with CFRP and bolted steel plates. J values which are a measure of crack driving force are also compared. Additionally, an optimization method based on the J values for various crack lengths is proposed in order to define fatigue parameters regarding the Paris Law. Obtained parameters than used to model fatigue life simulations in order to demonstrate the life-extension characteristics of the repair methods. The overall efficiency of the proposed repair methods is demonstrated both via experiments and numerical modeling.

1.3 Hyphothesis

An orthotropic steel deck (OSD) consists of a deck plate supported in orthogonal directions via a system of longitudinal stiffener ribs and transverse crossbeams. These are, in turn, spanned by main girders. All connections are done through welding. One of the most important problems in OSDs' service life is fatigue. This because these structures include extremely sensitive welding spots with respect to fatigue thus their service life can be unexpectedly short. An important fatigue prone location is the one at the rib-to-rib butt-welded connections of the trapezoidal longitudinal rib orthotropic steel deck (OSD). This mainly due to the low stiffness of the rib plate with respect to wheel loads. Moreover, the ever-increasing nature of heavy traffic makes the fatigue an even greater problem. An obvious remedy is to reduce the stress levels occurring in these sensitive locations. Recent decades have witnessed an increased amount of studies on this subject and several repairment methods have been proposed. Numerous repair methods have been suggested. The general idea is to use a stiffer overlay instead of the wearing asphalte layer. These types of propositions and similar alternatives have been feasible where the dead-weight is not a concern like fixed bridges. But OSDs have also great usage in movable bridges as well where the weight of the repairment becomes a serious constraint.

In this thesis, the characteristic fatigue life, propagation of fatigue cracking, and the mechanics of the failure at the rib-to-rib (RR) butt-welded connections of the trapezoidal longitudinal rib orthotropic steel deck (OSD) under cyclic loading are studied. The fatigue life study of OSD ribs in this thesis consists of six (6) chapters. Chapter 1 is the introduction chapter. It briefly states the objectives of the thesis and includes a literature survey. Chapter 2 gives general information about the OSD bridge ribs. The structural components, fatigue considerations, and information on repairment techniques are explained here. In Chapter 3 an experimental study is undertaken over full-scale specimens. Details and results of experiments conducted on prepared specimens are given here. The cyclic test rig, geometrical and material properties, fatigue life-related measurements are explained in detail. For verification issues, a static test was performed, and the experimental setup was verified with strain gage measurements which are compared to finite element

simulations of the test rig. In Chapter 4 two methods for the repair of the damaged specimens of Chapter 3 are proposed and tested. These are carbon-fiber-reinforced polymer layers (CFRP) and bolted steel plates (BSP) methods. Both alternatives are promising light-weight (between 2 and 13 kg/m2) methods for prolonging the life-span of orthotropic steel decks. The details of repairment for both methods and results of cyclic fatigue life experiments are given. In Chapter 5 finite element simulations of the experiments given in Chapters 3 and 4 are included. Detailed modeling processes and comparisons with the experimental results are given in this chapter. Also, simulations on fatigue crack growth and predictions on fatigue-related material properties based on Paris Law are included as well. Finally, Chapter 6 includes conclusions.

2
ORTHOTROPIC STEEL DECK BRIDGES

2.1 General Information on (OSD) Bridge

An OSD bridge structure is made of steel plates with stiffeners welded in 2D in-plane directions (longitudinal-ribs and transversal-cross beams) which are perpendicular and working concerning the bending. Bridges are generally under bending in the longitudinal direction so main girders in this direction are the primarily responsible parts for the load-bearing capacity. A cross-sectional perspective view of a typical OSD is shown in Fig. (2.1). The name orthotropic is derived from orthogonal and anisotropic where the first one is due to load carrying system is orthogonal (perpendicular in longitudinal and transversal directions) and the latter is due to the difference of their (ribs and cross beams) stiffness.

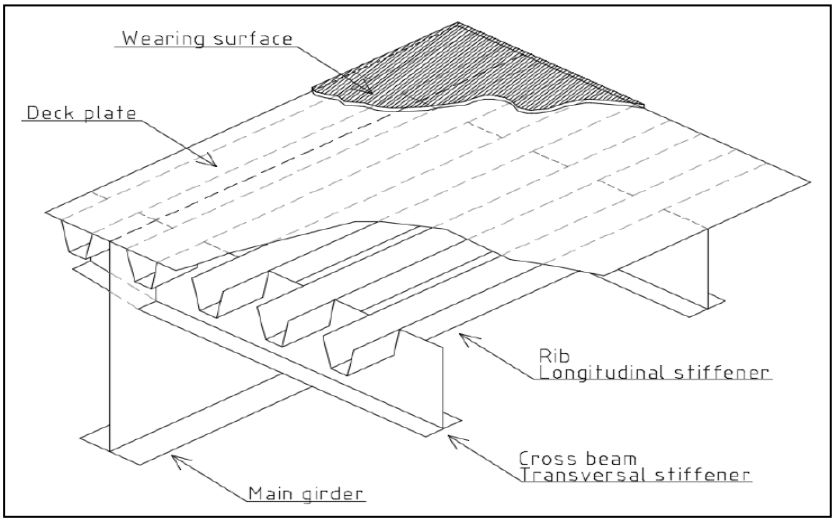

Figure 2.1 Principal layout of an orthotropic bridge deck [66]

The main structural advantage of the OSD systems is lying in the configuration where the entire deck structure is acting as the top flange for the main girders. In this manner, overall stiffness is increased and a more economical and efficient system is obtained. [67] OSD bridge systems are generally designed in two different configurations. One is a plate girder and the other is the box girder system. In Fig.

(2.2). one can see the plate girder system which is also called “battle deck floor”. This design generally employed through the 1930s bridge constructions.

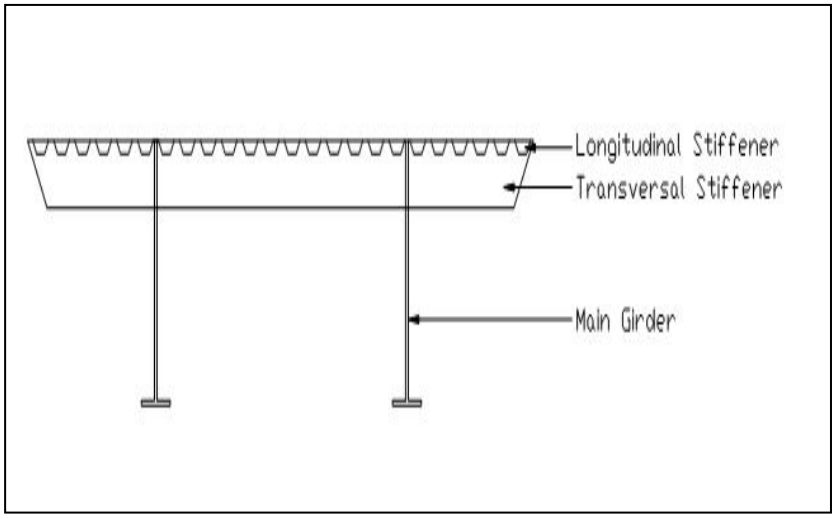

Figure 2.2 Plate girder deck [67]

As an advancement, to increase torsional stiffness and also withstand horizontal loads such as wind, the cross-section is strengthened with lateral bracings at the bottom side. This configuration is the main essence of the box girder system [67]. Besides being stiffer concerning asymmetrical loadings with increased torsional stiffness this design also offers a maintenance platform for the inspections and repairments of the bridge even under traffic load. Some subtypes of the box girder design can be seen in Figs. (2.3), (2.4) and (2.5) for the single, multi-cell, and box with struts (where the overhanging deck is supported with struts) types respectively. [68]

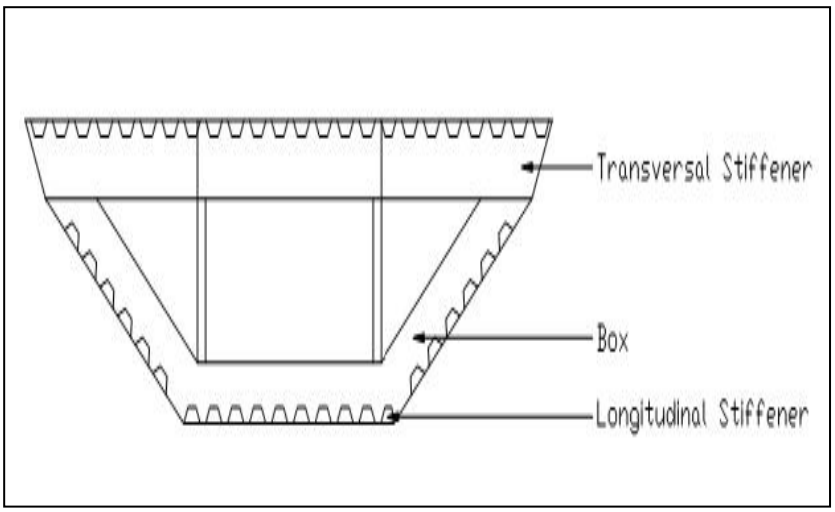

Figure 2.3 Single-cell box girder deck [68]

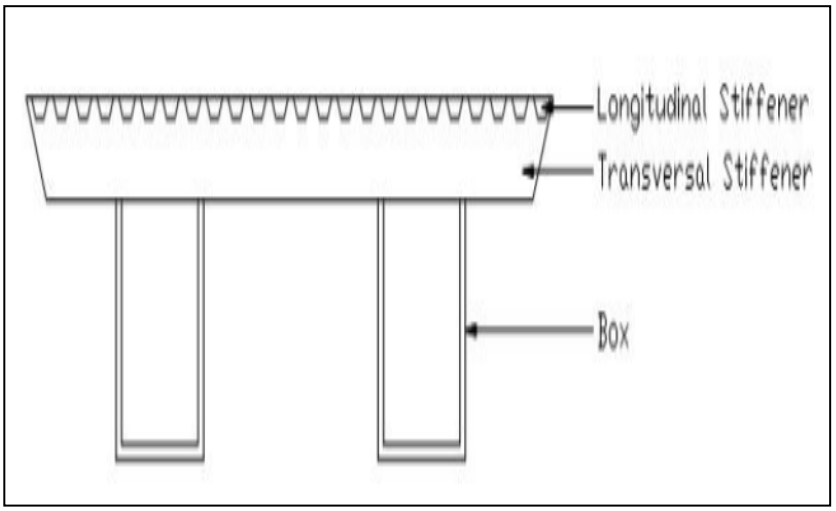

Figure 2.4 Multi-cell box girder bridge [68]

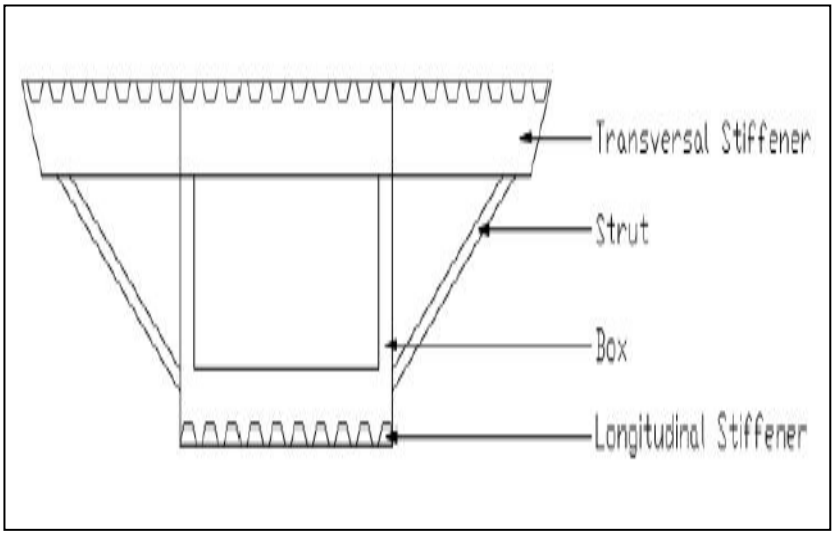

Figure 2.5 Box girder type, struts support overhanging deck [68]

2.2 Fatigue Crack Occurrences in (OSD) Bridge

2.2.1 Introduction

One of the main considerations for the OSD bridge safety is the fatigue cracks due to continuous cyclic loading. These cracks have been observed and identified increasingly especially in the last few decades as the traffic loads have been consistently increasing. Thus studies and manuals concerning this fact have been published at an increasing rate. AISC Design Manual Wolchuk [69] and BS 5400 [70] are some of them. As indicated in "Fatigue and Fracture in Steel Bridges", Fisher [71], the main reason for the brittle fatigue fracture of the OSD systems is due to designers' overestimation of the stiffness levels of specific details. Briefly, some

details (especially around connections) have lower fatigue resistance capacities then intended. Concerning the lower resistance of specific details researcher in Japan identified and grouped cracks in OSD systems into four main categories while working on the Hanshin Expressway [72]. These are depicted in Fig. (2.6) and can be explicitly given as cracks in welded sections of the following connections:

- Deck plate, rib to the deck (Category 1)
- Rib splice (Category 2)
- Deck plate, vertical stiffener (Category 3)
- Rib to cross beam (Category 4)

Investigations revealed that there is an increasing trend in the fatigue cracks in OSD bridges. From 7.8% (105/1347 bridges) in 2006 to 10.5% (142/1347 bridges) in 2007. Another striking fact is the construction times as most of them were built around the 90s (84 of 142) with 60 of them after the Kobe earthquake. This fact alone shows the importance of the fatigue life characteristics of the OSD bridge structures under heavy traffic loading. Similarly, in the Netherlands, studies done by Kolstein [40] resulted in the identification of six crucial locations for fatigue failure in OSD systems, all again around welded connections:

- Deck plate to rib between cross beams
- Deck plate to rib at cross beams
- Rib splice
- Rib to cross beam
- Deck plate to vertical stiffener
- Butt-welded

This list is an extension of the previous list [72]. The first two locations can be gathered in category 1 (Deck plate, rib to deck), and the last one concerning the butt welds can be considered in the categories 2 (Rib splice) and 4 (Rib to cross beam). One can see typical crack formations with associated categories in Fig. (2.6). Of course with so many different details and connection types, an OSD can experience a combination of these cracks or maybe sometimes an entirely different type.

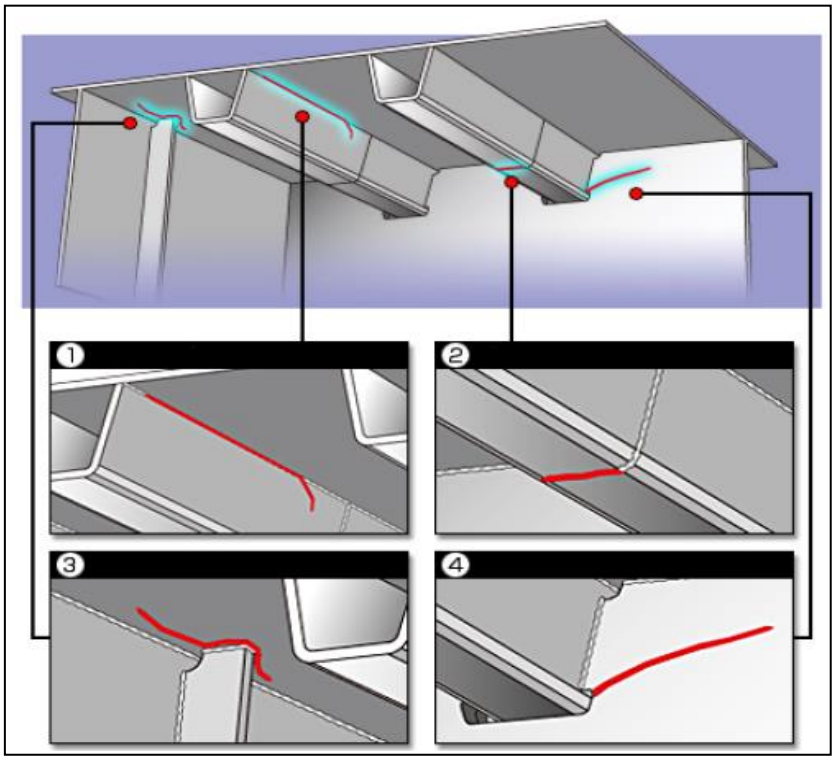

Figure 2.6 Fatigue crack categories of OSD (1) rib to deck, (2) rib splice, (3) deck plate and vertical stiffener, and (4) rib to cross beam [72]

This study is concerned with category 2 (Rib splice) type cracks in closed trapezoidal ribs thus we will include more detailed information on this category for the sake of completeness.

2.2.2 Rib Splice Type Cracks

Investigation revealed that fatigue cracks in rib splice weld connections are not uncommon. Observations on Harbour Bridge (New Zealand) by Beamish et al. [73] and Billings et al. [74], on bridges in the Netherlands [39], and Hanshin Expressway in Japan revealed this type of cracks. This form of cracks generally arising around the root of the weld or weld which forms the connection between the rib and the backing strip. Fig. (2.7) shows these two types of sources with cross-sections. In design, the locations of rib connections are generally selected where minimum bending moments occur. Bending moments are due to heavy traffic loads and directly responsible for the higher tensile stress ranges. We can see a weld root crack in Fig. (2.8) which is detected via visual inspection from the outside of an OSD. Moreover, it can be seen that the crack is well advanced and propagated through the deck plate as well.

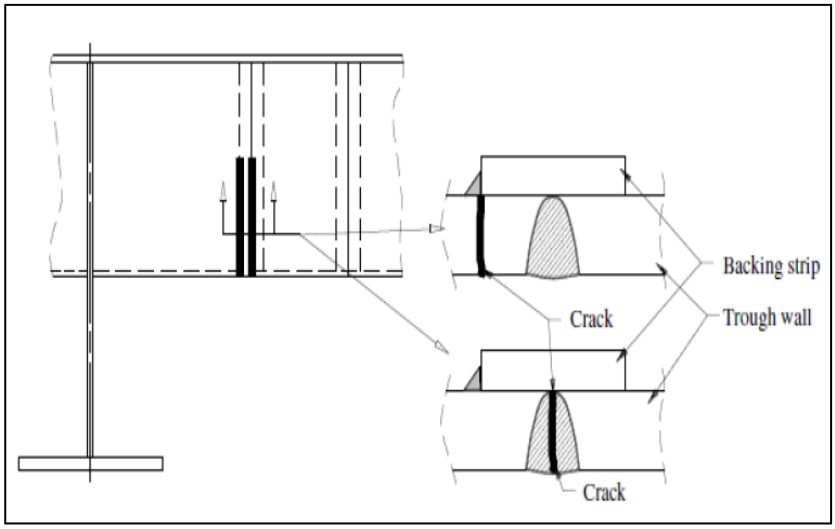

Figure 2.7 Rib splice crack formations [39]

Figure 2.8 Visual identification of a rib splice weld root crack [75]

2.2.3 Summary

Among the several fatigue cracks mentioned at the beginning of section one of the utmost crack type associated with the heavy traffic, the load is the rib to rib crack type. As explained before these are due to the continuous cyclic nature of the heavy axle loads. These loads cause considerable bending moments which in turn result in high levels of tensile stresses in the longitudinal direction as the OSD is forced to out-of-plane bending. These fatigue cracks which are propagating through the rib walls (along weld root or along with the connection between the backing strip and rib wall) constitute one of the most important cases for the operational safety of the OSD.

2.3 Repairment of Orthotropic Steel Bridges

Several methods have been implemented for the fatigue crack cases of the OSD bridges.

- The foremost point is the regular and throughout inspection of the OSD. This will help to assess the general structural health of the system and would allow timely interventions.

- Once the crack is identified they can be arrested by drilling holes.

- If the crack propagation rates are high and cracks are already affecting multiple parts, these parts can be repaired via welding (Gas Metal Arc Welding GMAW, Submerged Arc Welding SAW or Shielded Metal Arc Welding SMAW) and/or replacing parts.

Fig. (2.9) shows a repairment application (both welding and bolted steel plates) for the Hanshin Expressway [75]. Drilling a hole to arrest a crack can be done as a part of the inspection/maintenance program. These holes are called a hey hole or a stop hole and they would be drilled at the leading tip of a crack. Other than the mitigation techniques sometimes (if the cracks are significant and pose threat to the operational capacity) it is required to opt for complete or partial overhauling by replacing and/or repairing crack exposed sections (deck plate or rib) of the bridge.

This procedure is utilized such that the stiffness of the bridge is restored to its original capacity. Sometimes the capacity can be increased to the levels above the original level by adding additional parts as well. As can be seen from Fig. (2.9) both welding the original parts and adding bolted steel plates can be applied at the same time.

Figure 2.9 Welding treatment for a rib-deck crack, hanshin expressway [75]

Here for the sake of completeness brief information on the popular repair methods which includes additional parts such as bonded steel plates and CFRP layers (both deemed light-weight options) are included.

2.4 Bond Steel Plate Reinforcement

One of the solutions for light-weight repair for the movable OSD bridges is the application of steel plates. These additional steel plates are configured such that they will resist the out-of-plane bending with the existing deck plate hence considerably increase the stiffness. Generally selected with 5 to 8 mm thickness these plates are bonded to the existing deck plate directly or in a sandwich formation. The important point is the adhesive selected for the bonding. Thus early studies were concerned with this bonding layer, Jong [39]. One of the first applications of this method was carried out by using Sikadur 30 adhesive via a glue comb and then fitting the additional plate on top. Full scale dynamic and static loading experiments were carried out on 1500x2600 mm steel specimens and it was found that delamination occurred through the adhesive layer [76]. Corte [77] tested

this configuration with an epoxy-based adhesive, PC5800/BL. He found that even after 5 million cycles no visible fatigue damage was observed for the deck plates which were 600x300 mm. One improvement due to Labordus [78] was the utilization of vacuum-infusing of the bond layer between plates. Cyclic tests on 6 mm thick steel plates showed no sign of fatigue damage for the beam specimens which were reinforced via low viscosity epoxy. Another improvement was due to Overduin et al. [79] who arranged a sandwich system. This sandwich system has the existing plate and the reinforcing plate (10 mm) as the skins and there would be a thick core (30 mm synthetic layer) that bonds them. Increased thickness of the core was also expected to increase the overall bending stiffness as well but the tests revealed that with 32 MPa Young's Modulus it was not effective. A solution to this problem was proposed by Kennedy et al. [80] by simply replacing the core with a stiffer one. In this case, this was made from polyurethane with a room temperature Young's modulus of 750 MPa. This solution constitutes the essence of the Sandwich Plate System (SPS) by Intelligent Engineering and it found initial application in the repairment of docks. Since then it has been used to build new bridges and also repairment of existing bridges as well, [81], and [82]. In an experimental and numerical study, Feldmann et al. [83] analyzed the performance of SPS for the repairment purpose of an existing OSD with the addition of a 6 mm reinforcing plate and a 20-30 mm thick core. Friedrich [84]; Matuschek et al. [85] worked on a pilot study which includes the utilization of SPS for the repairment of the Schonwasserpark Bridge, Krefeld, Germany. Also in China, Zhang et al. [86] studied newly constructed and repaired bridge decks via SPS. These fixed bridges include up to 50 mm of asphalt overlay on top of the sandwich system. Another important study is due to Teixeira de Freitas, Kolstein and Bijlaard [51]. In their work, they considered two (bonded and sandwich methods) light-weight repairment approach for movable OSD bridges. The primary objective was to reduce stress levels and improve fatigue life. The general layout of both approaches can be seen in Fig. (2.10). As can be seen, they both include an additional reinforcing plate. In both cases, experiments revealed that shear stress developing at the interfaces (within the adhesive layer for the bonded system and core-plate boundary for the sandwich system) is the primary factor for the fatigue damage.

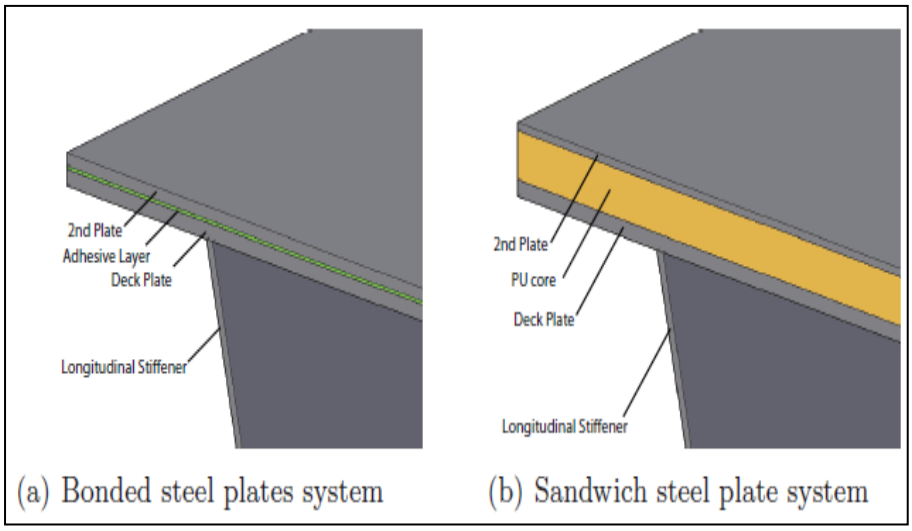

Figure 2.10 Detail of the steel plate reinforcement systems [51]

2.5 Bond CFRP Layer Reinforcement

Usage of carbon fiber reinforced polymer (CFRP) has been gaining great attention for the restoration to the original capacity or even increasing the original performance levels an structure. The application can be done for individual components of a structure or sometimes for the whole structure. The performance of the structure can be greatly enhanced in terms of ductility, crack resistance, stiffness, stability, etc. [87,89]. These benefits of CFRP appeared in many applications, especially for the bridges in the USA which were rendered insufficient, structurally, concerning newer construction codes [90]. There were also inevitable reasons as well such as the increased service loads, structural deterioration due to elements; especially corrosion, etc. or for some cases, the mechanical response of the structure required major enhancements for previously unanticipated loading regimes like cyclic loading. These bridges required extensive overhauling to meet the ever tightened public safety standards [88]. Today many studies established the reliability, efficiency, and cost-effectiveness of the usage of CFRP not only for repair and rehabilitation of existing structures but also for the construction of new structures. Due to wide usage of CFRP with increasing applications especially for concrete structures American Concrete Institute committee 440 (ACI 440) published a guide that addresses all aspects of repair and design of CFRP usage with

reinforced concrete. The CFRP consists of a layerwise structure. Each layer called the lamina is formed by fibers (unidirectional within a lamina) arranged inside a thin layer of the polymer matrix. In the case of CFRP, as the letter indicates carbon, fibers are made from carbon. There can be other types like aramid (AFRP), glass (GFRP), etc. All in common is called as FRP or fiber-reinforced polymers. Fibers' primary role is to provide necessary stiffness and strength. The primary role of the matrix is to maintain overall structural stability, to transfer loads between fibers, and to protect fibers from the elements and damage. Polyester, nylon, epoxy are some common materials for matrix applications. Alternative arrangements of fibers lead to different types of FRP composites such as bidirectional arrangement for two-way plates or FRP robs which can be a serious alternative to the RC steel bars [91]. Externally attached FRP sheets were used for the strengthening and capacity increase of RC bridge slabs by Fathelbab et al. [92]. In their work performance of several configurations of FRP sheets (different stiffness and arrangements) were parametrically evaluated via a commercial finite elements package (ANSYS) by applying non-linear analyses. They concluded that stiffness, strength, and ductility of slabs with FRP applications were greatly enhanced concerning the control specimen (RC only). Fig. (2.11) includes a tainted valve which is held by crack damaged struts. Riveros et al. [93] worked this case as an innovative application of CFRP assisted repair. They carried out finite element analyses for the configurations of the valve before and after repair and evaluated the fatigue enhancement in terms of fitness for service. Fig. (2.12) shows their innovative CFRP usage on site. They concluded that analyses revealed an increase of fatigue life up 2 to 4 times the fatigue life of the original structure.

Figure 2.11 Cracks in valve's strut arms (flange and flange-web) [93]

Figure 2.12 CFRP applied on struts of the valve [93]

In a study by Schnerch et al. [94], application high modulus CFRP for the steel bridges were explored. One crucial aspect was the neat installation of CFRP. In this way, debonding issues would not hinder the true performance of CFRP retrofitting. A compilation of application of proper bonding techniques gathered from the field experience and the literature was provided by the researchers in guideline form. The guide includes all the key aspects of adhesive and material preparation, and also detailing issues especially oriented for the applications which include high modulus CFRP usage in steel-concrete composite bridge systems. The main target was to enhance the flexural capacity of the bridge girders concerning increasing demand due to service loads. The capacity analysis was based on moment-curvature relations and they also proposed a bond model that estimates the shearing stresses

within the adhesive layer. Failure criteria of the adhesive given by the researchers were based on maximum principal stress. Briefly dictates that this value should be smaller than the adhesive's characteristic strength. Fig. (2.13) shows a detail in the application of the bonding of the CFRP high modulus sheet. Finally, they concluded that due to its great performance enhancement characteristics, CFRP, for the retrofitting of steel bridges offers great potential with its convenience in design and application.

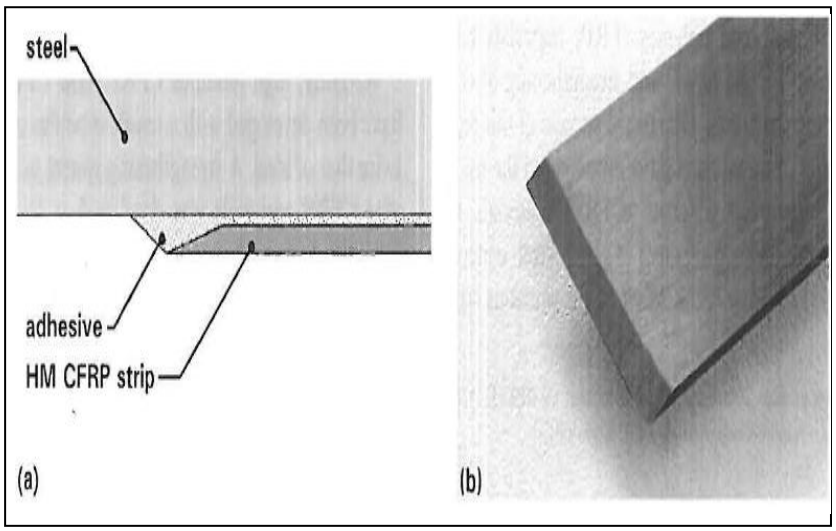

Figure 2.13 CFRP bonding application [94]

3

BEHAVIOR OF FATIGUE CRACK AT THE RIB TO RIB BUTT WELDED CONNECTIONS IN ORTHOTROPIC STEEL DECKS

3.1 Introduction

Rib-to-rib (RR) butt-welded connections are one of the most probable locations for encountering fatigue failure in OSDs, and fatigue cracks related to these locations have been observed in existing OSD bridges. Due to dynamic factors in their service life bridges with an orthotropic steel deck (OSD) are prone to fatigue cracking and failure. The present chapter presents the studies concerning the cases which use (RR) butt-welded connections are limited in the literature. In this study, a cyclic loading experiment is carried out for the investigation of the fatigue life and crack propagation characteristics of butt-welded connections. A static numerical simulation was performed, and the experimental setup was verified with strain gage measurements at the beginning of the tests. Failure modes and stiffness curves were obtained. Crack growth characteristics are observed as provided by dye-penetrant and dynamic stiffness crack detection methods. Crack lengths against the number of cycles were obtained and failure cycles were recorded for construction of the fatigue strength (S-N) Curves as given in AASHTO (2007). Cracked specimens performed in E' category while the control specimen showed infinite fatigue life. Also, it is seen that the dye-penetrant method is more efficient than the dynamic stiffness detection method.

3.2 Experimental Set up with Numerical Verification

The trapezoidal longitudinal rib examined in this study is illustrated in Fig. (3.1). The cross-sections of the rib studied in this case were taken similar to that of existing ribs (Fig. 1.1) used in the Fatih Sultan Mehmet (FSM) Bridge in Istanbul, Brownjohn, Dumanoglu and Severn [95]. The connected rib part is 1500 mm long and has a depth of 256 mm. The deck plate is 400 mm wide and its thickness is t_d =12 mm. The rib has a trapezoidal section as shown in Fig. (3.1) with a plate thickness of t_r =6 mm. Two 675 mm main ribs are welded and connected with a 140 mm central rib. The arc curvature radius of each rib measured 25 mm. The part is supported from the edges and loaded in the middle of the span as in a three-point bending formation.

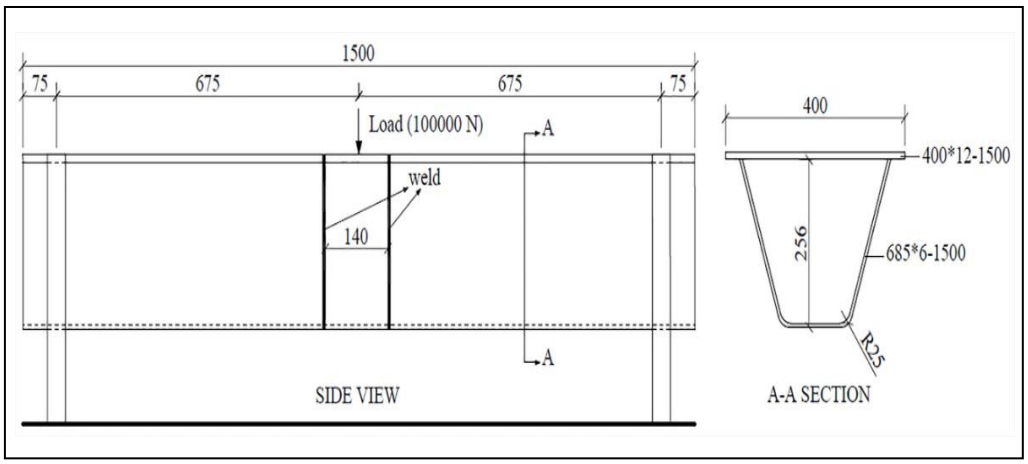

Figure 3.1 Trapezoidal longitudinal rib details (dimensions in mm)

According to the drawing in Fig. (3.1), in the experiment, six full-scale (RR) butt-welded connections were built. Specimens are formed with a deck plate, two trapezoidal ribs, and a connecting rib as details were given. The legs of the ribs were connected to the deck plate using PJP weld, while complete joint penetration (CJP) was applied at the RR connection edges. This was carried out using carbon dioxide gas arc welding, in complete accordance with the American National Standard Welding Code [96]. The details of a typical specimen are illustrated in Fig. (3.2).

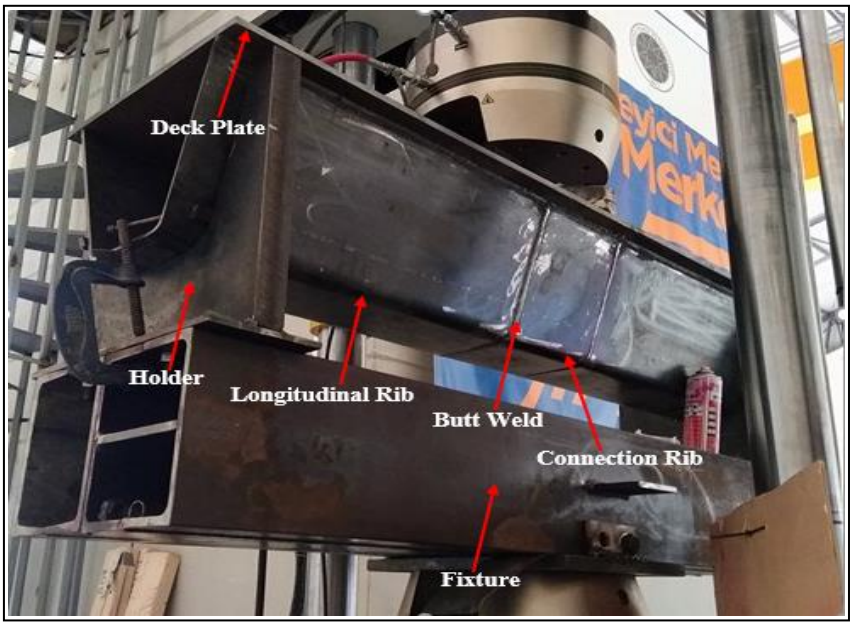

Figure 3.2 Experimental specimen details

3.3 Test Rig

Prior to testing, the longitudinal rib and deck plate were horizontally erected and locked onto the foundation "fixture" using fastening holders. A simply supported beam arrangement is devised. Each holder sat on the longitudinal fixture at the plate (which was 400 mm in length, 150 mm in width, and 50 mm thick) and welded to the holder and fastened to the fixture with rivets to prevent any potential transverse movement in the rigid body of the specimen while the cyclic loading is occurring, as illustrated in Fig. (3.2). The fixture was 1,500 mm in length, 360 mm in width and 240 mm in height. The specimens were tested experimentally following two methods, namely static calibration, and dynamic fatigue tests. A model 8803 Instron test machine conducted the work.

3.4 Set up Verification

3.4.1 Strain Gage Measurements

Five strain gages were attached to the control specimen from the rib bottom side in the longitudinal direction in order to measure the strains near the (RR) butt-welded connections, as illustrated in Fig. (3.3). The first step (considered to be the most important step in strain gage installation) was surface preparation, which was necessary to produce a chemically clean surface with appropriate roughness,

alkalinity, and layout lines. The surface preparation was performed in accordance with the Vishay (2009) Micro-Measurements Application Note B-129-8 [97]. A static load was successfully applied to the specimen. While the static test was being performed, specimens were loaded within the elastic range monotonically and load was raised to its maximum value in a step-wise manner. A load of 100,000 N was applied at the center of the specimen and strain values were obtained at each gage location.

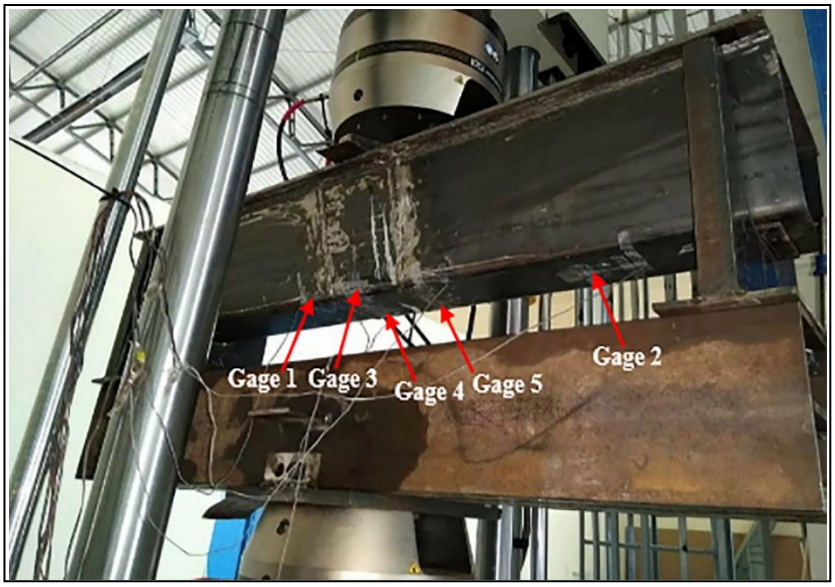

Figure 3.3 Gage installation in the field

3.4.2 Material Properties and FE Modeling of Ribs

All of the plates used to manufacture the specimens were S235 steel material. Following static calibration and dynamic fatigue tests, tensile testing coupons were cut from the web (rib steel plates) and flange (deck steel plates) of specimen 2. The rib coupons (RC1 through RC3) had a 6 mm test thickness, while the deck coupons (DC1 through DC3) had a 12 mm test thickness, and the tests performed in accordance with ASTM E8/E8M (2009) [98]. The measured material properties are shown in Table 3.1, which indicates the modulus of elasticity (E), yield stress (σ_y), and ultimate stress (σ_u). The test was conducted using an Instron machine, as illustrated in Fig. (3.4).

Table 3.1 Tensile coupon test results

Coupon No	Modulus of Elasticity [MPa]	Yield Stress [MPa]	Ultimate Stress [MPa]
RC-01	192,679	268.28	392.53
RC-02	190,652	269.72	390.97
RC-03	201,607	294.34	397.34
Average:	194,979	277.45	393.61
DC-01	199,054	275.88	413.76
DC-02	197,896	291.31	440.70
DC-03	202,573	301.58	428.40
Average:	199,841	289.59	427.62

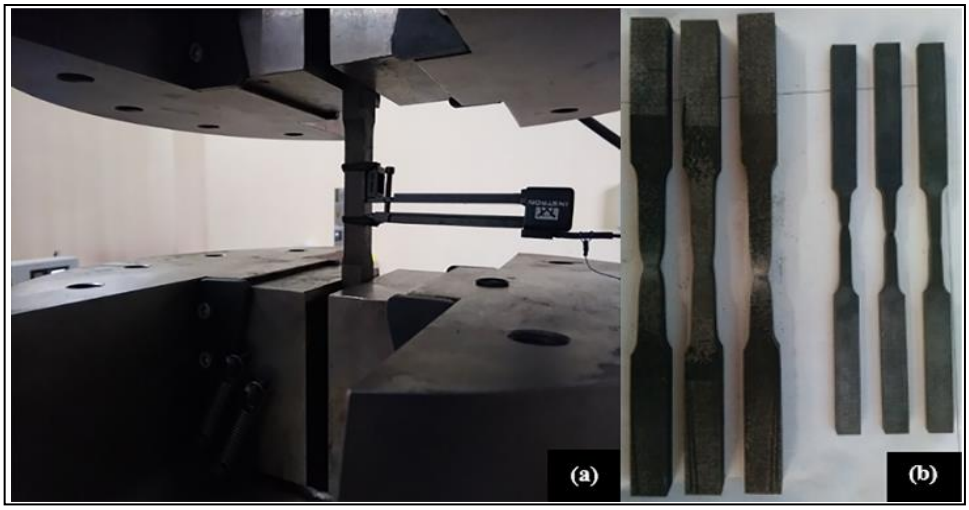

Figure 3.4 (a) Coupons while testing, and (b) coupons geometry following test

In order to verify the experimental set up before commencing to execute a cyclic test, the rig was modeled via the finite element analysis program ABAQUS [99]. The longitudinal ribs, deck plate welds, and connection ribs were defined using S235 steel material with the elastic-plastic material model (metal plasticity). The Young's modulus is taken as 195 GPa and 200 GPa for ribs and deck plates respectively. A

Poisson's ratio of 0.3 is used for the whole model. A bilinear curve is used for the fit of the elasto-plastic material model to the experimental yield stress and ultimate stress. The average values for the yield and ultimate stresses are used from Table 1. The load is applied with a rigid cylindrical rod since the loading apparatus of the machine is assumed to relatively rigid with respect to the other structural members. All of the materials in the FE model were defined using a solid homogeneous material type. The boundary conditions of the longitudinal rib and deck plate at each end location were constrained with respect to rigid body displacements but are allowed to rotate freely.

The connections between the longitudinal rib and deck plate were modeled using a tie constraint in the analysis. Also, the interaction among the connection rib, weld, and longitudinal rib was selected as a tie constraint to provide the full connection. Hard contact interaction and friction were defined between the loading rod and the deck plate. The holders and the support assembly are assumed to be rigid and only the holder parts are modeled with discrete rigid elements as can be seen in Fig. (3.5).

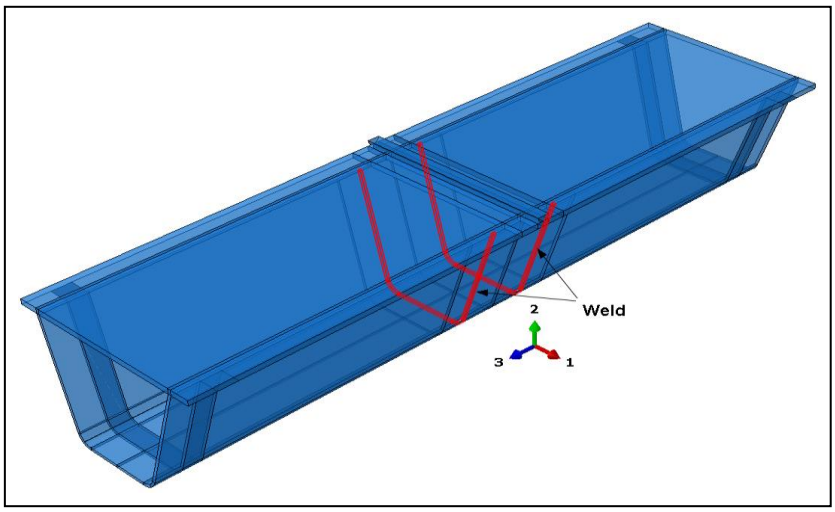

Figure 3.5 Trapezoidal longitudinal rib with connection region

Metal plasticity is used in the analysis despite the load level was not over the elastic range. Thus yielding and other nonlinear effects were of no interest Håkansson [100] Except for the target connections which include the connections rib, welds, and a small part of the longitudinal ribs in the middle of the model, the mesh size for the entire model was approximately 25 mm. The mesh size in connection regions was selected at 5 mm. Eight-node linear brick element (C3D8R) defined for the

whole mesh element type, as illustrated in Fig. (3.6). An axial load of 100,000 N of concentrated force was applied to the center of the deck plate. This is considered the maximum load of one wheel when a truck is fully loaded with a dynamic amplification factor.

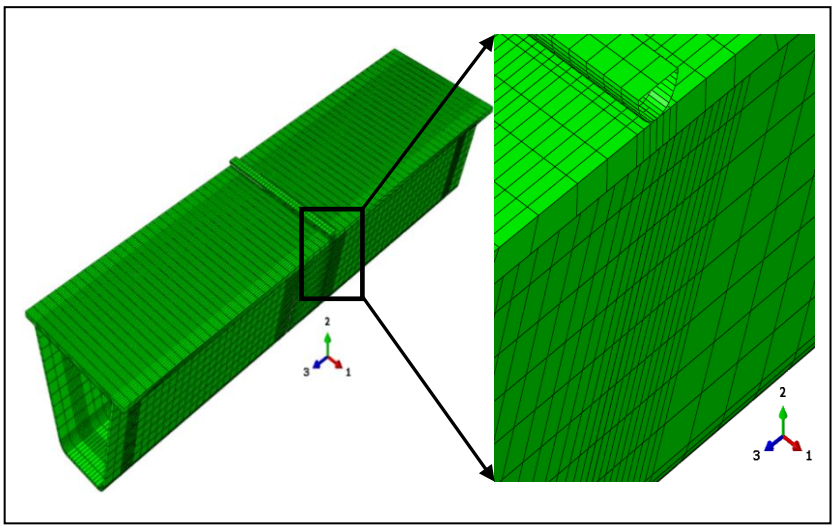

Figure 3.6 Finite element assembly mesh with target connections

3.4.3 Numerical Results and Discussion

As the expected bottom path of the rib was subjected to the maximum principal stresses, deflection, and deformations compared to the other system components when the load is applied in the middle of the rib. It is also seen that the weld stresses around the connection rib were concentrated, and the connection region could be susceptible to fatigue type cracking. The stresses on the trapezoidal ribs exhibited a single-sign stress distribution, particularly the compression region along the force direction. Moreover, the maximum deformation locations were close to the bottom side of the trapezoidal rib, as indicated in Fig. (3.7). This result reveals the places where the cracks most probably began to grow, as illustrated in Fig. (1.1).

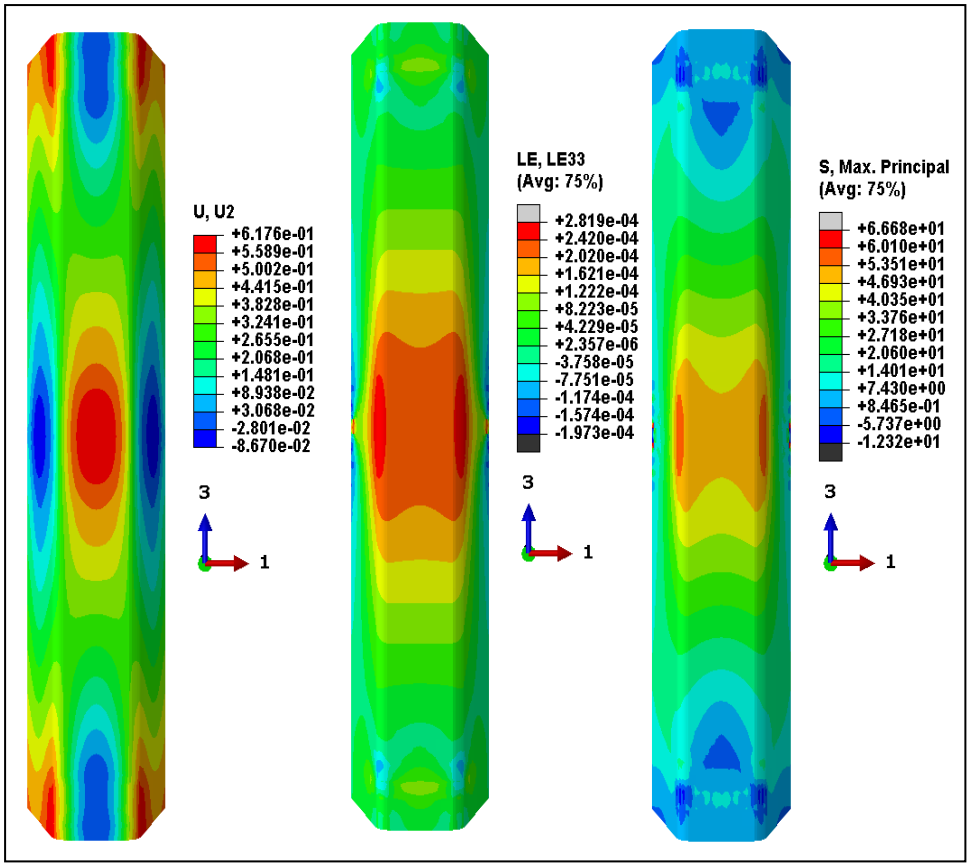

Figure 3.7 Vertical deflection (U2 - mm), longitudinal strain (LE33 - mm/mm), and maximum principal stress (MPa) contours

The main point of the numerical approach in this study was to determine the strain values in the same strain gage positions that were fixed on the specimen in the experimental static loading test so that set up can be verified. The three different longitudinal paths that were examined numerically are illustrated in Fig. (3.8). These paths were taken along the bottom of the model, which considered the most critical locations and would be exposed to the greatest deformations. Path 1 passed through Strain Gages 1 and 3, Path 2 passed through Strain Gage 2, and Path 3 passed through Strain Gages 4 and 5. The details for these gages are displayed in Table 3.2.

Table 3.2 Strain gage locations in the model

Gage No	Approximate Position
Gage 1	5 mm from weld joints
Gage 2	300 mm from weld joints
Gage 3	Center of model 750 mm from beginning of model edge
Gage 4	Center of model 750 mm from beginning of model edge
Gage 5	5 mm from weld joints

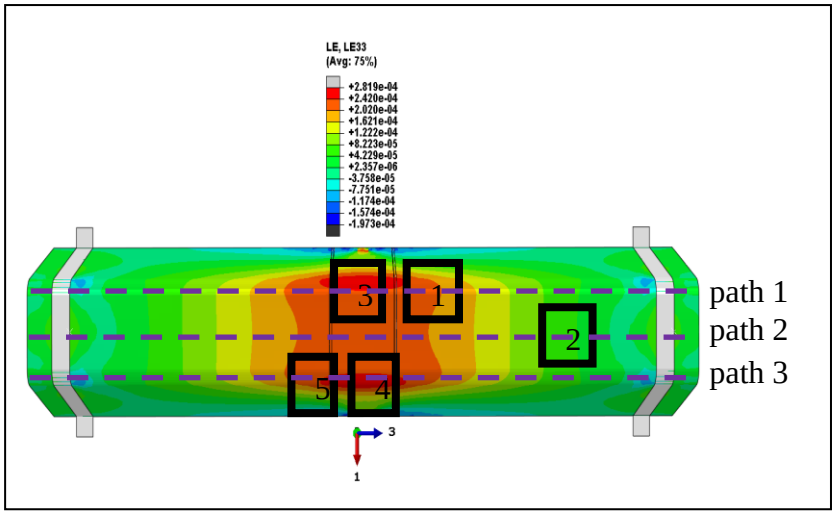

Figure 3.8 Location of strain gages

As can be seen from Fig. (3.9) strain data correlates well with the numerical model and all assumptions made for rigid parts can be considered realistic. This also shows that the holder fixture does not have any effects on the experiment. Thus cyclic test indeed will reveal true fatigue characteristics of the RR butt connection.

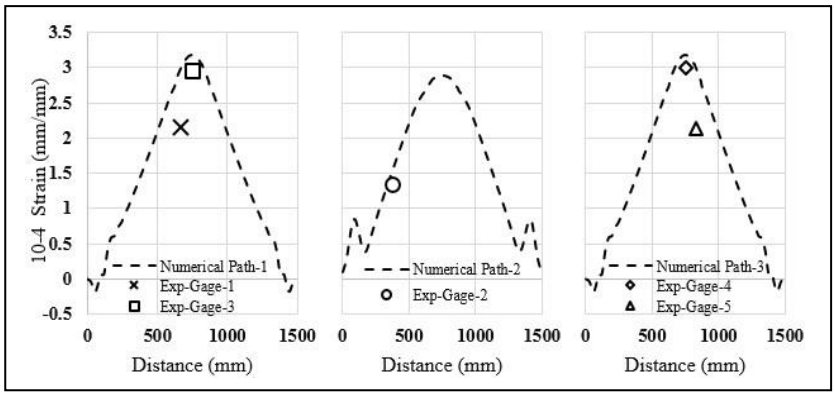

Figure 3.9 Comparison of strain gage values of numerical and experimental approaches along longitudinal paths

3.5 Experimental Fatigue Investigation

3.5.1 Fatigue Data Measurement

Following the completion of the static calibration load tests, all data were analyzed, and it was decided to conduct dynamic fatigue with test parameters. The experimental fatigue loading formed a sinusoidal shape with only a compression part. Cyclic fatigue loads were applied for all specimens so that the minimum load was one-tenth of the maximum ($R = P_{min}/P_{max} = 0.1$)and the maximum applied load was 100,000 N. a 2 Hz of constant cyclic loading frequency was selected in the sinusoidal form under load control. As soon as the specified criteria for failure of vertical rigidity were achieved, the fatigue tests were terminated. The specimens were tested using these parameters until failure occurred. Crack length measurements were made by eye and recorded approximately at every 5,000 cycles for each specimen, and the test was run continuously. The important aspect of the fatigue analysis was to determine the extent to which the crack grew under each cycle of applied loading and counting the number of cycles that would lead to failure that could be carried out Liao [101].

3.5.2 Observations of Fatigue Failure

3.5.2.1 Identification of Crack Propagation

Fatigue cracks at the (RR) butt-welded connections were mainly caused by out-of-plane bending, which is the mode I loading. The failure modes of the five trapezoidal rib specimens with initial cracks were similar, represented by an opening mode at the bottom of the ribs and indicated by local displacements that are symmetric with respect to the x-y and x-z planes, and the two fracture surfaces were displaced perpendicular to one another in opposite directions Barsom and Rolfe [102]. Fig. (3.10) illustrates the typical failure modes of the five specimens with initial cracks, where fatigue cracks were all observed on the butt-welded connections, generally near to the center of the rib arc.

Figure 3.10 Failure mode at the bottom of the rib

The beginning of the crack and the process of its growth will occur in three phases:

Phase I: An initial crack with a length of 50 mm and a depth of 6 mm is manually created at the central arc of the butt weld on one side of the connection from the bottom of the rib for the five trapezoidal specimens by using a cutting tool, as shown in Fig. (3.11). The main reason for implementing the initial crack is to reduce the dynamic fatigue test time. It had been found that the control specimen reached 1.2 million cycles, which is more than ten consecutive days of continuous examination without any noticeable cracks, following which the test was stopped. The secondary reason is that it may be easier to investigate the propagation characteristics of possible rib cracks. Therefore, the determination of cracking became more accurate and cracks could be observed with the naked eye. Because the study focused on the areas around the initial crack tips, which were manually arranged, by using either the dye-penetrant or dynamic stiffness crack detection method, both of which were implemented in this study. The crack initiation locations are consistent with the large stress concentration that was identified from the static calibration test and computer simulations.

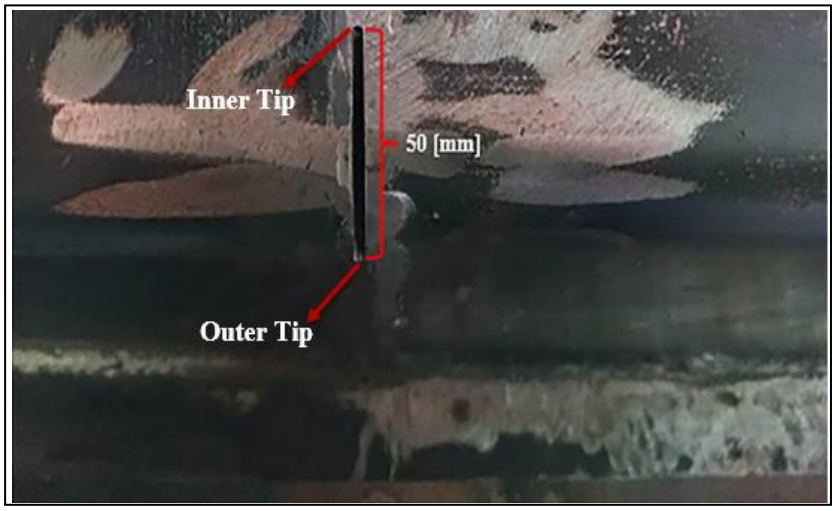

Figure 3.11 Initial crack at transverse butt-welded connections

Phase II: As the cyclic loading continued, the crack gradually propagated, up to the outer tip proximal to the terminating point of the rib wall, and finally reached the rib edge. The paths of the crack growth at all times continued along with the toes of the butt weld on the rib. Relative to other states, the rate of crack growth during this phase was low. Also, crack propagate faster in the lower direction. During this propagation phase, as their opening widths gradually enlarged, the cracks had become increasingly visible to the naked eye when using dye-penetrant crack detection, as illustrated in Fig. (3.12). The test was monitored and the specimen was inspected for possible fatigue cracking at regular intervals. In the dye penetrant method, the procedure recommendations were firstly achieved by spraying BT68 spray onto the specimen on the parts where cracks were expected to occur, the function of which is to penetrate inside the cracks rapidly. Repeated spraying BT69 served to clean only the surface part that was sprayed with BT68, following which it was wiped dry with a cotton cloth. The use of these two sprays made the cracks visible to the naked eye, and the method was applied without stopping the test. This phase concluded upon the onset of cracks appearing on the upper surface of connections, and the displacements of the maximum crack openings on the butt-welded connection of the rib bottom surface were found to be up to 1mm.

Figure 3.12 Detection of crack propagation using a dye-penetrant method

Phase III: The lower tip finally propagated through the arc of the rib and passed this section. Meanwhile, the upper crack tip accelerated. The outer tip of the crack, which ran through the thickness of the weld, was extended in the vertical direction perpendicular to the loading axis (towards the inner tip) step by step and increasing crack parts ran through the weld. Consequently, parallel to the weld joints, a visible longitudinal crack formed on the wall and bottom surface of the rib plate, and the measured opening widths were up to 5 mm, as seen in Fig. (3.13).

Figure 3.13 Extended fatigue crack thickness along butt-welded connections

Furthermore, the inner tip of the crack continued its propagation along its initial path to the un-cracked edge of the rib plate. The rate of the growth of the crack during this phase was noticeably higher than previous instances, as the tips of the crack were less constrained than previously. This final phase finished upon the specimen having completely cracked and all the connections failed when the rib plates tore completely.

3.5.2.2 Fatigue Crack Growth with Dye-Penetrant Method

Variability in the length of the cracks, as can be seen on the rib bottom surfaces and butt-welded connections during the test, is illustrated in Figs. (3.12) and (3.13). It is evident that the cracks continued to increase in vertical length from start until the end of the test, and there were no obvious distinguishing boundaries between the above phases. Moreover, the rate of the growth in crack length, curve slopes in Fig. (3.14) constantly increased while the test was occurring, implying that the stress intensity factors at the crack tips increased with an increase in the length of the crack, Fu et al. [103]. Normally in the early phase, nearly linear increments in crack length were observed with the number of cycles upper tip reaches to the deck. The crack growth rate afterward started improving with the continuation of the cyclic loading.

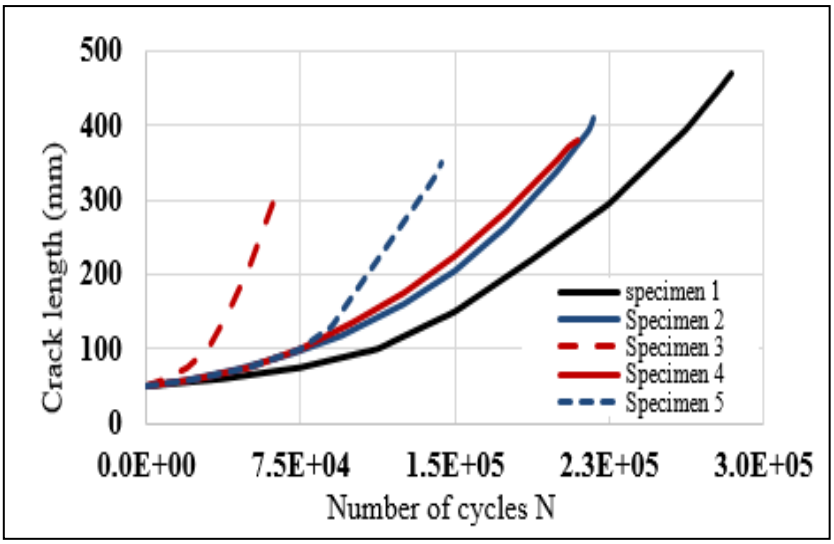

Figure 3.14 Crack length versus number of cycles (R = 0.1)

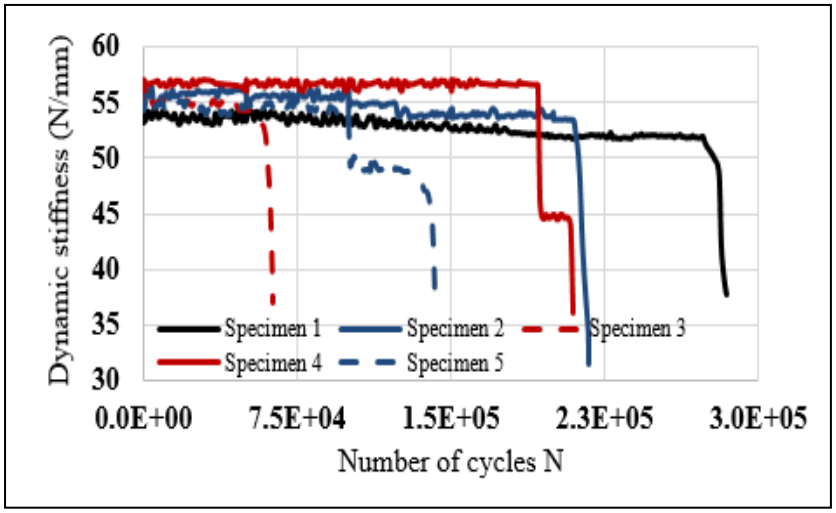

Figure 3.15 Dynamic stiffness versus cycles for cracked specimens

At a certain number of cycles (7,500), the crack began to propagate when it was 2 mm in length. Crack location investigations were performed using the dye-penetrant method, as mentioned previously, following which the cracks were monitored and registered manually versus every 5,000 cycles until the specimen was exposed to fatigue issues. The crack growth began from both surface edges of the initial crack, where the maximum bending stress was generated and penetrated to the center of the weld thickness. Once the crack had begun to penetrate to the weld thickness middle, the curve of crack growth at the center of the weld connections was almost parallel to the weld stretch shape, indicating that the growth rates of the crack at the center and weld stretch shape were nearly identical. The measured propagation of the crack lengths and cycle numbers of the cracks for each specimen are listed in Table 3.3.

Table 3.3 Propagation crack length versus number of cycles to failure

No. of Specimen	No. of Cycles to Failure	Propagation Crack Length to Failure [mm]
Specimen 1	284,555	420
Specimen 2	217,260	360
Specimen 3	63,288	260
Specimen 4	209,529	330
Specimen 5	143,467	300
Control Specimen	Runout	No crack

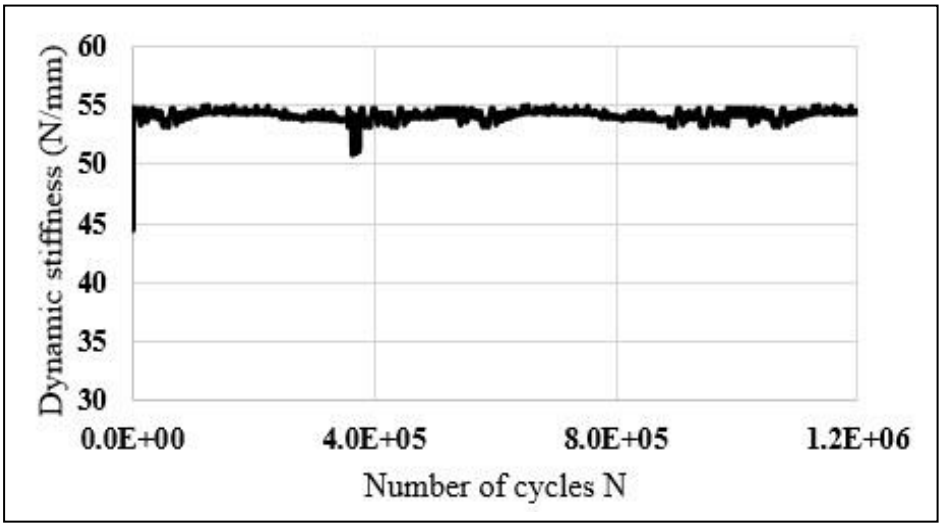

Figure 3.16 Dynamic stiffness versus cycles for the control specimen

3.5.2.3 Determination of Crack Propagation with Dynamic Stiffness Data

The instantaneous or dynamic stiffness of the specimens was a parameter inferred from direct test measurements. Dynamic stiffness, in turn, is defined as the ratio of the load range to the displacement range over a cycle thus:

$$K_{dyn} = \Delta_p/\Delta_y \tag{3.1}$$

Where Δ_p is the change in the applied load per fatigue cycle and Δ_y is the change in displacement per cycle. The change in dynamic stiffness basically allowed to monitor the response with increasing cycle count. This change stemmed from the fact that crack is initiated and propagating in the model. As discussed in Section 3.5.2.2, the fatigue crack growth in a specimen was expected to cause a decrease in dynamic stiffness, as recorded by the controller. The data used to calculate the dynamic stiffness were measured by the Instron testing machine and recorded by the controller. All data were plotted using an Excel spreadsheet. In order to display the subtle changes in dynamic stiffness as effectively as possible, each plot indicates the narrowest dynamic stiffness range that the data recorded for that specimen would allow. Dynamic stiffness generally began to decrease at a certain point following the initiation of crack propagation for specimens with initial cracks. The decrease in the dynamic stiffness of a specimen did not coincide perfectly with the visual crack detection. In general, the dynamic stiffness did not begin to decrease until approximately 7500 cycles after crack propagation, as detected using the dye penetrant. Changes in dynamic stiffness recorded for the specimens that developed fatigue cracks appeared to predict the fatigue cracking onset accurately. However, when the testing specimens were under 60.772 MPa of a nominal weld toe stress, problems with this crack detection method became apparent.

A decrease in dynamic stiffness was demonstrated to be a direct indication of fatigue crack growth. The fatigue crack propagation could be predicted by recording and monitoring changes in the dynamic stiffness of a specimen throughout the fatigue test duration of a fatigue test. Moreover, Fig. (3.15) presents the stiffness values versus every cycle during cycling load until fatigue. It was observed throughout the cycling load that the change in the stiffness value was small and almost a straight line, but the value suddenly changed downwards, which means that the specimens with initial

cracks failed, Kaan et al. [104]. However, as seen in Fig. (3.16), the stiffness line for the control specimen still does not exhibit any slope change, indicating that no noticeable cracks appeared during the test.

3.5.2.4 Fatigue Life

As failure was predicted to occur at the weld connections, all specimens were tested at a nominal stress range of 60.772 MPa, taken at the center of the butt-welded connections from the rib bottom side with 100,000 N of applied loading. Where the stress range was too small, the maximum stress state was taken from the actual state and not selected as being higher. Each of the specimens with initial cracks exhibited markedly shorter fatigue lives than the control specimen that was tested within the same stress range. Fig. (3.17) presents this effect and shows how it indicates the number of cycles accumulated for each specimen in the form of an S–N diagram with the AASHTO (2007) [105] fatigue design curves. The S–N curve is a relation between the stress range under constant amplitude loading and the number of cycles until fracture, Alemdar et al. [106]. Specimens with initial cracks underperformed the AASHTO Category E' fatigue curve by a significant margin, which may be explained by the lowest fatigue strength quality of the welds alone at the bottom of the ribs.

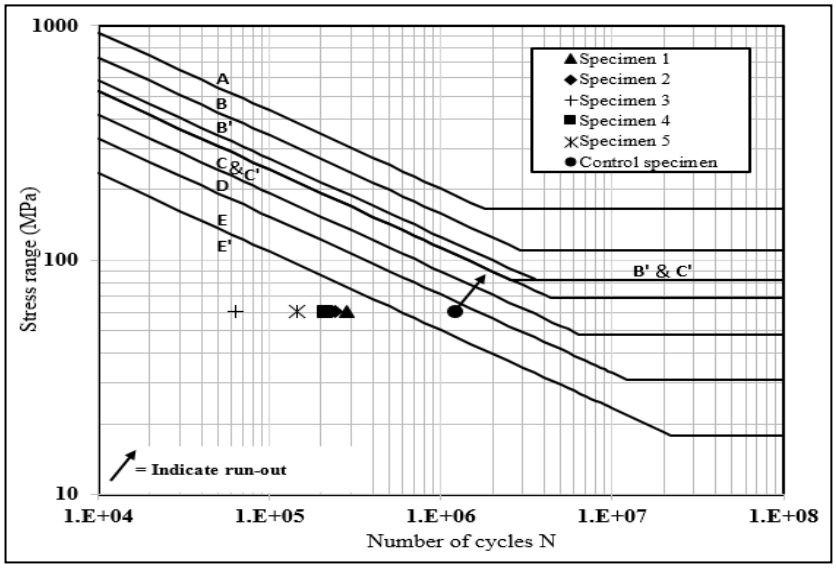

Figure 3.17 S-N diagram illustrating results of testing of six trapezoidal ribs in AASHTO (2007) fatigue curves

3.6 Conclusions Experimental Work

The conclusions below were established based on experimental tests.

- The principal stresses on the bottom side of the trapezoidal rib, particularly at the connecting region, were higher than in other parts of the structural component; thus, fatigue cracks appeared from the bottom of the ribs.

- The maximum deformations on the trapezoidal rib cross-section occurred closer to the bottom side of the rib. This demonstrates that the rib wall exhibits out-of-plane bending through the transverse directions. Following the crack appearance, they easily propagate as a result of out-of-plane bending.

- All specimens with initial cracks developed fatigue cracks at the center of the transverse butt-welded connections where the initial crack developed. In these specimens, the cracks propagated at either the center or one end of the initial transverse weld toe and extended into the web in an orthogonal direction to the longitudinal axis of the specimens. Once a crack had propagated in these specimens, the crack growth rate increased exponentially, until yielding of the reduced web section resulted in failure.

- During fatigue testing, it was concluded that the most effective method of detecting the onset of fatigue crack propagation was the modified dye-penetrant method. Another less effective method that was employed to detect the onset of fatigue crack propagation was the dynamic stiffness method.

- By comparing the lives of fatigue specimens, it was concluded that specimens tested at the center of the transverse butt-welded connections from the bottom side of the trapezoidal rib provided an effective means of predicting the fatigue life. The fatigue life of specimens with initial cracks tested at a nominal weld toe stress range of 60.772 MPa achieved a level at or below the AASHTO Category E' detail, while the control specimen stayed on or above the expected behavior for the AASHTO Category E.

- The numerical analysis and experimental test data exhibited very strong agreement. Furthermore, although the stress range was low, the fatigue cracks propagated easily.

- One apparent difference between actual situations and the experimental results is that the fatigue cracks that propagated following the weld direction reached the deck plate, while in actual situations, fatigue cracks originating from the weld direction maybe one-third of the weld height. The reason for this may be that in real situations, the rib continues, whereas, in the experimental specimens, it is only 1500 mm in length.

- Two methods of crack detection revealed quite similar characteristics in their own terms. For example, crack size- number of cycles graph of Dye-Penetrant method in Fig. (3.14) shows a sudden jump in crack growth rate around 105 cycles whereas crack stiffness-number of cycles graph of dynamic crack stiffness detection method in Fig. (3.15) shows a sudden loss of stiffness at the same number of cycles (105).

4

AN EXPERIMENTAL STUDY ON THE REPAIRMENT OF RIB TO RIB BUTT WELDED CONNECTION CRACKS IN ORTHOTROPIC STEEL DECKS VIA CFRP LAYERS AND BOLTED STEEL PLATES

4.1 Introduction

Orthotropic steel decks (OSDs) made up most of the steel bridges worldwide. They are mainly suffering from fatigue prone connections, corrosion and maintenance issues. Reports indicate that 88000 bridges in US and Canada are suffering from some form of structural deficiency and over 82000 bridges are functionally obsolete [107]. As the traffic loads tend to increase most of these steel bridges require urgent attention. They should be replaced completely or to be retrofitted according to the standards which is a far less costly option. Retrofitting has also some other major advantages in terms of time considerations and service interruptions. Considering this serious safety issues, US declared Transportation Equity Act in motion in order to raise funding for the ever increasing number of structurally deficit bridges.

One of the most common method for the retfrofitting of the bridges consist of increasing size of the sections via adding material. A typical application includes welding external steel plates. Most of the time welding introduces weak spots or defects which can be prone to the fatigue [108]. However, several disadvantages such as corrosion problems, difficulty in handling and performance, also fatigue prone locations in (OSDs) bring problems that have induced to the research for new methods. It ıs obvious that OSDs should be made stiffer so that stress levels at weldments decrease and their fatigue life increase.

It is obvious to utilize highly resistant materials in repairment, for example nonmetallic materials such as carbon-fiber-reinforced polymers layers (CFRP).

On the other hand, mechanical details such as bolted steel plates (BSP), which have better fatigue life, and take less time in implementing and not highly-priced.

Advanced structural properties of CFRP materials make them quite attractive for the repairment of steel structures. Most commonly available CFRP materials are made of high-strength filaments with tensile strength typically over 2 GPa, such as carbon placed in a polymeric resin matrix.

Usage of CFRP in concrete structures proved to be effective. This fact has been shown for various repairment scenarios. As a result CFRP becomes much more widely used in concrete structure. In order to increase structural performance in tersm of higher load capacity and increased ductility CFRP sheets and layers are applied on to RC members. The US Department of Transportation (USDOT) and Federal Highway Administration (FHWA) have supported multiple projects which resulted in design codes for bridge repairment.

CFRP to metal type bonds firstly used in mechanical engineering. CFRP layers have been used for repairing metallic airfoils [109, 110]. Also CFRP showed promising achievements for the repairment of marine structures [111, 112]. In case civil engineering, initial applications started with repairment of steel girders w/out weld, corrosion and finally against fatigue type cracks in welds.

CFRP has various advantages over repairment with welding extra steel plates. One of most important is the cost effectiveness of CFRP due to labor, material and service interruptions. Also its ease of application due to light-weight is very important. Another factor that makes CFRP advantageous is, as long as a proper bond forms, it has more mechanical performance with respect to steel plates due to its higher tensile strength.

However, orthotropic steel decks (OSDs) are also widely used in movable bridges. As explained earlier dead-weight of the selected repairment becomes a serious constraint in selection of the appropriate method. This study investigates the effectiveness of repairing fatigue damage at the (RRBW) connections of (OSDs) with adhesively bonded carbon fiber reinforced polymer layers (CFRP) and bolted steel plates (BSP) experimentally. Both retrofitting methods were used to stiffen (RR) butt-welded connections in the existing trapezoidal longitudinal ribs over cracks. In

the bolted steel plates method, the steel plates with a thickness of 10 mm are bolted to the existing longitudinal ribs by bolts. This method has been applied recently to repair the orthotropic fatigue cracks on the Fatih Sultan Mehmet (FSM) Bridge in Istanbul [47], as illustrated in Fig. (4.1).

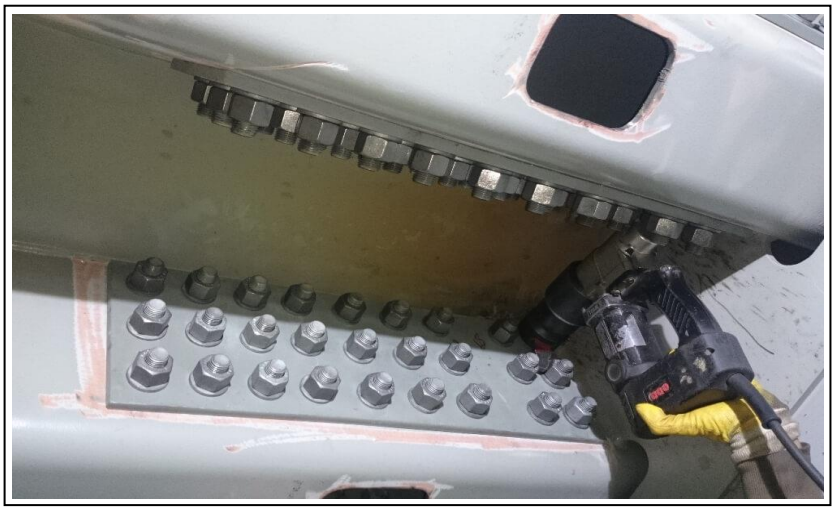

Figure 4.1 Bolted steel plates method [47]

In the bonded CFRP layers method, the five layers of CFRP with the total thickness of 3 mm are bonded to the existing damaged longitudinal ribs with an epoxy resin and considered one of the new repairment methods to repair the damage caused by fatigue cracks at the (RR) butt-welded connections of orthotropic steel decks (OSDs).

From the extensive literature review, it is understood that very limited research work has been conducted in this area especially for the retrofitting of rib-to-rib butt-welded connections of orthotropic steel decks (OSDs) due to fatigue damage. At present, there is a lack of suitable repair for fatigue damage at the rib to-rib (RR) butt-welded connections of orthotropic steel decks (OSDs) by using the bolted steel plates (BSP) method and the bonded CFRP layers method. This study aims to address the fatigue life and dynamic stiffness behavior of the repaired trapezoidal longitudinal ribs on orthotropic steel bridge decks in a controlled fashion for (RR) butt-welded connections to avoid any extra fatigue problems on the repaired trapezoidal longitudinal ribs of OSDs. Each repairing method was applied to the damaged ribs in the longitudinal direction allows for increasing the bending stiffness of the repair. Both methods are light-weight (between 2 and 13 kg/m2), and especially useful for movable bridge applications. The aim of applying the repair

is to reduce the stress levels in the (RRBW) connections and extend the fatigue life of OSDs under cyclic loading. Experimental tests have been conducted to investigate the fatigue behavior of the bolted steel plates (BSP) method and the bonded CFRP layers method by performing fatigue strength (S-N) curves as given in AASHTO (2007) which are potentially useful for the evaluation of fatigue life of repaired specimens. The dynamic stiffness curve should also be studied to investigate the bond efficiency and how well the stiffness of repaired specimens has improved.

Test results showed that as long as the bond between the ribs and the repairment sections are maintained both methods resulted in an insufficient reduction in stress demand and the fatigue life of the RRBW connections was extended from AASHTO fatigue-design Category E' for the unrepaired configuration to the infinite fatigue life range. Also, drastic improvements in the dynamic stiffness curves were observed. Overall, the performance of these two lightweight methods for repairing movable OSDs proved to be efficient and durable. Thus assessment of value in the design of the repairment of (RR) butt-welded connections in OSDs has been established.

4.2 Objective

The overall objective of the research described in this chapter was to determine the effectiveness of bonded CFRP layers method and bolted steel plates (BSP) method to repair existing fatigue damage at the rib-to-rib (RR) butt-welded connections of OSDs under cyclic fatigue loading, and to restore the full cross-sectional properties of the cracked trapezoidal longitudinal ribs to its original strength. The significance of these two lightweight methods is that it is simpler to implement and more cost-effective than existing retrofit measures. The performance of the repairment methods was investigated experimentally using 6 mm trapezoidal longitudinal ribs assemblies subjected to cyclic loading.

4.3 Retrofitting Procedures

The experimental work focused on applying two lightweight methods to develop the retrofitting procedure of the damaged trapezoidal longitudinal ribs depending on the combination of laboratory trials, past experience, literature review, recommendations from CFRP manufactures, and implementation procedures of bolted steel plates (BSP) method. Experimental repair methods then performed on four specimens of full-scale trapezoidal longitudinal ribs that were damaged by fatigue cracks at the (RR) butt-welded connections [113], as illustrated in Fig. (3.10) in chapter three. Two of the four fatigue crack-induced full-scale trapezoidal longitudinal ribs were repaired by adding five layers of CFRP with an epoxy resin and the remaining two were repaired by adding steel plates with bolts and subjected to cyclic loading.

4.3.1 Retrofitting Method Using Bonded CFRP Layers

Carbon fiber reinforced polymer (CFRP) layers method is being increasingly used in steel structures and defined as composite materials. In this case, the composite consists of two parts: a matrix and reinforcement fibers. In CFRP, the reinforcement is carbon fibers, which provides the strength, stiffness, and load-carrying capacity. The matrix is usually a polymer resin, such as epoxy, to bind the reinforcements together [114]. Because CFRP consists of two distinct elements, the material properties depend on these two elements. Therefore, the main properties of CFRP layers depend on the type and orientation (transverse or longitudinal direction) of carbon fibers, the percentage of resin material, and curing conditions. The performance of this technique depends mainly on the quality of the application of the adhesive material which transfers loads between steel plates and CFRP layers. Since the transfer mechanism is mainly affected by surface conditions of the bonded materials to ensure the integrity of the bond proper preparation was required for both surfaces of the damaged ribs and the CFRP layers. Hence, firstly the compression webs and the bottom of the damaged ribs were prepared by using a handheld grinder with abrasive disk to remove any rust, paint or foreign object and also to obtain sufficient roughness for surfaces. Surfaces are then cleaned by acetone and propyl alcohol to obtain clean and chemically active surfaces, as illustrated in

Fig. (4.2). At the same time, the surfaces of CFRP layers were treated by a very fine sandpaper (grit P240) to provide improved bond strength.

Figure 4.2 Preparing the surfaces

Secondly, the application procedure of the CFRP layers started by marking the locations of the CFRP layers on the damaged ribs. CFRP layers with 600 mm longitudinal length were considered centrally to the ribs from the bottom side and both sides of the compression webs simultaneously in order to maintain a robust connection between cracked and un-cracked rib sections. After mixing and applying the epoxy on the CFRP layers and positioning the CFRP layers as explained above, layers are rolled over to extract the excessive epoxy and the air in order to ensure good contact. A total of 8 liters of epoxy was used for two CFRP retrofitted specimens with 5 layers of CFRP each. The care and the attention were given to details at the edges of the CFRP layers. The treatment of edges is crucial to ensure the strong bond as indicated by Bocciarelli et al. [115]. In their experimental study on retrofitting the tensile steel members with CFRP plates, they showed that the debonding of the CFRP plates started in the edge zones of high-stress concentration or the gaps in the case of joints. Also, another analytical study presented by Youssef [116] to predict the linear and nonlinear behavior of steel beams rehabilitated using FRP sheets found that the maximum value of the adhesive shear stress was developing at the edges of the FRP sheets.

Briefly, five layers of CFRP with the total thickness of 3 mm (0.165 mm for each layer without resin) and the dimensions of 600×687 mm were bonded to the damaged

ribs with following the above procedure. The two prepared specimens were cured for one week, as illustrated in Fig. (4.3).

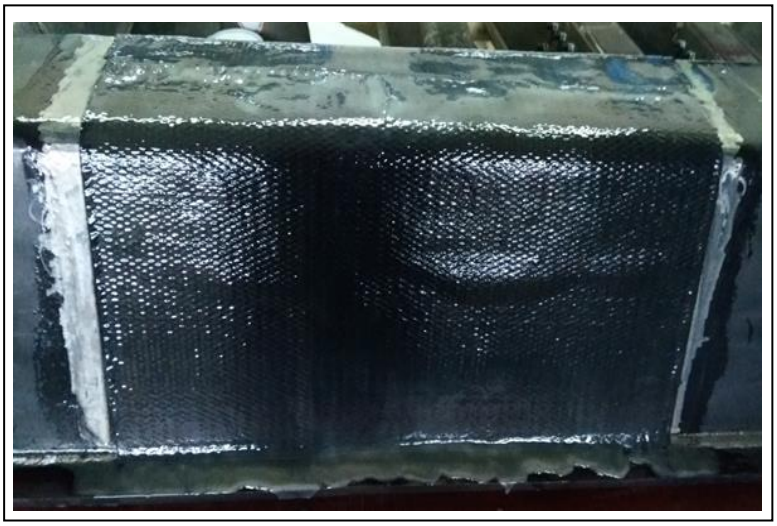

Figure 4.3 Adding the CFRP layers

4.3.2 Retrofitting Method Using Bolted Steel Plates

The philosophy of bolted steel plates (BSP) method to repair fatigue damage is based on adding a cross-sectional area and maintaining a robust connection between un-cracked parts, which in turn reduces stress ranges and restores the full cross-sectional properties of the un-cracked ribs. This technique is particularly useful when full-depth crack forms in (RR) butt-welded connections. In order to increase the overall stiffness steel plates were designed thicker with a value of 10 mm assuming that the webs of the ribs are no longer transferring the loads. Thus the design process is similar to that used for a bolted field splice connection. In this method, the steel plates were bolted to the damaged ribs by the high-strength bolts (type 8.8). The high-strength bolted connection can be considered an AASHTO Category B detail [117]. The width of the steel plates is selected approximately equal to the depth of the trapezoidal ribs and length is selected as 600 mm (same as CFRP) in order to maintain a robust load transfer between un-cracked parts. Thus overall dimensions are 600×250×10 mm (L×W×t). 22 holes with 20 mm diameter each were drilled on plates and the corresponding locations on ribs. The same horizontal and vertical distances of 70 mm between the holes were maintained in accordance with the edge distance requirements per ASTM A325 (2004) [118], as illustrated in Fig. (4.4).

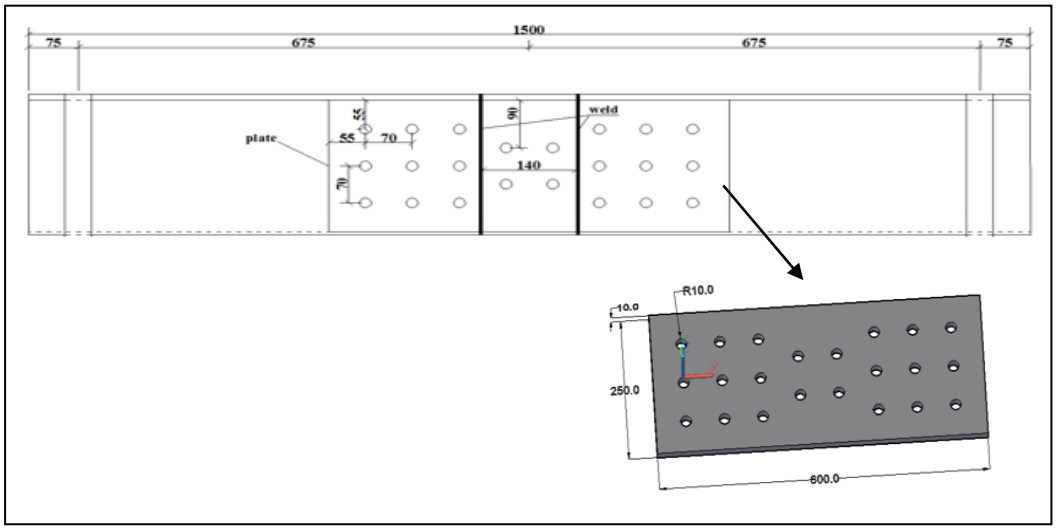

Figure 4.4 The details of the bolted steel plates (BSP) method (dimensions in mm)

After drilling contacting surfaces were cleaned to remove oil, grease, dirt, and cutting fluids to restore the friction between the surfaces. Lastly, all bolts were fastened with snug tighten to make sure that all the surfaces are mated and all bolts are in full as illustrated in Fig. (4.5).

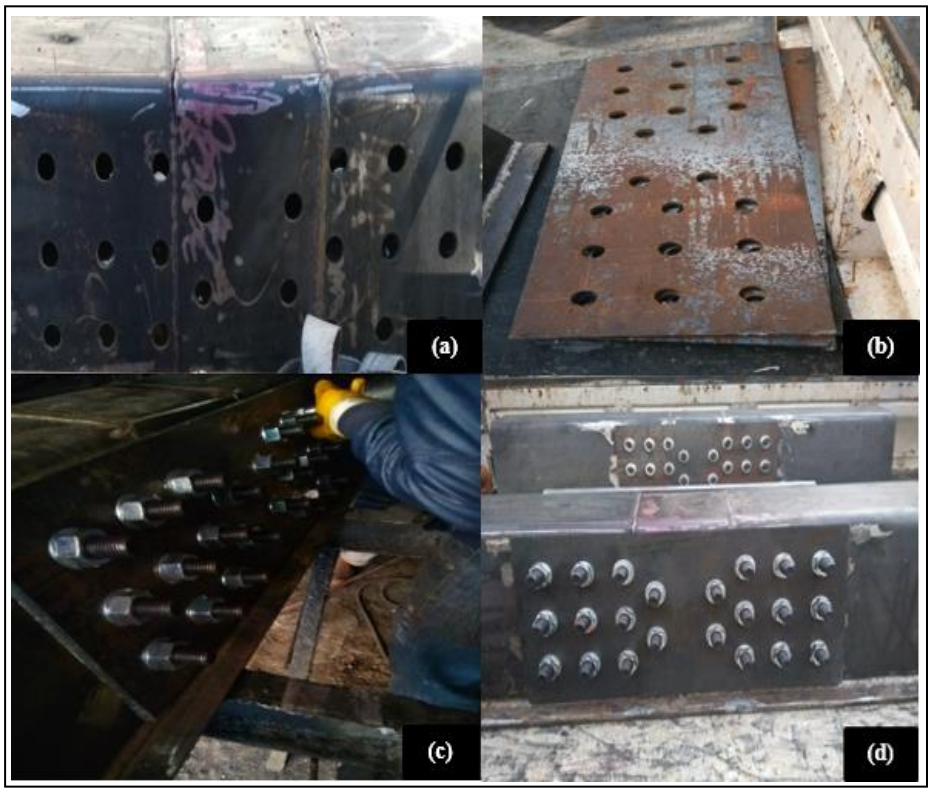

Figure 4.5 (a) Drilling the holes on the damaged ribs wall, (b) drilling the holes on the adding steel plates, (c) fastened the bolts, and (d) bolted steel plates to the damaged ribs wall

4.3.3 Test Rig and Procedure

Prior to testing, the longitudinal rib and deck plate were horizontally erected and fixed by using fastening holders. A simply supported arrangement was used. Each holder is bolted to a rigid base box with a length of 1500 mm which itself also bolted to the testing machine in order to prohibit rigid body motions as can be seen in Fig. (3.2). The specimens were tested experimentally by using the cyclic fatigue-loading test. Cyclic fatigue loads were applied to the mid-section of the deck plate with a rigid cylinder which was attached to the boom of the machine as can be seen in Fig. (4.6). A model 8803 Instron test machine was used. The experimental fatigue loading of the sinusoidal (2 Hz) form only with the compression part was utilized. The frequency was kept constant under load control condition. The minimum load was one-tenth of the maximum ($R=P_{min}/P_{max}=0.1$) and the maximum load was 100,000 N. This is assumed as the maximum load (with dynamic amplification factor) of one wheel when a truck is fully loaded.

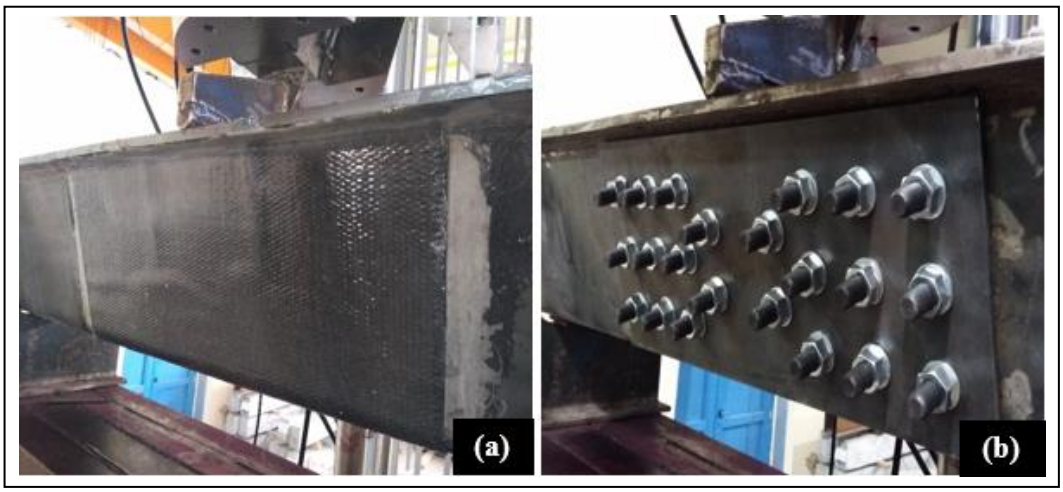

Figure 4.6 An axial load applied to the center of the deck plate of the repaired specimens (a) bonded CFRP layers, and (b) bolted steel plates (BSP)

The maximum load level was selected such that the un-damaged and initially cracked specimens would have maximum stress levels of 60.8 MPa at the bottom face and 144.3 MPa at the crack tip of the rib plate respectively. These values are well below the yield stress value of the rib plate material. Which were obtained via typical uniaxial tests on extracted coupons. All repaired specimens were tested by using these parameters and the test was set to stop when the number of cycles

reaches 1.2 million cycles, which would be assumed as an indication to exceed the limit of the infinite fatigue life range as shown in Table 4.1.

Table 4.1 Fatigue test results

Specimens No	Cycles to Damage	Method	Run-out Cycles	Stress Range (MPa)
1	284,555	BSP	1,200,000	60.772
2	217,260	BSP	1,200,000	60.772
3	209,529	CFRP	1,200,000	60.772
4	143,467	CFRP	1,200,000	60.772

4.4 Experimental Results and Discussions

4.4.1 Fatigue Life

All specimens were tested at a nominal stress range of 60.8 MPa, taken at the center of the welded connections from the ribs bottom side with the 100,000 N applied loading. Each of the repaired specimens showed significantly longer fatigue lives than the specimens with fatigue cracks tested within the same stress range. It was found that all the retrofitted specimens reached 1.2 million cycles (continuous testing for 7 days) without any damage accumulation, as shown in Table 4.1. No sign of looseness in the bolts, no sign of delamination in CFRP layers, and no sign of loss of adhesion between CFRP and steel were observed. Cracks were arrested completely and no further increase in crack length was found. A good indicator of the performances of these methods can be given via S-N diagrams. The initially cracked specimens [113] without retrofitting showed a performance level of somewhere below E' category of AASHTO (2007) fatigue design curves [105] whereas retrofitted specimens' performance run-out at high-stress ranges towards infinite life. Fig. (4.7) presents this effect and indicates the number of cycles accumulated for each specimen under constant amplitude loading with the stress range [119], in the form of an S–N diagram.

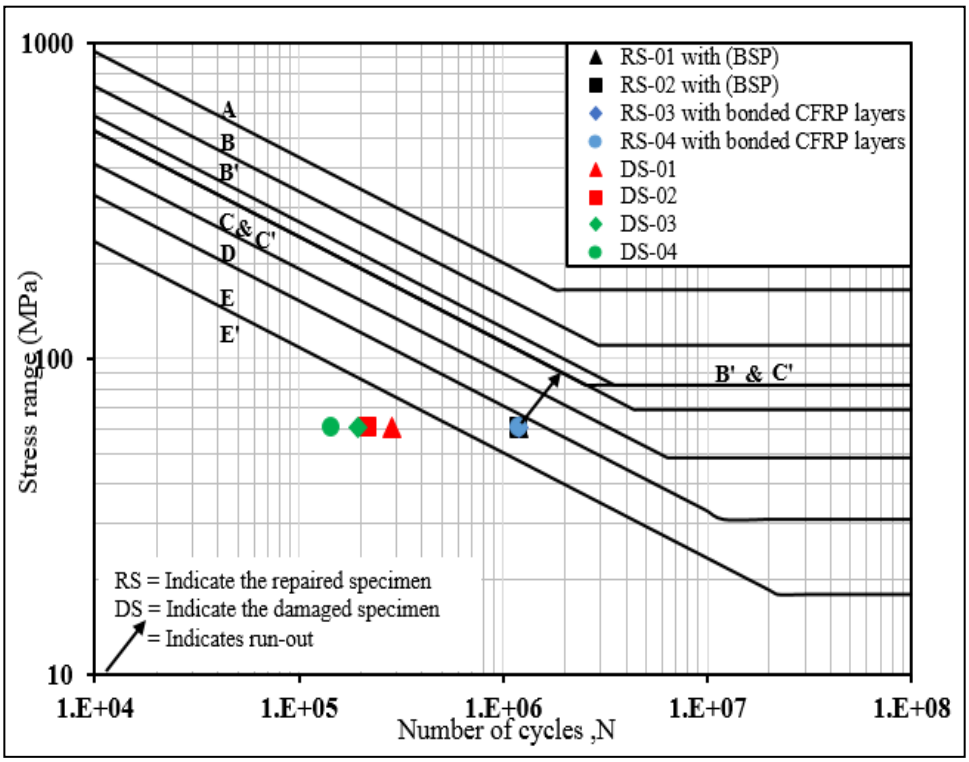

Figure 4.7 Diagram illustrating the results of testing of four trapezoidal longitudinal ribs in AASHTO (2007) fatigue curves before and after applying the retrofitting procedure

The measured material properties of bolted steel plates (BSP) method and bonded CFRP layers method used in this work are shown in Table 4.2. Following the dynamic calibration test, tensile testing coupons were cut from the steel plates used in the repairment. The coupons of the bolted steel plates (BSP)method (BC1 through BC3) had a 10 mm test thickness. The tests performed in accordance with ASTM E8/E8M (2009)[98] and loading was continuous until failure.

The coupons of the CFRP layers had a 3 mm test thickness, and then coupons tests performed according to the ASTM 3039D/3039M (2000)[120]. The measured material properties showed the average modulus of elasticity [E], the average yield stress [σ_y], and the average ultimate stress [σ_u], as illustrated in Fig. (4.8).

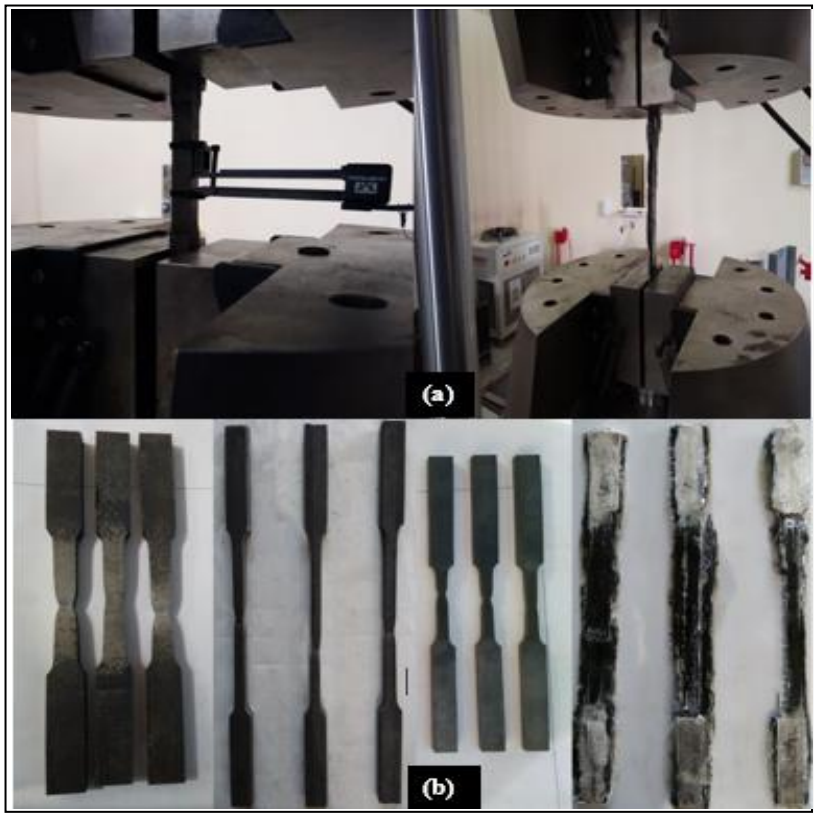

Figure 4.8 (a) Coupons while testing, and (b) coupons geometry following test

Table 4.2 Material test results

Bolted Steel Plate				
Coupon ID	**No. of Coupons**	**Average Modulus of Elasticity (MPa)**	**Average Yield Stress (MPa)**	**Average Ultimate Stress (MPa)**
BC	3	196,751	284.393	402.573
CFRP				
No. of Coupons	**No. of Layers**	**Average Modulus of Elasticity (MPa)**	**Standard Deviation (MPa)**	**Strain at Break (mm/mm)**
3	5	61,700	300	0.761

4.4.2 Dynamic Stiffness Data

The instantaneous or dynamic stiffness of the specimens is a parameter inferred from direct test measurements. As explained before dynamic stiffness is the ratio of the load range to the corresponding deflection range:

$$K_{dyn} = \Delta_p/\Delta_y \tag{4.1}$$

Here Δ_p is the load range and Δ_y is the corresponding deflection range over one fatigue cycle. The data used to calculate the dynamic stiffness were measured by the Instron testing machine and recorded by the controller. All data were plotted using an Excel spreadsheet. In order to display the subtle changes in dynamic stiffness as effectively as possible, each plot indicates the smallest possible change in the dynamic stiffness range which can be detected by the machine. Moreover, this curve presents the stiffness values versus every cycle during cycling load until the end of the test. It was observed that the dynamic stiffness curves of specimens retrofitted with the bonded CFRP layers exhibit the smallest change in the slope whereas there is a comparatively sharp drop of the stiffness values of the specimens with bolted steel plates (BSP) method. The stiffness values saturate after this drop. This behavior can be explained by the superior bonding between the CFRP layers and ribs from the beginning and throughout the tests. While for the bolted steel plates (BSP) method even though there was no looseness in the bolts and no propagation in the cracks apparently a duration is needed so that ribs and bolted plates assume the intimate and mutual load-bearing configuration. Overall retrofitting the damaged ribs with bolted steel plates (BSP) method showing practically somewhat less efficiency compared to the retrofitting with the bonded CFRP layers method in terms of cooperation [121]. Nevertheless, the dynamic stiffness curves of the retrofitted specimens were drastically improved compared with the dynamic stiffness curves of the damaged specimens, as illustrated in Fig. (4.9). Despite excessive damage before retrofitting, the repaired specimens still run-out.

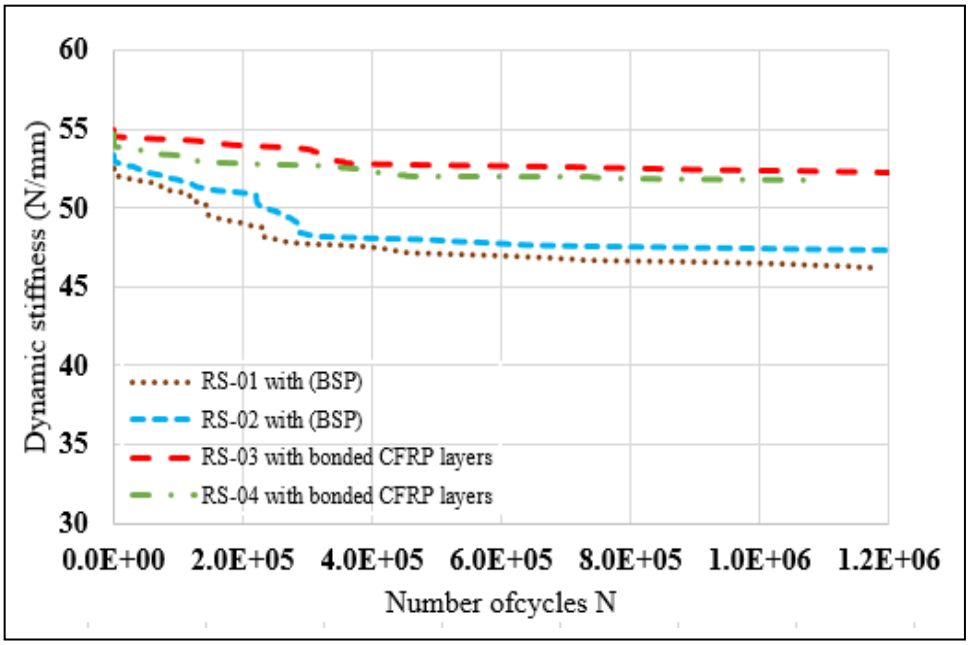

Figure 4.9 Dynamic stiffness versus cycles for repaired specimens

4.5 Conclusions Experimental Work

The conclusions below were established utilizing experimental fatigue tests.

- Considering two lightweight methods for repairing (RR) butt-welded connections of orthotropic steel decks (OSDs), the local stress reduction in weldment is higher for the CFRP layers than for the bolted steel plates (BSP) method. The bonded CFRP layers method reduces the global stresses more than the bolted steel plates (BSP) method. It is seen that shear stresses due to wheel loads up to 100 kN are considerably lower than the determined fatigue levels of both repairment methods. Therefore, it is expected that both repairment methods can achieve the desired performance within the mentioned load range.

- To repair one fatigue crack at the (RR) butt-welded connection of orthotropic steel decks (OSDs), it was concluded that the weight which will be added to the structure by using the bonded CFRP layers method is (2.226) Kg, while the (13.511) Kg will be added by using the bolted steel plates (BSP) method. Consequently, these methods can be considered lightweight and simpler to implement.

- By comparing the lives of fatigue specimens in Fig. (4.7), it was concluded that specimens tested at the center of the transverse welded connections from the bottom side of the trapezoidal ribs provided an effective means of predicting the fatigue life. The fatigue life of specimens with fatigue cracks tested at a nominal weld toe stress range of 60.772 MPa achieved a level at or below the AASHTO Category E' detail, while the repaired specimens exhibited behavior passing the limit of the infinite fatigue life range at or above the curve expected for the AASHTO Category E detail. This behavior indicates the efficacy of the bonded (CFRP) layers method and the bolted steel plates (BSP) method to repair fatigue damage at the (RR) butt-welded connections of orthotropic steel decks (OSDs).

- According to the dynamic stiffness curve in Fig. (4.9), it was concluded that the repairment by using the bonded CFRP layers method provided a most effective bonding between the CFRP layers and the damaged ribs during fatigue testing than the bolted steel plates (BSP) method that showed a slight deterioration in the dynamic stiffness curve.

- The dynamic stiffness curve of the repaired specimens was drastically improved compared with the dynamic stiffness curve of the damaged specimens, as illustrated in Figs. (3.15), and (4.9). Indicating that no noticeable cracks propagation, no debonding in the CFRP layers, and no looseness in the bolts appeared during fatigue testing even though that the repaired specimens still run-out.

5
A NUMERICAL STUDY ON THE FATIGUE CRACK PROPAGATION AT THE RIB TO RIB BUTT WELDED CONNECTIONS IN (OSD) BRIDGES

5.1 Finite Element Analysis

In order to better understand the stress levels for the cracked and retrofitted specimens an elasto-plastic finite element stress analysis is performed in 3D with a commercial FEA package (ABAQUSTM). The cracks were explicitly produced and the load was applied in a quasi-static manner from zero to maximum value. Static stiffness values, stress concentration levels were produced for original un-repaired, bolted steel plate and CFRP retrofitted cases. For bolted steel plates frictional contact (Coulomb Friction with a coefficient of 0.3) was assumed between the steel plates and ribs, and between the bolt holes and bolts. CFRP layers were tie constrained on the ribs. Extensive mesh refinement was applied around crack tips. Two identical models were produced. One with solid elements (Solid Model) and the other with shell elements (Shell Model). The same mesh structure is utilized for both models. Their results are compared and the validity of the shell model is verified. This is done because the shell model offers tremendous computational efficiency over the solid model, especially for cyclic fatigue calculations. Fig. (5.1) shows SP 3D solid model for the case repaired with Bonded Steel Plates (SP). Fig. (5.2) shows the overall mesh structure for the SP model.

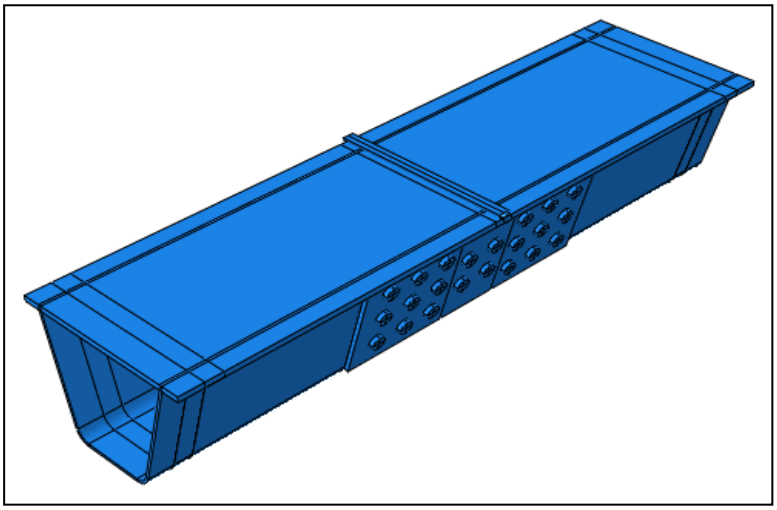

Figure 5.1 SP solid model

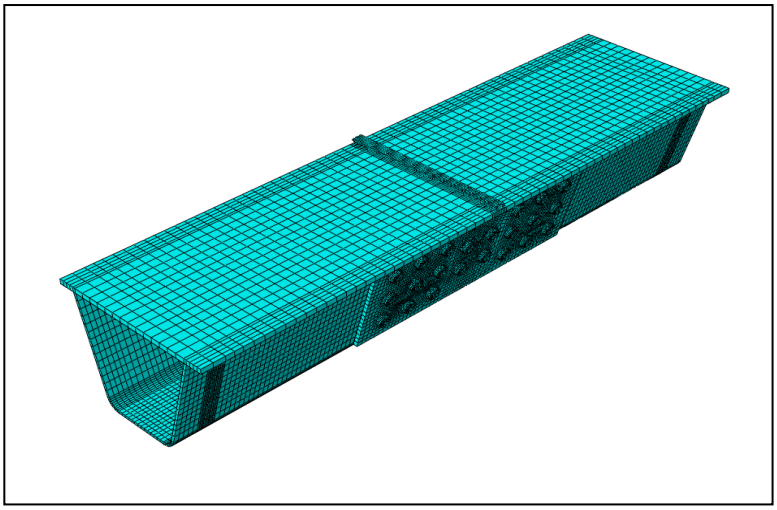

Figure 5.2 SP mesh structure

NR, CFRP, and SP models have 20704, 25384, and 77844 C3D8R type elements respectively. The explicit blunt crack tip introduced in order to mitigate the effects of encountered singularity. In fact, it is well known that local yielding at the crack tip in real materials results in a deviation from a sharp crack tip. The radius of the crack tip is selected such that it is one-thousandth of the size of yield region ahead of the crack tip as recommended in the ABAQUS™ manual. In our problem, this is simply taken as 0.01 mm with an average yield region size of ≈10 mm ahead of the crack tip. Von Mises plasticity is used with combined hardening. Yield stress at zero plastic strain is selected as 280 MPa with an ultimate stress level of 400 MPa at %15 plastic strain. Fig. (5.3) shows the refinement level with the magnification of the blunt crack tip.

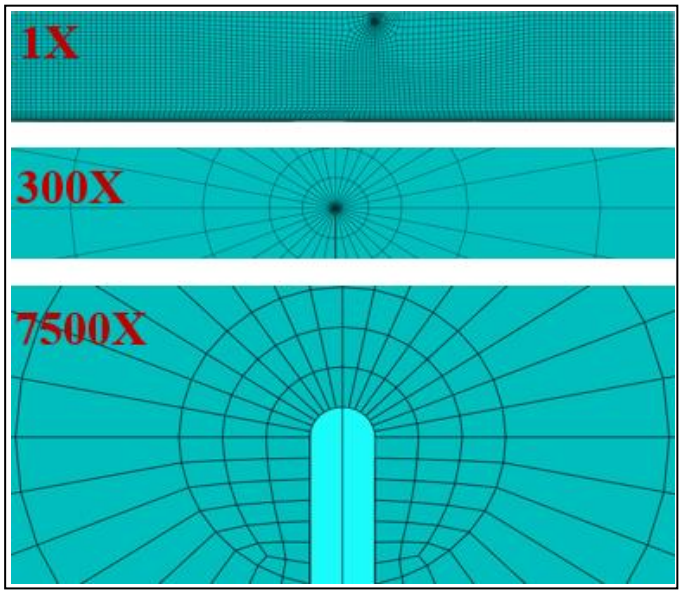

Figure 5.3 Mesh refinement around explicit blunt crack tip

The complete failure of the specimens occurred when the bottom crack reached to another side of the bottom plate and (simultaneously) up crack reached to the upper edge of the sidewall of the channel. As a representative configuration that is close to the failure, the crack lengths of 220 mm (top) and 110 mm (bottom) measured from the initial cut curved section of the channel were used in the analysis. Mises stresses ahead of bottom crack and up crack are shown in Figs. (5.4), and (5.5) respectively. Here the results from shell-models with almost identical mesh structures are given as well. Results indicate the close agreement between the computationally expensive solid models and their shell-based counterparts. The overall Mises stress contours are shown in Fig. (5.7a) and close-ups in Fig. (5.7b) at full load. It is evident that the plastic region is significantly diminished for the repaired cases. This effect is more pronounced for the CFRP case than that of the SP case.

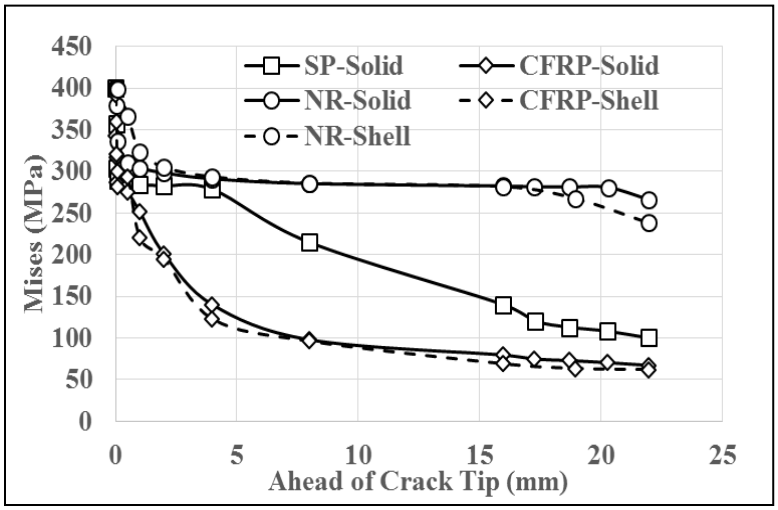

Figure 5.4 Mises stresses ahead of bottom crack

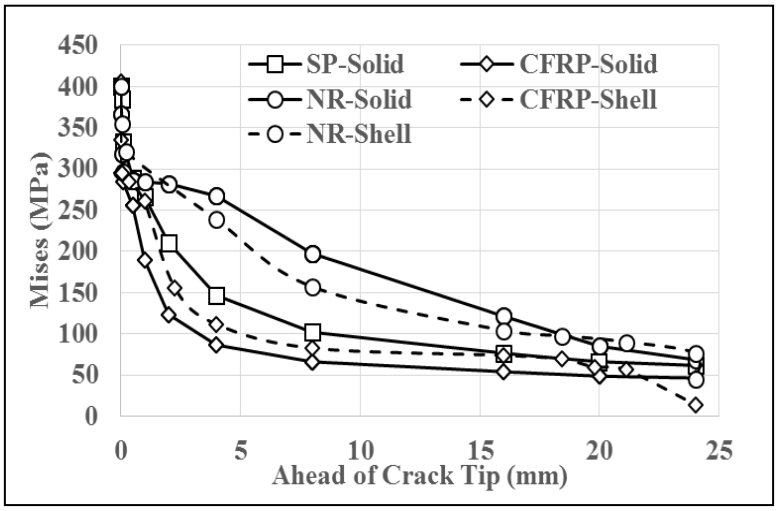

Figure 5.5 Mises stresses ahead of up crack

Results showing Mises stress values indicate that stress levels rapidly drop under yield limit for up crack, within 5 mm ahead of the crack tip. Bottom crack stress levels are more persistent around the yield limit up to 20 mm ahead of the crack tip, in Fig. (5.7). These regions of plastic deformation are limited with respect to the overall specimen dimensions and crack length. Thus we made the assumption of small scale yielding and applied the linear fracture mechanics concepts for the fatigue life analysis in the next section. Also, the J values are calculated for both solid and shell models, and shown in Fig. (5.6). These average values were calculated from the contour lines around the crack tip with ten contours. It is again seen that the computationally efficient shell model produces acceptable results when compared with the demanding solid model.

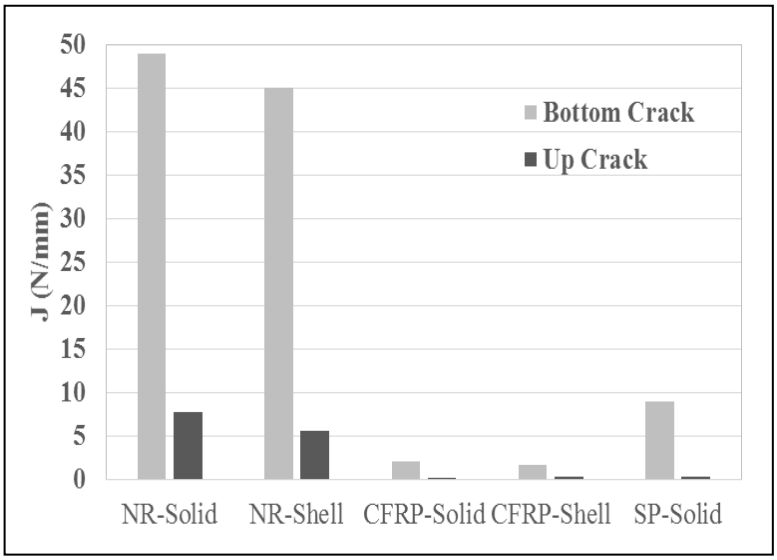

Figure 5.6 Avg. strain energy release rate values (J-N/mm)

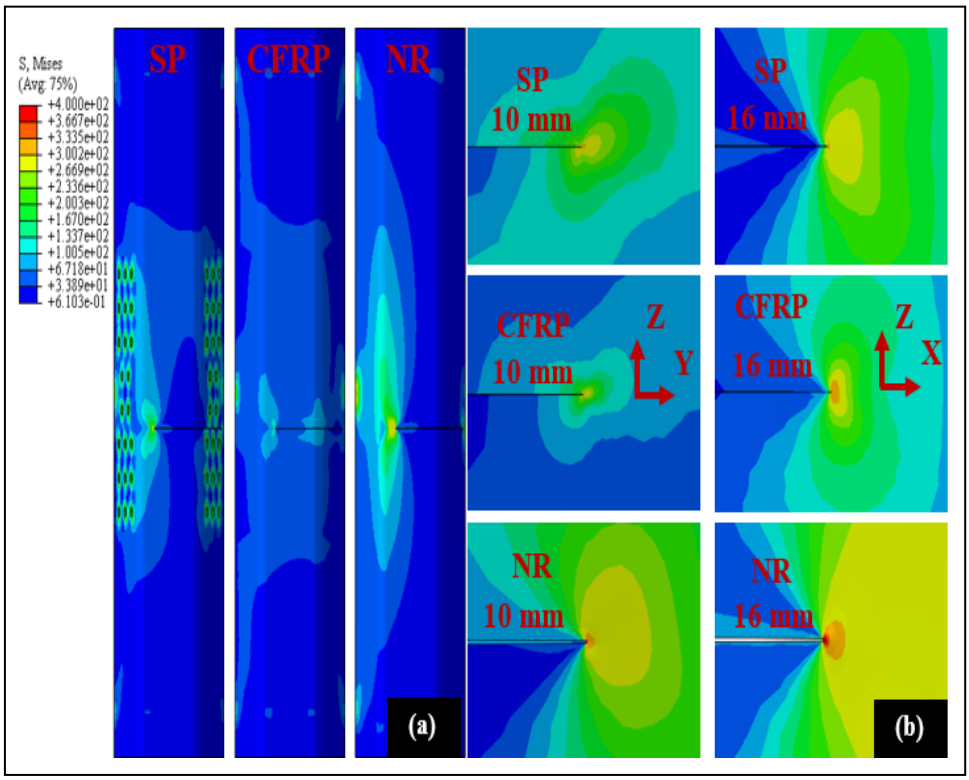

Figure 5.7 Mises stress contours (a) overall mises contours, and (b) crack tip close-up (left: bottom-right: up)

5.2 Fatigue Life Analysis

In order to assess fatigue life of the specimens we utilized the virtual crack closure technique (VCCT) based on the well-known Paris Law (5.1).

$$\frac{da}{dN} = C^* \Delta K^{m^*} \tag{5.1}$$

Here a is crack length, N is the number of cycles, ΔK is the stress intensity factor range, $\Delta K = K_{max} - K_{min}$, and C^* and m^* are material specific parameters. Paris law basically relates the crack growth rate to the stress intensity range. ABAQUS™ will be used for the cyclic crack calculations. ABAQUS assumes J values instead of K values in a similar manner.

$$\frac{da}{dN} = C \Delta J^m \tag{5.2}$$

Here C and m are the counterparts of the C^* and m^* in the original Paris Law. The relation between J and K, $J = K^2/E$, with the loading ratio $\gamma = K_{max}/K_{min}$ result in the correspondences $m^* = 2m$ and $C^* = C((1+\gamma)/(E(1+\gamma)))^m$. Like the original relation (5.2) is a power type relation and manifests itself as a linear line in the log-log plot of da/dN-ΔJ plane. In the experiments cyclic life of unrepaired specimen (NR) was monitored with a-N curves. Crack lengths for corresponding accumulated number of cycles N is recorded. At the time of the experiments fatigue life analysis had not been considered thus instead of separately monitoring the lengths of up crack and down crack, total crack length (a_T) was recorded which is the summation of up (a_{UP}) and down (a_{DW}) crack lengths.

$$a_{UP} + a_{DW} = a_T \tag{5.3}$$

Since this is an unsymmetrical crack case (characteristics of the crack tips are very different) the Paris Law in terms of J values can be written for both cracks, each with different crack growth rates and J ranges but with the same material constants C and m.

$$\frac{da_{UP}}{dN} = C \Delta {J_{UP}}^m \tag{5.4.a}$$

$$\frac{da_{DW}}{dN} = C\Delta J_{DW}{}^{m} \tag{5.4.b}$$

Ratio of (5.4.a) to (5.4.b), *R* which is a function of both cracks' lengths can be utilized to find the material constants *C* and m.

$$R(a_{UP}, a_{DW}) = \frac{da_{UP}}{da_{DW}} = (\bar{R})^m = \left(\frac{\Delta J_{UP}}{\Delta J_{DW}}\right)^m \tag{5.5}$$

In order to define the R function for all values of up and down crack length variations, *J* value range surfaces i.e. $\Delta J_{UP}(a_{UP}, a_{DW})$ and $\Delta J_{DW}(a_{UP}, a_{DW})$ functions were produced. Based on the NR shell model an automated ABAQUS script was developed such that *J* values for up and down cracks can be calculated for any desired crack length combinations(a_{UP}, a_{DW}). Up crack is running along the rib wall so it can reach a maximum length of 231 mm, down crack is running through the bottom rib and then through arc so it can reach a length of 220 mm. In fact these are the typical values when specimen enters to critical failure region. We have devised that with an increment of $\Delta a_{UP} = \Delta a_{DW} = 11mm$ ΔJ_{UP} and ΔJ_{DW} values can be calculated at discrete points.

$$(a_{UP})_i = 11i \; for \; i = 0,1, \dots ,21 \tag{5.6.a}$$

$$(a_{DW})_j = 11j \; for \; j = 0,1, \dots ,20 \tag{5.6.b}$$

This corresponds crack lengths of up to 231 mm and up to 220 mm for up and down cracks respectively. These values are close to the total failure state and together with the increments of 11 mm they are thought to result in a reasonable resolution of the *J* values. As can be seen in Fig. (5.8) for each (*i, j*) pair crack tips are automatically repositioned and remeshed and J values are calculated at each crack tips.

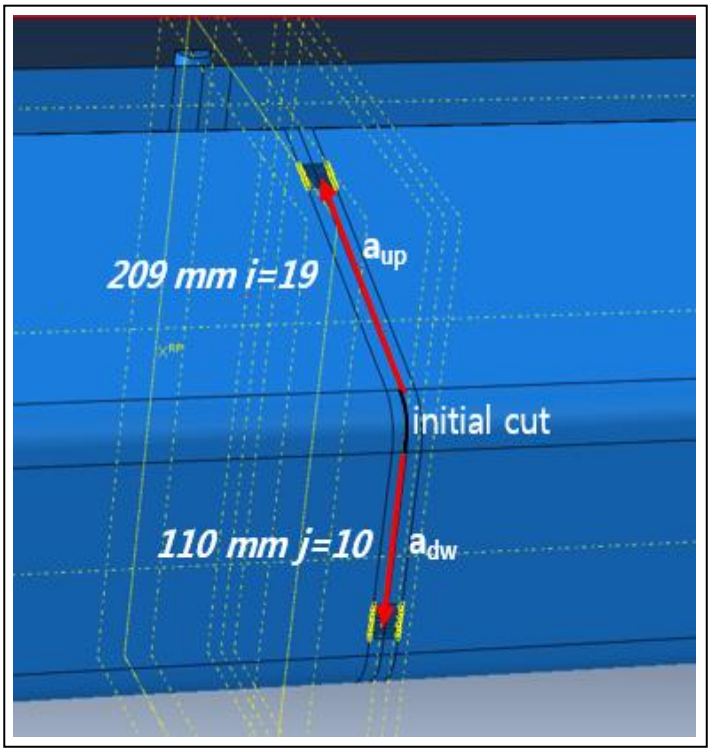

Figure 5.8 An instance (*i=19, j=10*), automatic remeshing

In total we have completed 22x21=462 runs and arrays of $(\Delta J_{UP})_{ij} = \Delta J_{UP}((a_{UP})_i, (a_{DW})_j)$ and$(\Delta J_{DW})_{ij} = \Delta J_{DW}((a_{UP})_i, (a_{DW})_j)$ were produced.

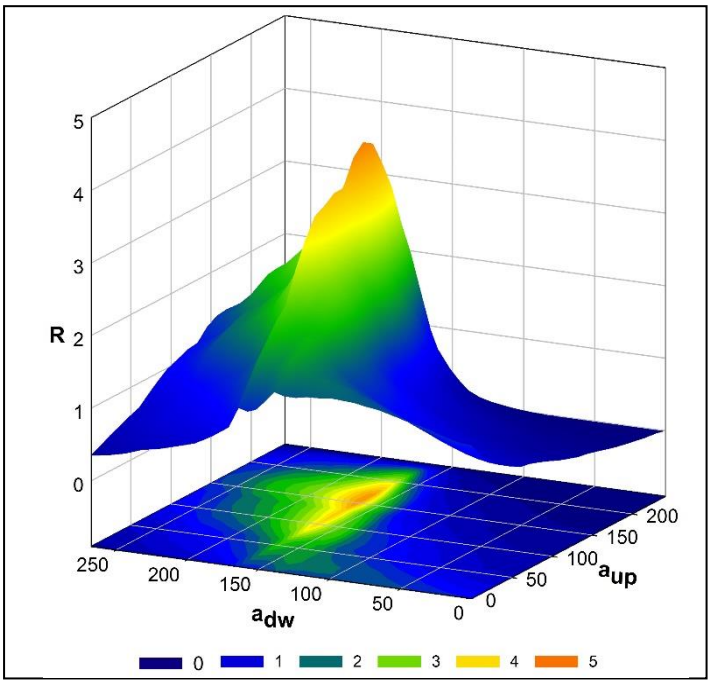

Figure 5.9 $\bar{R}(a_{UP}, a_{DW})$ Surface graph

The surface graph for $\bar{R}$ is given in Fig. (5.9). A multivariable interpolation function $\bar{R}(x, y)$ can be fitted for discrete $\bar{R}$ thus continuous interpolation function$\bar{R}(x, y)$ can be evaluated for all values of $0 \leq x \leq 231\ for\ a_{UP}$ and$0 \leq y \leq 220\ for\ a_{DW}$. Now we can define a path across the *x-y* plane such that at every point on the path satisfies Eq. (5.5):

$$\bar{R}^m(x, y) = \frac{\Delta a_{UP}}{\Delta a_{DW}}\Big|_{x,y} \tag{5.7}$$

In order to achieve this iterations must be carried out over m such that the local ratio of crack length increments (right hand side of Eq. 5.5) matches with the local ratio of J values to the power *m* (left hand side of Eq. 5, i.e.$\bar{R}^m$). The experimental measurements for the total crack length is shown in Fig. (5.10) for NR specimens. Inspection of Fig. (5.10) reveals experimental discrepancy between different specimens. Nevertheless we have selected specimens NR-2 and NR-3 which have similar response characteristics as the basis of the algorithm for the deduction of material parameters.

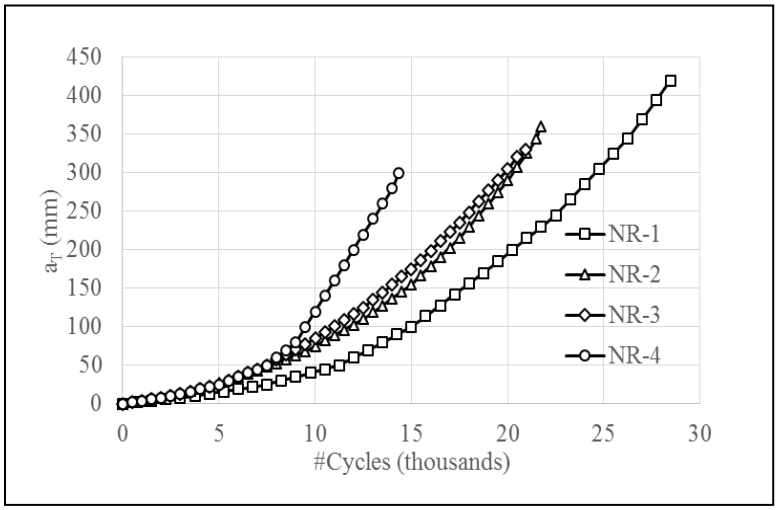

Figure 5.10 Experimental a-N curves

The algorithm begins with fitting the discrete a-N data set with a polynomial *f(N) with* $0 \leq N \leq N_{max}$ where N_{max} is the maximum number of cycles recorded. A 3rd order fit seems to adequately represent the data. The calculation of the slope of the experimental a-N curves can be done by simply using forward differences for *i=1,2,..,S-1*:

$$\left.\frac{da_T}{dN}\right|_{N_i} \approx \left.\frac{\Delta a_T}{\Delta N}\right|_i = \frac{a_{T_{i+1}} - a_{T_i}}{N_{i+1} - N_i} \tag{5.8}$$

Here *S* is the total number of data points in a typical a-N data set (S corresponding to N_{max}). But taking derivative of the fitted polynomial *f(N)* gives smoother results. Thus instead of discrete derivative Δa-ΔN we can simply use *g(N)=df(N)/dN*. Instead of working directly with discrete data sets using fitted functions gives more flexibility in choice of ΔN and greater smoothness. Thus we can discretize the functions with desired level of resolution. Now per Eq. (5.3) and remembering that we have denoted a_{UP} and a_{DW} as *x* and *y* respectively:

$$x + y = a_T \tag{5.9.a}$$

Also taking derivatives of both sides in Eq. (5.9.a) we get:

$$dx/dN + dy/dN = da_T/dN \tag{5.9.b}$$

We can introduce any number of intervals S* with corresponding interval length $\Delta N = N_{max}/S^*$ and rewrite (5.9.a) and (5.9.b) in discrete forms:

$$x_i + y_i = f_i \tag{5.10.a}$$

$$\left(\frac{dx}{dN}\right)_i + \left(\frac{dy}{dN}\right)_i = g_i \tag{5.10.b}$$

Similarly discrete form of Eq. (5.7) can be obtained as

$$\bar{R}^m(x_i, y_i) = \left(\frac{dx}{dN}\right)_i \Big/ \left(\frac{dy}{dN}\right)_i \tag{5.11}$$

Here $f_i = f(N_i)$, $g_i = g(N_i)$, and $N_i = i\Delta N$ for *i=0,1,2,…,S** with *S*=200* seems to give reasonable resolution. Now using Eqs. (5.10.a) and (5.10.b) with Eq. (5.11) $(dy/dN)_i$ can be solved and$(dx/dN)_i$ can be directly calculated for a given *m*. Starting with $x_0 = y_0 = 0$ (zero crack lengths initially), the algorithm is simply:

$for\ i = 1,2, \dots, S^*$

$$\begin{cases} \left(\frac{dy}{dN}\right)_i = \frac{g_{i-1}}{1+\bar{R}(x_{i-1},y_{i-1})^m} \\ \left(\frac{dx}{dN}\right)_i = g_{i-1} - \left(\frac{dy}{dN}\right)_i \\ x_i = x_{i-1} + \left(\frac{dx}{dN}\right)_i \Delta N \\ y_i = y_{i-1} + \left(\frac{dy}{dN}\right)_i \Delta N \end{cases} \tag{5.12}$$

Once for a given m (x_i, y_i) for *i=0,1,2,...,S** are calculated and corresponding $\Delta J_{UP_i} = \Delta J_{UP}(x_i, y_i)$ and $\Delta J_{DW_i} = \Delta J_{DW}(x_i, y_i)$ can be obtained. Discrete sets $\left(\left(\frac{dx}{dN}\right)_i, \Delta J_{UP_i}\right)$ and $\left(\left(\frac{dy}{dN}\right)_i, \Delta J_{DW_i}\right)$ can be plotted on a log-log graph. Since logarithmic forms of the Eqs. (5.4.a) and (5.4.b) are simply linear curves, discrete sets can be fitted (Least Squares) with linear functions for both up and down responses in order to obtain C_{UP}, m_{UP} and C_{DW}, m_{DW}

$$H_{UP}(\overline{\Delta J}) = \overline{C_{UP}} + m_{UP}\overline{\Delta J} \tag{5.13.a}$$

$$H_{DW}(\overline{\Delta J}) = \overline{C_{DW}} + m_{DW}\overline{\Delta J} \tag{5.13.b}$$

Here $\overline{C_{UP}} = logC_{UP}$, $\overline{C_{DW}} = logC_{DW}$ and $\overline{\Delta J} = log\Delta J$ also logarithm is common logarithm (base 10). Since both cracks are propagating in the same material these two functions should be equal in some sense. We can define an error function whose argument is *m* over the squared difference of the functions (5.13.a) and (5.13.b)

$$ERRF(m) = \int_{\overline{\Delta J}_{min}}^{\overline{\Delta J}_{max}} (H_{UP}(\overline{\Delta J}) - H_{DW}(\overline{\Delta J}))^2 d\overline{\Delta J} \tag{5.14}$$

The error function can be minimized with any of the common minimization methods like Conjugate Gradient, Levenberg-Marquardt etc. Application of the procedure for NR-2 and NR-3 data sets (see Fig. 10) produced quite reasonable results. In Figs. (11 and 12) we see closely matched responses for both up and down cracks.

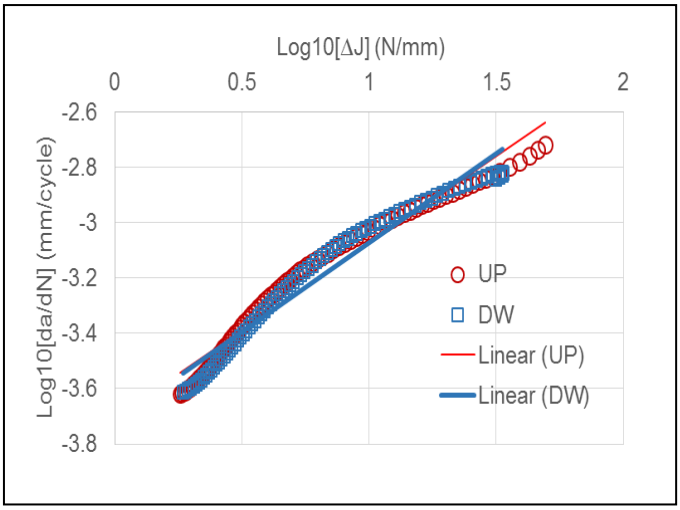

Figure 5.11 Optimized NR-2

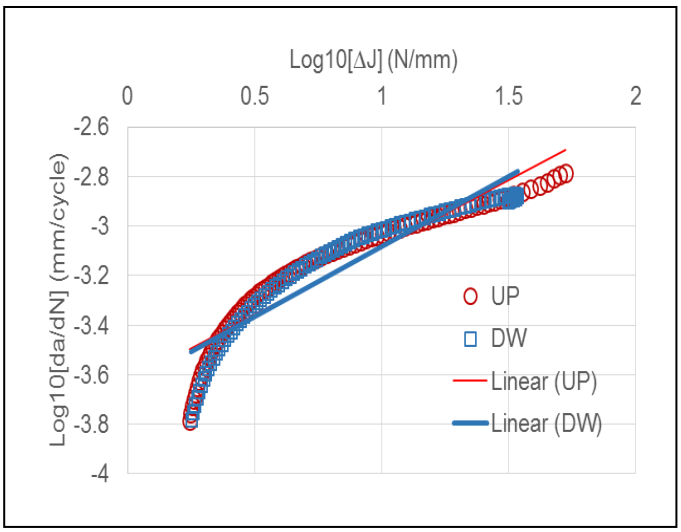

Figure 5.12 Optimized NR-3

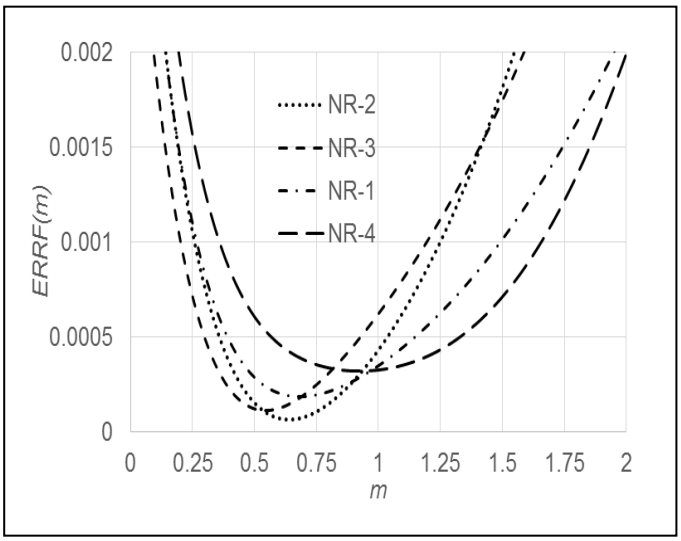

Figure 5.13 Error functions

Fig. (5.13) includes the graph of error function *ERRF* with respect to *m* parameter for all cases. As expected optimization procedure leads to the minimization of the defined error and minimum locations provide the smallest difference between up and down responses. Table 5.1 shows optimized *m* values and corresponding m_{UP}, m_{DW}, C_{UP}, and C_{DW} values. As can be seen in- the table that results are consistent for each specimen. Since the crack is propagating through weldment, inconsistencies and differences between specimens should be expected.

Table 5.1 Optimization results

		NR-1	**NR-2**	**NR-3**	**NR-4**
opt.	m	0.68	0.64	0.54	0.92
corres.	m_{up}	0.68	0.63	0.54	0.89
	m_{dw}	0.71	0.65	0.57	0.92
	C_{up}	1.5E-04	2.0E-04	2.4E-04	1.8E-04
	C_{dw}	1.4E-04	1.9E-04	2.2E-04	1.7E-04
avg.	m	0.70	0.64	0.56	0.91
	C	1.5E-04	1.9E-04	2.3E-04	1.7E-04
	m^*	1.39	1.28	1.11	1.81
	C^*	3.5E-08	8.9E-08	2.9E-07	3.3E-09

Table 5.1 also includes equivalent parameters m^* and C^* in the original Paris Law which is based on stress intensity factors. A simple approach for crack lengths can be directly obtained by using the determined parameters by simply utilizing numerical integration of Eqs. (5.15.a) and (5.15.b):

$$N_k = \int_0^{a_{UP}} \frac{1}{C\Delta {J_{UP}}^m} da_{UP} \approx \sum_{i=1}^{k} \frac{\Delta x_i}{C\Delta J_{UP}(x_i,y_i)^m} \qquad (5.15.a)$$

$$N_k = \int_0^{a_{DW}} \frac{1}{C\Delta {J_{UP}}^m} da_{UP} \approx \sum_{i=1}^{k} \frac{\Delta y_i}{C\Delta J_{DW}(x_i,y_i)^m} \qquad (5.15.b)$$

Here $1<k<S^*$ and N_k is the corresponding number of cycles for the k^{th} step of crack length. Fig. (5.14) shows comparisons of the results with that of numerical integration.

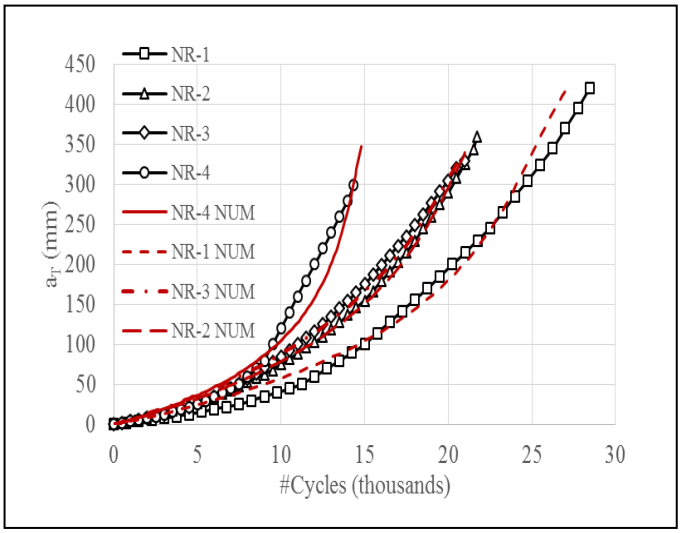

Figure 5.14 Comparison of simple model w/ integration

The agreement between numerical and experimental results seen in Fig. (5.14) is also another implication of the success of the optimization-based parameter estimation developed in this study. Now we can directly use the optimized parameters in 3D finite element simulations. As indicated before 3D models with shell elements will be the basis.

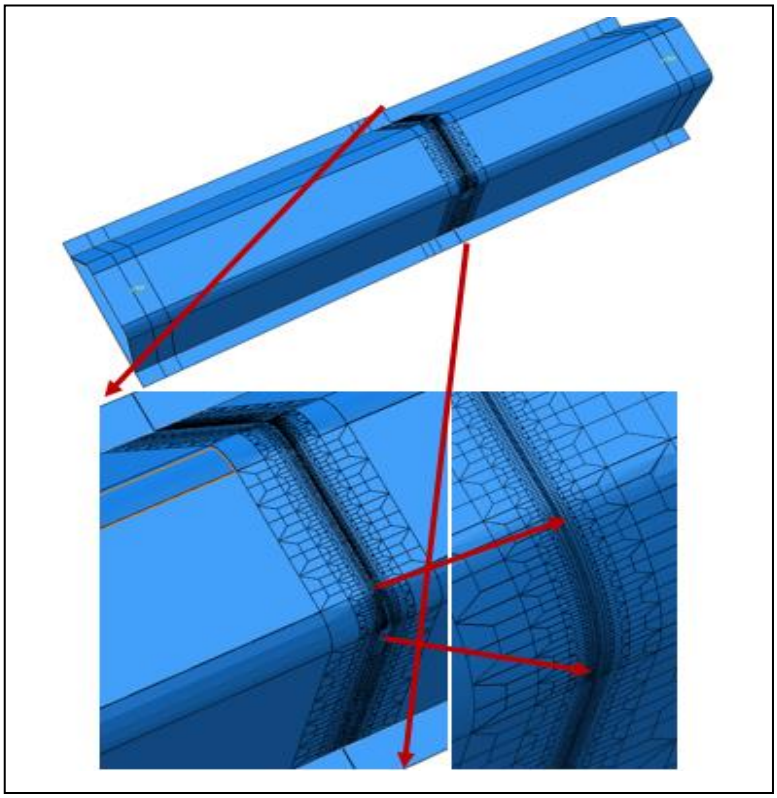

Figure 5.15 Refinement for 3D FEM cyclic fatigue simulations

Fig. (5.15) shows the 3D shell structure with mesh refinement throughout the weldment. A virtual crack closure technique (VCCT) of ABAQUS™ is utilized. In this method, the crack path is predetermined along the weld line as in the actual case. Basically, two separate parts (back and front channels) with corresponding matching refinement levels are bonded along this line except for the arc region which corresponds to the initial cut. The five-layer refinement results in an element size of l≈0.5 mm on the crack path which offers enough resolution and reasonable runtimes. The partition is done by an automated script developed for ABAQUS™. The algorithm is based on the calculation of the number of increments in the cycle count which is required to propagate crack one element length at the current crack tip.

$$\frac{\Delta a}{\Delta N} = C\Delta J^m \tag{5.16}$$

Element length l along the crack at the tip is dictated by the refinement level ($l = \Delta a$). Thus per Eq. (5.16) the required number of cycles are calculated for the given material parameters C, m and the current energy release rate range ΔJ of the crack tip.

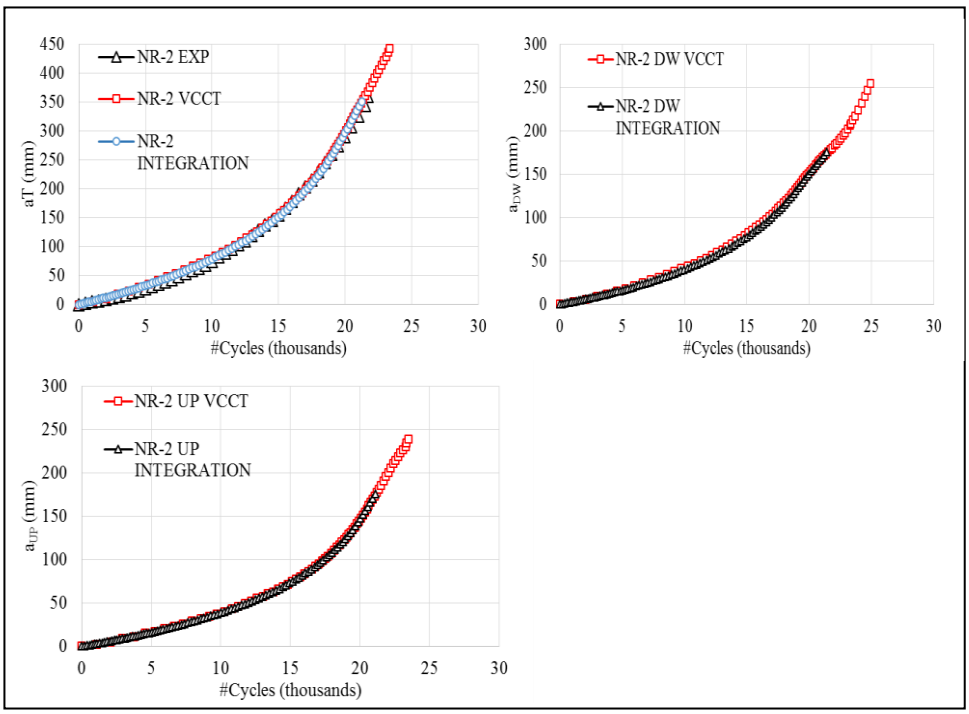

Figure 5.16 Comparison of results NR-2

Once the number of cycle increments ΔN required to release one node ahead of the crack tip is calculated for the current state total number of cycles is updated $N \leftarrow \Delta N + N$ and procedure is repeated for the next node on the path. Results for NR-2 were produced with the corresponding values of C and m parameters given in Table 5.1. Fig. (5.16) compare results obtained directly from the experiment with the VCCT results by ABAQUS™. Also results obtained by direct integration Eqs. (5.15.a-b) are included. Here we can see that for up and down crack propagations VCCT and integration results match quite well. Overall we have seen that the optimization procedure produced remarkable results in the resolution of the up and down cracks and determination of the propagation parameters C and m.

We can now incorporate our findings in 3D shell models of CFRP and Steel Plates reinforcement cases. Fig. (5.17) shows automated script produced models. The green dashed line is representing the debond region prior to analysis right after the failure. It is going through all the way up to the top plate from one side and through the arc on the other side. For CFRP tie constraint is enforced between the steel channel and the CFRP layer. For the SP model all contact surfaces between reinforcing steel plates, steel channels, bolts' shank, and nut are modeled with dry friction with a coefficient of friction of 0.4. Bolts are produced as single units with nuts and shank are monolithic. Shanks are modeled as beam elements whereas nuts are modeled as shell elements as well. Fig. (5.18) shows a single bolt with rendered beam and shell thicknesses.

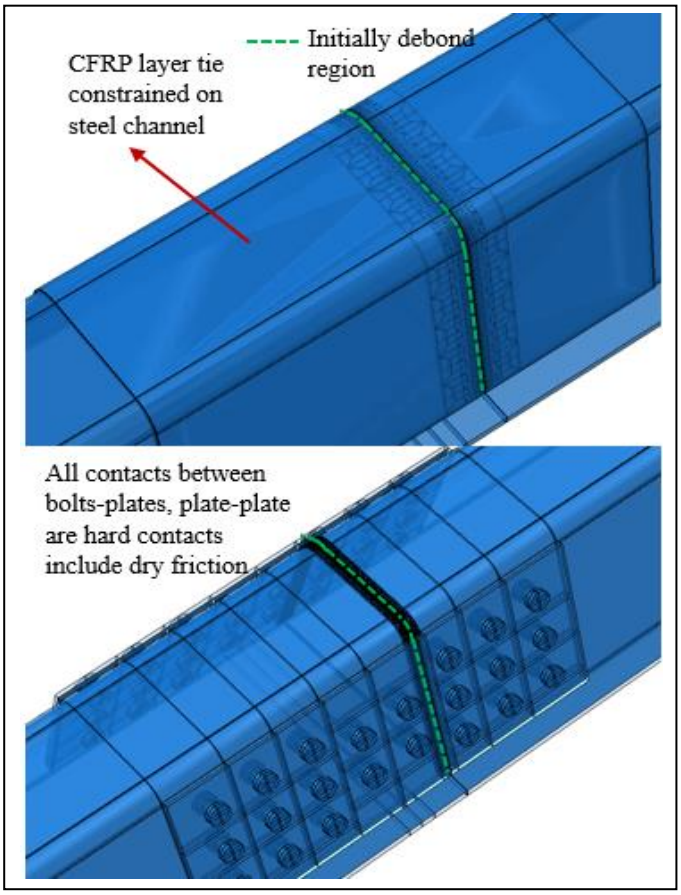

Figure 5.17 Transparent views of CFRP and SP models

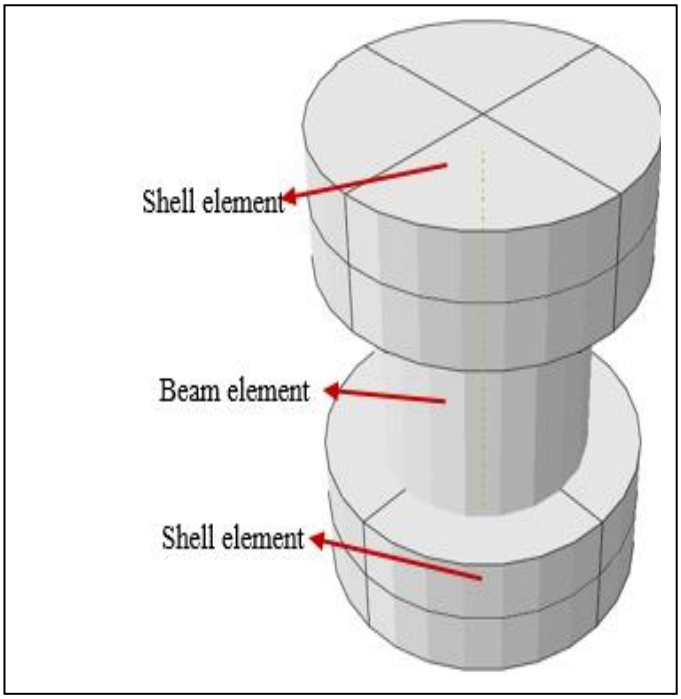

Figure 5.18 Bolt model w/ beam and shell elements

The primary monitoring would be on the dynamic stiffness. Figs. (19 and 20) show experimental dynamic stiffness curves and the model simulations together. We see a good level of agreement in terms of stress levels and initial stiffness loss. One interesting modeling aspect is the introduction of bolt pre-tension. Applying a pre-tension level of 30 kN for each bolt before the cyclic regime in the model resulted in a smoother response. This was somewhat expected as components are connected better this way and noise due to slips between components during cyclic loading is reduced. In fact, this is closer to the reality of the experiments. We did not precisely control the torque applied for the bolts during installation but the pneumatic torque wrench specifications, with respect to air-pressure and bolt diameter parameters, resulted in torque values around 30 kN for the bolts used in the experiments. That was the reason for the selection of 30 kN pre-tension level in the model. CFRP model behaved nearly uniformly as in the experiments. The magnitude of the stiffness was obtained between two CFRP test results and fairly flat for 1 million cycles. The models do not include any wear of the repairments i.e. loosening of nuts or debonding of epoxy. We deduce from the agreement between the experimental model results that these issues are not threatening factors for the performance of repairment as long as a careful and sound procedure is carried out during repairmen.

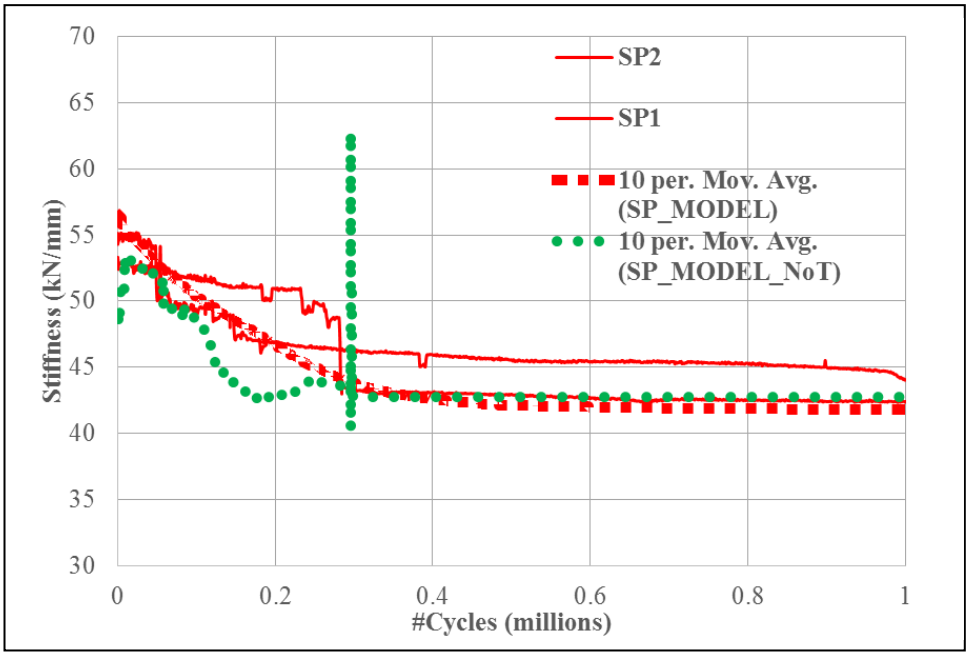

Figure 5.19 Dynamic stiffness versus cycles for bolted steel plate specimens

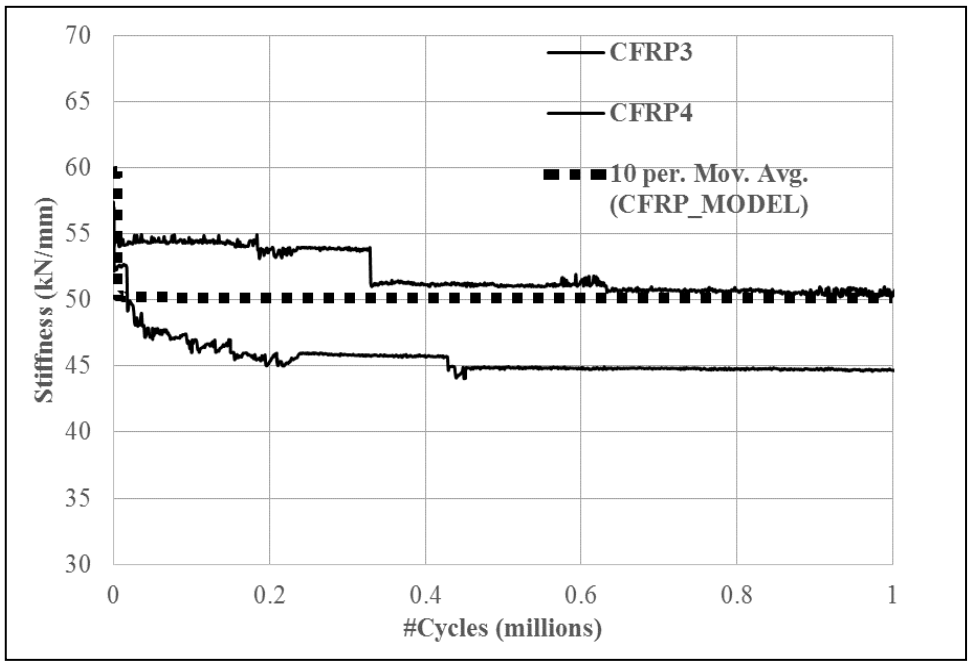

Figure 5.20 Dynamic stiffness versus cycles for CFRP specimens

5.3 Conclusions Numerical Work

The conclusions below were established by means of the FE models analysis and experimental fatigue tests.

- Two light-weight methods; CFRP and bolted steel plates are proposed for the retrofitting of fatigue crack-damaged specimens. The repaired specimens were tested under the cyclic load of 100 kN and found to be run-out.

- In order to better assess the mechanical state of the cracked specimens 3D FE models were developed. Models both with solid elements and with more economical shell elements were considered. Energy release rates and Mises stresses ahead of crack tips were studied. Cracks were explicitly modeled with introducing a keyhole at the tip in order to simulate bluntness. It is found that repairment significantly diminishes stress levels and energy release rates which is a common measure of the crack driving force. Also, results from solid and shell elements were in agreement. Stress results also indicate that plasticity around the crack tip is small compared to the crack and specimen sizes. Thus it would be possible to model cyclic fatigue with linear fracture mechanics approximately.

- Considering two lightweight methods for repairing (RR) butt-welded connections of orthotropic steel decks (OSDs), the local stress reduction close to the welds is higher for the CFRP method than for the bonded steel plates method. The bonded CFRP method is more effective in reducing the overall stress levels with respect to the bonded steel plates method. This founding is in agreement with FE models as well.

- In order to assess the cyclic fatigue performance mechanically, first a method to determine the crack propagation parameters per Paris Law is established. For this, an automated script is developed and energy release rate ratios for different lengths of up and down cracks were calculated. This formed the surface functions for energy release rates. Then depending on the fact that both up and down cracks would have the same material parameters an optimization procedure is proposed over the responses of both cracks. The recording was based on the total crack length in the experiments. The optimization procedure is used to resolve up and down crack lengths such that their responses match. An error function based on the integral of the square of the difference between up and down propagation functions is minimized for a given total crack length data. This way optimized parameters were obtained for different specimens.

- Optimized parameters are then used to establish crack length with respect to the number of cycles with simple numerical integration of Paris Law and it is seen that a good agreement is observed between numerical and experimental total crack lengths. Then a FE shell model with excessive refinement around the crack path is developed based on the virtual crack closure technique (VCCT). This model is used with CFRP and bolted steel plates and a direct cycle fatigue analysis is carried on. Recorded dynamic stiffness values from experiments and models were compared and found to be in agreement as well.

- As found in tests and analyses both repairment methods are safe in terms of the shear stresses developed due to the loads up to 100 kN. Therefore, for both methods, it is unexpected that any damage due to fatigue would occur due to wheel loads. This fact is well established with the cyclic models which do not include any

degradation mechanism. We see that models are in good agreement with the experimental results in terms of dynamic stiffness values for 1 million cycles.

- Both from experiments and cyclic models we observe that the CFRP method provides greater overall stability in terms of dynamic stiffness values. This is due to the more effective bonding of CFRP layers to the channel. Bolted steel repairment shows slight deterioration in dynamic stiffness curve which can be attributed slippage, slight looseness of bolts, and local small scale yielding. It is also found that pre-tension of the bolts is effective on the results as well. It is observed from the models that applying pre-tension to the bolts results in a more stable response (no abrupt jumps due to slippage) with respect to bolts w/out any pre-tension.

- To repair one fatigue crack at the (RR) butt-welded connection of orthotropic steel decks (OSDs), it was concluded that the weight which will be added to the structure by using the bonded CFRP layers method is (2.226) kg, while (13.511) kg will be added by using the bonded steel plates method. Consequently, these methods can be considered lightweight and simpler to implement.

- By comparing the lives of fatigue specimens in Fig. 8, it was concluded that specimens tested at the center of the transverse welded connections from the bottom side of the trapezoidal ribs provided an effective means of predicting the fatigue life. The fatigue life of specimens with fatigue cracks tested at a nominal weld toe stress range of 61 MPa achieved a level at or below the AASHTO Category E' detail, while the repaired specimens exhibited behavior passing the limit of the infinite fatigue life range at or above the curve expected for the AASHTO Category E detail. This behavior indicates the efficacy of the bonded (CFRP) layers method and the bolted steel plates method to repair fatigue damage at the (RR) butt-welded connections of orthotropic steel decks (OSDs).

- The dynamic stiffness curve of the repaired specimens was drastically improved with respect to damaged specimens, as illustrated in Fig.5.19 and Fig.5.20. Indicating that no noticeable crack propagation, no debonding in the CFRP layers, and no significant looseness in the bolts appeared during fatigue testing even though that the repaired specimens still run-out.

6
RESULTS AND DISCUSSION

6.1 Main Conclusions

Two light-weight methods for the repairment of butt-welded OSD bridges were proposed. The repairment is tested on the conditions of butt-weld cracks. One of the methods is the CFRP layers method and the other one is the bolted steel plates method. Butt-welded girder specimens were prepared for the experimental work. An initial cut of 50 mm is introduced at the arc section of the channels. Cyclic tests under 100 kN wheel load are conducted on an Instron machine. Specimens generally failed around 200-250k cycles as the crack propagates from upside through the wall of the channel and from downside through the bottom of the channel. Dynamic stiffness values and total crack length vs the number of cycles were monitored and recorded throughout the experiments. Then some of the damaged (failed) specimens were repaired with CFRP layers and others were repaired with bolted steel plates. All the details regarding the repairs are established clearly in the thesis's sections 2, 3, and 4. Experimental results indicate repairments worked as expected and even after 1 million cycles repaired specimens do not show any sign of wear or performance loss and can be considered runout. Also, an extensive FE study is carried out as well. In order to better understand the mechanical state behind the crack propagation, stresses, and dynamic stiffness under cyclic load we have developed 3D FE models of the entire rib. Both solid elements and more economical shell elements were used in the models. Stress states on the models with plasticity and explicit blunt cracks were monitored. It is seen that repaired models showed significant diminishment of Mises stresses ahead of the crack tip. Energy release rates were also calculated and compared. It is also seen that repaired specimens have significantly lower values of energy release rate which is a common measure for the crack driving force. It should be also mentioned that CFRP is more effective in reducing the overall stresses with respect to the bolted steel plates. Small

scale yielding encountered during simulations allowed us to use linear elastic fracture mechanics for the cyclic analysis. In order to start the analysis, we first obtained fracture parameters that can be used in Paris Law. For this, we resolved total crack length into up and down crack lengths. These were not recorded separately when conducting the experiments. Nevertheless, we proposed an optimization procedure that minimizes the difference between the crack propagation functions of up and down cracks based on the fact that the same material parameter should be used for both cracks. Up and Optimized parameters were tested with the integration of Paris Law and total crack length obtained from this numerical integration is compared with experimental data. A good agreement is obtained. Then a 3D shell FE model with excessive refinement around the crack path (through weldment) is developed with a virtual crack closure technique (VCCT). The parameters obtained from optimization are used with VCCT for direct cyclic fatigue analysis of repaired specimens. Experimental dynamic stiffness values were compared with the model produced values. A good agreement is observed. We see that the CFRP method works better than the bolted steel plates method. We also introduced pre-tension to the bolts in the model. As expected pre-tensioned bolts resulted in a smoother response in the dynamic stiffness curve. This was expected because pre-tension increases the frictional forces and avoids slippage between parts during cyclic loading.

Also, models do not include any degradation mechanism and still able to capture the dynamic stiffness behavior. This is also an indication of the runout as no visible wear, tear, debonding observed on CFRP layers, and no bolt loosening, visible yielding, permanent slip observed on bolted steel plates. The following points can be derived from the thesis as important highlights:

- Primary tensile stresses occurred at the bottom of the ribs. These cause tensile stress concentrations especially in welding details which are prone to fatigue type cracks.

- Considerable out-of-plane bending can occur in the rib walls which manifests itself as enlargement in transverse directions. Cracks can easily propagate when they reach rib walls.

- Specimens that are induced initial cracks all developed into fatigue type cracks. These cracks run through the web in an orthogonal direction to the longitudinal axis of the specimens. Once cracks propagate into the web section their propagation rate increased exponentially till failure of the specimen when cracks reached deck plate.

- It is seen that the modified dye-penetrant method was the most effective way of detecting cracks on the early onset of propagation. The dynamic stiffness method seems also effective but not per dye-penetrant method.

- Comparison of fatigue life of the specimens revealed a level at or below the AASHTO Category E' detail with around 60 MPa nominal weld toe stress, while the control specimen stayed on or above the expected behavior for the AASHTO Category E.

- Static numerical calculations established the soundness of the testing rig. Numerical and experimental strain values displayed remarkable agreement.

- It is seen that CFRP is more effective in reducing the local stress concentrations around crack tips when compared to the Bolted Steel application. Also, CFRP reduces more effectively the overall stress values at other details of the connection. Both methods seem efficient as expected wheel loads of up to 100 kN can be considered lower than their fatigue capacity threshold and we can conclude that both repairment methods can achieve desired performance within the mentioned load range.

- Both methods can be deemed lightweight as they are adding to the structure (2.226) Kg and (13.511) Kg for CFRP per repaired connection. Consequently, these methods can be considered lightweight and simpler to implement.

- Repaired specimens also indicated infinite fatigue life range at or above the curve expected for the AASHTO Category E detail. This revelation indicates the efficiency and performance of both methods of repairment.

- Dynamics stiffness results (4.9) indicate that CFRP maintains a better overall response as it covers the damaged section as a whole dynamic stiffness degradation characteristics are better when compared to the bolted steel plates which are only

transferring loads through bolts and thus showed a slight deterioration in the dynamic stiffness curve.

- Both methods drastically improved dynamic stiffness curves (Figs. (3.15), and (4.9)), and even after 1 million cycles (run-out) no noticeable crack growth, no CFRP debonding, and no looseness in the bolts appeared during fatigue testing.

- Understanding the mechanical response in detail required the development of extensive FE models. 3D models using both solid elements and shell elements were developed and compared to each other in terms of energy release rates and Mises stresses ahead of crack tips. A keyhole is placed at the crack tips for better representing the blunting of the crack tip and yielding due to stress concentrations. It is seen that repairment dropped stresses ahead of crack tip significantly and also the energy release rates were diminished. 3D solid and shell elements produced very similar results. Also, it is found that the yielding was localized so that it would be possible to model cyclic fatigue with linear fracture mechanics approximately.

- Models also indicated the better performance of CFRP in reducing the stresses around crack tip over the Bolted Steel Plates. CFRP method is also more effective in reducing the overall stress levels with respect to the Bolted steel plates method. Revelations of the FE models are in agreement with those observed in experiments.

- Paris Law is proposed for the numerical fatigue model. This requires material parameters related to the law. In order to obtain these parameters first the experimentally recorded crack sizes (a-N curves) were separated for up and down cracks. Since up and down cracks are propagating into the same material an optimization procedure is developed such that these parameters for both of the crack tips match. For the optimization procedure first, an automated script is developed and energy release rate ratios for different lengths of up and down cracks were calculated. The ratio of these values is used to resolve up and down crack lengths such that their responses match. Minimization is carried over an error function which is defined as the integral of the square of the difference between up and down propagation functions. This way optimized parameters were obtained for different specimens.

- Parameters which are obtained after the optimization is first used in the simple integration of the Paris Law. The results of this simple integration served as a confirmation of the optimization method since they compared quite well with the experimental data. Finally, a FE shell model with automatic refinement around the crack path is developed based on the virtual crack closure technique (VCCT). Fatigue is simulated for CFRP and BSP on this model is failed specimens using the direct cycle fatigue analysis. Recorded dynamic stiffness values from experiments and models were compared and found to be in agreement as well.

- Models showed that shear stresses pose no problem as far as 100 kN wheel loads are considered. Thus no damage is expected for this load level for both methods. The numerical fatigue model does not include any degradation mechanism and showed a very similar dynamic stiffness response with respect to the experiments. We see that models are in good agreement with the experimental results in terms of dynamic stiffness values for 1 million cycles.

- Numerical models and experiments both verified that CFRP offers greater structural stability in terms of dynamic stiffness values. As explained before this is primarily due to the over-all CFRP cover and more effective bonding through a greater surface area. Whereas slippage, slight looseness of bolts, and local small scale yielding can be attributed to the slight deteriorations of the dynamic stiffness results of the Bolted steel plates method. Another important finding was the introduction of the pre-tensioning of the bolts. It is observed from the models that applying pre-tension to the bolts results in a more stable response (no abrupt jumps due to slippage) with respect to bolts w/out any pre-tension. This should be directly linked to increased friction and a hence better bond between steel plates and rib walls.

6.2 Future Work

The ribs were constructed with U type channels. Different cross-sections can be used and the effect of cross-section type would be studied. Effects of large scale plasticity with even higher wheel loads can be a subject of interest as well. Environmental effects (cold, hot weather, humidity, sea salt, etc.) should be studied in order to assess the efficiency of the proposed methods within different scenarios. Controlled experiments can be proposed and advanced numerical methods which would include appropriate degradation mechanisms can be used to understand the mechanics. Numerical methods other than VCCT, like ductile damage and degradation can be employed in the simulation of the loss of the bonding material. Ductile rupture through the structural parts can be studied with different damage models in the literature. Impacts of variable amplitude and frequency loading over the fatigue life can also be studied. Instead of CFRP layers, CFRP based plates can be used and evaluated for repairment. Overall a procedural repairment manual can be produced for these light-weight methods which would be effective in a wide range of requirements for OSD bridges.

REFERENCES

[1] F. Alemdar, "Evaluation of the Performance of Stress Measures for Longitudinal Ribs on Orthotropic deck Using Finite Element Analysis," in *Steel Bridge Symposium, Istanbul*, 2015.

[2] X. Ju and K. Tateishi, "Fatigue Crack Behavior at Rib-To-Deck Weld Bead in Orthotropic Steel Deck," *Adv. Struct. Eng.*, vol. 17, no. 10, pp. 1459–1468, 2014.

[3] R. Liu, B. Wang, and Y. Liu, "Distortion induced fatigue of deck plate at rib intersection with diaphragm in orthotropic steel deck," *Int. J. Steel Struct.*, vol. 15, no. 3, pp. 623–632, 2015.

[4] H.-B. Sim, C.-M. Uang, and C. Sikorsky, "Effects of Fabrication Procedures on Fatigue Resistance of Welded Joints in Steel Orthotropic Decks," *J. Bridg. Eng.*, vol. 14, no. 5, pp. 366–373, 2009.

[5] H.-B. Sim and C.-M. Uang, "Stress Analyses and Parametric Study on Full-Scale Fatigue Tests of Rib-to-Deck Welded Joints in Steel Orthotropic Decks," *J. Bridg. Eng.*, vol. 17, no. 5, pp. 765–773, 2012.

[6] Z. G. Xiao, K. Yamada, S. Ya, and X. L. Zhao, "Stress analyses and fatigue evaluation of rib-to-deck joints in steel orthotropic decks," *Int. J. Fatigue*, vol. 30, no. 8, pp. 1387–1397, 2008.

[7] S. Ya, K. Yamada, and T. Ishikawa, "Fatigue Evaluation of Rib-to-Deck Welded Joints of Orthotropic Steel Bridge Deck," *J. Bridg. Eng.*, vol. 16, no. 4, pp. 492–499, 2011.

[8] R. Liu, Y. Liu, B. Ji, M. Wang, and Y. Tian, "Hot spot stress analysis on rib-deck welded joint in orthotropic steel decks," *J. Constr. Steel Res.*, vol. 97, pp. 1–9, 2014.

[9] M. S. Pfeil, R. C. Battista, and A. J. R. Mergulhão, "Stress concentration in steel bridge orthotropic decks," *J. Constr. Steel Res.*, vol. 61, no. 8, pp. 1172–1184, 2005.

[10] R. Connor, "Influence of Cutout Geometry on Stresses at Welded Rib-to-Diaphragm Connections in Steel Orthotropic Bridge Decks," *Transp. Res. Rec. J. Transp. Res. Board*, vol. 1892, pp. 78–87, 2004.

[11] R. J. Connor and J. W. Fisher, "Consistent Approach to Calculating Stresses for Fatigue Design of Welded Rib-to-Web Connections in Steel Orthotropic Bridge Decks," *J. Bridg. Eng.*, vol. 11, no. 5, pp. 517–525, 2006.

[12] AASHTO, *AASHTO LRFD Bridge Design Specifications*, Sixth Edition. American Association of State Highway and Transportation Officials, 2012.

[13] J. Choi and D. Kim, "Stress Characteristics and Fatigue Crack Behaviour of the

Longitudinal Rib-to-Cross Beam Joints in an Orthotropic Steel Deck," *Adv. Struct. Eng.*, vol. 11, no. 2, pp. 189–198, 2008.

[14] C. K. Oh, K. J. Hong, D. Bae, H. Do, and T. Han, "Analytical and experimental studies on optimal details of orthotropic steel decks for long span bridges," *Int. J. Steel Struct.*, vol. 11, no. 2, pp. 227–234, 2011.

[15] Z. G. Xiao, K. Yamada, J. Inoue, and K. Yamaguchi, "Fatigue cracks in longitudinal ribs of steel orthotropic deck," *Int. J. Fatigue*, vol. 28, no. 4, pp. 409–416, 2006.

[16] K. Yokozeki and C. Miki, "Fatigue evaluation for longitudinal-to-transverse rib connection of orthotropic steel deck by using structural hot spot stress," *Weld. World*, vol. 60, no. 1, pp. 83–92, 2016.

[17] Y.-M. Liu, Q.-H. Zhang, P. Zhang, C. Cui, and Y.-Z. Bu, "Study on fatigue life of U-rib butt weld in orthotropic steel bridge deck of Hong Kong-Zhuhai-Macao Bridge," *Zhongguo Gonglu Xuebao/China J. Highw. Transp.*, vol. 29, no. (12): 25-33, 2016.

[18] B. Cheng, X. Ye, X. Cao, D. D. Mbako, and Y. Cao, "Experimental study on fatigue failure of rib-to-deck welded connections in orthotropic steel bridge decks," *Int. J. Fatigue*, vol. 103, pp. 157–167, 2017.

[19] S. Kainuma, M. Yang, Y. S. Jeong, S. Inokuchi, A. Kawabata, and D. Uchida, "Experimental investigation for structural parameter effects on fatigue behavior of rib-to-deck welded joints in orthotropic steel decks," *Eng. Fail. Anal.*, vol. 79, pp. 520–537, 2017.

[20] X. Wei and S. Jiang, "Fatigue Life Prediction on Rib-to-Deck Welded Joints of Steel Bridge Deck Based on LEFM," *Xinan Jiaotong Daxue Xuebao/Journal Southwest Jiaotong Univ.*, vol. 52, no. 1, pp. 16–22, 2017.

[21] Q.-H. Zhang, Y.-M. Liu, Y.-Z. Bu, and Q. Li, "Study on Fatigue Performance of Orthotropic Composite Bridge Deck with Large Longitudinal Ribs," *Zhongguo Gonglu Xuebao/China J. Highw. Transp.*, vol. 30, no. 3, pp. 226–235, 2017.

[22] Q.-H. Zhang, P. Zhang, Y.-M. Liu, J. Yu, and Z.-T. Ye, "Study of Mechanical Behavior of New Type of Orthotropic Composite Bridge Deck with Large Longitudinal U Ribs," *Bridg. Constr*, 2017.

[23] A. Zhu, M. Li, H. Zhu, G. Xu, H. Xiao, and H. Ge, "Fatigue behaviour of orthotropic steel bridge decks with inner bulkheads," *J. Constr. Steel Res.*, vol. 146, pp. 63–75, 2018.

[24] Z. Fu, B. Ji, C. Zhang, and D. Li, "Experimental study on the fatigue performance of roof and U-rib welds of orthotropic steel bridge decks," *KSCE J. Civ. Eng.*, vol. 22, no. 1, pp. 270–278, 2018.

[25] Ming Li; Yasuo Suzuki; Kunitaro Hashimoto; and Kunitomo Sugiura, "Experimental Study on Fatigue Resistance of Rib-to-Deck Joint in Orthotropic Steel Bridge Deck," *J. Bridg. Eng.*, vol. 23, no. 2, 2018.

[26] C. Cui, Y. Bu, Y. Bao, Q. Zhang, and Z. Ye, "Strain Energy-Based Fatigue Life Evaluation of Deck-to-Rib Welded Joints in OSD Considering Combined Effects of Stochastic Traffic Load and Welded Residual Stress," *J. Bridg. Eng.*, vol. 23, no. 2, 2018.

[27] M. Yang, S. Kainuma, and Y. S. Jeong, "Structural behavior of orthotropic steel decks with artificial cracks in longitudinal ribs," *J. Constr. Steel Res.*, vol. 141, pp. 132–144, 2018.

[28] S. Kainuma, J. H. Ahn, Y. S. Jeong, H. Sugiyama, and M. Iwasaki, "Evaluation of structural responses on artificial fatigue crack for bulb rib orthotropic deck," *Adv. Struct. Eng.*, vol. 18, no. 9, pp. 1355–1369, 2015.

[29] G. Alencar, A. M. P. de Jesus, R. A. B. Calçada, and J. G. S. d. Silva, "Fatigue life evaluation of a composite steel-concrete roadway bridge through the hot-spot stress method considering progressive pavement deterioration," *Eng. Struct*, 2018.

[30] M. Aygül, M. Al-Emrani, L. Frýba, and S. Urushadze, "Evaluation of the fatigue strength of an orthotropic bridge deck detail using hot spot stress approach," in *Proc. of the Int. Conf. on Advances in Welding Science and Technology for Construction, Energy and Transportation, AWST 2010, held in Conj. with the 63rd Annual Assembly of IIW 2010*, 2010.

[31] M. Aygül, M. Al-Emrani, Z. Barsoum, and J. Leander, "Investigation of distortion-induced fatigue cracked welded details using 3D crack propagation analysis," *Int. J. Fatigue*, vol. 64, pp. 54–66, 2014.

[32] M. Aygül, M. Al-Emrani, Z. Barsoum, and J. Leander, "An investigation of distortion-induced fatigue cracking under variable amplitude loading using 3D crack propagation analysis," *Eng. Fail. Anal.*, vol. 45, 2014.

[33] B. R. Wolchuk, "Lessons from Weld Cracks in Orthotropic Decks on Three European Bridges," *J. Struct. Eng.*, vol. 116, no. 1, pp. 75–84, 1990.

[34] H.-B. Sim, C.-M. Uang, and C. Sikorsky, "Effects of Fabrication Procedures on Fatigue Resistance of Welded Joints in Steel Orthotropic Decks," *J. Bridg. Eng.*, vol. 14, no. 5, pp. 366–373, 2009.

[35] M. S. G. Cullimore and J. W. Smith, "Local stresses in orthotropic steel bridge decks caused by wheel loads," *J. Constr. Steel Res.*, vol. 1, no. 2, pp. 17–26, 1981.

[36] M. T. Yarnold, J. L. Wilson, W. C. Jen, and B. T. Yen, "Local buckling analysis of trapezoidal rib orthotropic bridge deck systems," *Bridg. Struct.*, vol. 3, no. 2, pp. 93–103, 2007.

[37] R. Fisher, J. and Sougata, "Fatigue damage in steel bridges and extending their life," *Adv. Steel Constr.*, vol. 11, no. 3, pp. 250–268, 2015.

[38] P. Ke, M. Guo, and L. Xia, "The Influence of Common Closed Longitudinal Rib Sections on Stress Distribution of Orthotropic Decks," in *International Conference on Architectural, Civil and Hydraulics Engineering, Atlantis Press*, 2015.

[39] F. B. P. Jong, "Renovation techniques for fatigue cracked orthotropic steel bridge decks," Delft University of Technology, 2006.

[40] M. H. Koistein, "Fatigue classification of welded joints in orthotropic steel bridge decks," Delft University of Technology, 2007.

[41] S. T. de Freitas, H. Kolstein, and F. Bijlaard, "Sandwich system for renovation of orthotropic steel bridge decks," *J. Sandw. Struct. Mater.*, vol. 13, no. 3, pp. 279–301, 2011.

[42] S. Ya, K. Yamada, and T. Ishikawa, "Fatigue Evaluation of Rib-to-Deck Welded Joints of Orthotropic Steel Bridge Deck," *J. Bridg. Eng.*, vol. 16, no. 4, pp. 492–499, 2011.

[43] X. Ju and K. Tateishi, "Fatigue Crack Behavior at Rib-To-Deck Weld Bead in Orthotropic Steel Deck," *Adv. Struct. Eng.*, vol. 17, no. 10, pp. 1459–1468, 2014.

[44] R. Liu, B. Wang, and Y. Liu, "Distortion induced fatigue of deck plate at rib intersection with diaphragm in orthotropic steel deck," *Int. J. Steel Struct.*, vol. 15, no. 3, pp. 623–632, 2015.

[45] R. Walter, "Cement based overlay for orthotropic steel bridge decks: A Multi-Scale Modeling Approach," Technical University of Denmark, 2005.

[46] J. Cao, X. Shao, Z. Zhang, and H. Zhao, "Retrofit of an orthotropic steel deck with compact reinforced reactive powder concrete," *Struct. Infrastruct. Eng.*, vol. 12, no. 3, pp. 411–429, 2016.

[47] Nunteknik, "Repairement of Orthotropic Cracks on Fatih Sultan Mehmet Bridge," Istanbul, Turkiye, 2017.

[48] M. Labordus, "Vacuum infused bonded steel reinforcing plates for bridge rehabilitation," in *International bridge technology conference and trade show, bridge engineering*, 2006.

[49] S. Teixeira de Freitas, H. Kolstein, and F. Bijlaard, *Structural monitoring of a strengthened orthotropic steel bridge deck using strain data*, vol. 11, no. 5, 2012.

[50] M. A. Alam, A. S. A. Jabbar, M. Z. Jumaat, and K. N. Mustapha, "Effective Method of Repairing RC Beam Using Externally Bonded Steel Plate," *Appl. Mech. Mater.*, vol. 567, no. June, pp. 399–404, 2014.

[51] S. Teixeira de Freitas, H. Kolstein, and F. Bijlaard, "Fatigue behavior of bonded and sandwich systems for strengthening orthotropic bridge decks," *Compos. Struct.*, vol. 97, pp. 117–128, 2013.

[52] F. Alemdar, D. Nagati, A. Matamoros, C. Bennett, and S. Rolfe, "Repairing Distortion-Induced Fatigue Cracks in Steel Bridge Girders Using Angles-with-Plate Retrofit Technique. I: Physical Simulations," *J. Struct. Eng.*, vol. 140, no. 5, 2014.

[53] B. Kaan, R. Barrett, C. Bennett, A. Matamoros, S. Rolfe, and A. P. L. Distinguished, "Fatigue Enhancement of Welded Coverplates Using Carbon-

Fiber Composites," *ASCE Struct. Congr*, 2008.

[54] B. N. Kaan, F. Alemdar, C. R. Bennett, A. Matamoros, R. Barrett-Gonzalez, and S. Rolfe, "Fatigue Enhancement of Welded Details in Steel Bridges Using CFRP Overlay Elements," *J. Compos. Constr.*, vol. 16, no. 2, 2012.

[55] F. Alemdar, B. Kaan, C. Bennett, A. Matamoros, and R. Barrett-gonzalez, "Parameters Affecting Behavior of CFRP Overlay Elements as Retrofit Measure for Fatigue Vulnerable Steel Bridge Girders," in *International Fatigue and Fracture Conference, At Philadelphia, PA*, 2009.

[56] F. Alemdar, A. B. Matamoros, C. R. Bennett, R. Barrett-Gonzalez, and S. T. Rolfe, "Improved method for bonding CFRP overlays to steel for fatigue repair," in *Structures Congress 2011 - Proceedings of the 2011 Structures Congress*, 2011.

[57] F. Alemdar *et al.*, "Use of CFRP Overlays to Repair Fatigue Damage in Steel Plates under Tension Loading," *J. Compos. Constr.*, vol. 18, no. 4, 2014.

[58] F. Alemdar, A. Matamoros, C. Bennett, R. Barrett-Gonzalez, and S. T. Rolfe, "Use of CFRP Overlays to Strengthen Welded Connections under Fatigue Loading," *J. Bridg. Eng.*, vol. 17, no. 3, 2012.

[59] J. J. Schubbe and S. Mall, "Investigation of a cracked thick aluminum panel repaired with a bonded composite patch," *Eng. Fract. Mech.*, vol. 63, no. 3, pp. 305–323, 1999.

[60] R. Haghani and M. Al-Emrani, "A new design model for adhesive joints used to bond FRP laminates to steel beams," in *Proceedings of the 6th International Conference on FRP Composites in Civil Engineering, CICE*, 2012.

[61] P. Nilsson and M. Al-Emrani, "Industrialized light-weight steel bridge concept using corrugated core steel sandwich plates," *Proceedings of the 19th IABSE Congress Stockholm*, 2016.

[62] V. Mara, R. Haghani, and M. Al-Emrani, "Improving the performance of bolted joints in composite structures using metal inserts," *J. Compos. Mater.*, vol. 50, no. 21, 2016.

[63] M. Heshmati, R. Haghani, and M. Al-Emrani, "Experimental evaluation of the durability of adhesively bonded CFRP/Steel joints in bridges," in *IABSE Congress Stockholm, 2016: Challenges in Design and Construction of an Innovative and Sustainable Built Environment*, 2016.

[64] M. Heshmati, R. Haghani, and M. Al-Emrani, "Environmental durability of FRP to steel bonded joints in brdiges," in *Maintenance, Monitoring, Safety, Risk and Resilience of Bridges and Bridge Networks - Proceedings of the 8th International Conference on Bridge Maintenance, Safety and Management, IABMAS 2016*, 2016.

[65] M. Heshmati, R. Haghani, and M. Al-Emrani, "Durability of CFRP/steel joints under cyclic wet-dry and freeze-thaw conditions," *Compos. Part B Eng.*, vol. 126, 2017.

[66] A. Karlsson, and C. Wesley, “Necessity of Advanced Fatigue Analysis for Orthotropic Steel Deck Bridges,” Chalmers University of Technology, Göteborg, Sweden, 2015.

[67] U. S. of Transportation, “Manual for Design, Construction, and Maintenance of Orthotropic Steel Deck Bridge.” US Department of Transportation, Federal Highway Administration, Publication no. FHWA-IF-12-027, USA, USA, 2012.

[68] A.R.Mangus, and S.Sun, *Orthotropic Deck Bridges*. In Bridge Engineering Handbook, Chapter 14, edited by Chen, W-F and Duan, L. CRC Press LLC, Boca Raton, Florida, USA, 2000.

[69] R.Wolchuk, “Design Manual for Orthotropic Steel Plate Deck Bridges.” American Institute of Steel Construction, New York, 1963.

[70] BSI, “Steel, concrete and composite bridges, code of practice for fatigue (BS 5400: Part 10).” British Standards Institution (BSI), London, 1980.

[71] J.W.Fisher, “Fatigue and fracture in steel bridges.” case studies Wiley, New York, 1984.

[72] Hanshin-expressway, “Fatigue Damage of Orthotropic Steel Decks and their Retrofit Measures,” Japanese, 2007.

[73] M. Beamish, P. Tindall, and I. Billings, “Auckland Harbour Bridge Fatigue Assessments,” 2006.

[74] I. Billings, A. Dickson, and M. Beamish, “Safety Assessment and Strengthening of the Auckland Harbour Bridge,” in *ICE Bridge Engineering Conference, Kuala Lumpur*, 2005.

[75] Hanshin-Expressway, “Research Council Report 2006 - Fatigue Damage of Orthotropic Steel Decks.” Hanshin Expressway Co, Ltd , Osaka, Japan, 2007.

[76] I.J. Straalen, and G.J. Hagen, “TNO 2003-BC-R0062: Proeven op stalen rijdekken - levensduurverlengende oplossing met een 6 mm dikke staalplaat gelijmde op het rijdek,” 2003.

[77] WD. Corte, “Renovation techniques for rib to deckplate fatigue cracking in orthotropic bridge decks,” *Sci. Res. Essays 6 (9), 1977–1986*, 2011.

[78] M. Labordus, “Vacuum infused bonded steel reinforcing plates for bridge rehabilitation,” in *International bridge technology conference and trade show, bridge engineering*, 2006.

[79] L. Overduin, A. Romeijn, and M. Kolstein, “Modelling of bridge deck systems for orthotropic steel bridges,” in *Proceedings National Conference on Computational Mechanics, Volos, Greece*, 1999.

[80] D. Kennedy, R. Dorton, and S. Alexander, “The sandwich plate system for bridge decks,” in *International Bridge Conference, Pittsburgh, USA, pp. 1–13*, 2002.

[81] S. Kennedy, and T. Murray, “Ultimate strength of an SPS bridge – The Shenley

Bridge," in *Annual Conference of the Transportation Association of Canada, Qu´ebec, Canada, pp. 1–13*, 2004.

[82] R. Vincent, and A. Ferro, "A new orthotropic bridge deck: Design, fabrication and construction of the shenley bridge incorporating an sps orthotropic bridge deck," in *Orthotropic Bridge Conference, Sacramento, California, USA*, 2004.

[83] M. Feldmann, G. Sedlacek, and A. Geler, "A system of steel-elastomer sandwich plates for strengthening orthotropic bridges decks," *Mech. Compos. Mater.*, vol. 43, no. 2, pp. 183–190, 2007.

[84] H. Friedrich, "Sch¨onwasserparkbr¨ucke: Untersuchungen zur thermischen Beanspruchung von SPS beim Einbau bitumin¨oser Fahrbahnbel¨age," *Stahlbau*, vol. 76, no. 7, pp. 472–477, 2007.

[85] J. Matuschek, T. Stihl, and S. Bild, "Verst¨arkung der orthotropen Stahlfahrbahn der Sch¨onwasserparkbr¨ucke mittels Stahl-Elastomer-Sandwich (SPS)," *Stahlbau*, vol. 76, no. 7, pp. 465–471, 2007.

[86] D. Zhang, Y. Li, and C. Cui, "A retrofitted case study of orthotropic steel bridge decks strengthened with sandwich plate system," *Adv. Mater. Res.*, pp. 163–167, 410–416, 2011.

[87] M. Arduini, A. Di Tommaso, and A. Nanni, "Brittle failure in FRP plate and sheet bonded beams," *ACI Struct. J.*, vol. 94, no. 4, pp. 363–370, 1997.

[88] D. I. Kachlakev, T. H. Miller, T. Potisuk, S. C. Yim, and K. Chansawat, "Finite element modeling of reinforced concrete structures strengthened with FRP laminates." Oregon, Dept, of Transportation, Research Group, 2001.

[89] N. F. Grace, G. Abdel-Sayed, and W. F. Ragheb, "Strengthening of concrete beams using innovative ductile fiber-reinforced polymer fabric," *Struct. J.*, vol. 99, no. 5, pp. 692–700, 2002.

[90] S. F. Brena, R. M. Bramblett, S. L. Wood, and M. E. Kreger, "Increasing flexural capacity of reinforced concrete beams using carbon fiber-reinforced polymer composites," *Struct. J.*, vol. 100, no. 1, pp. 36–46, 2003.

[91] S. F. Brena, S. L. Wood, and M. E. Kreger, "Full-scale tests of bridge components strengthened using carbon fiber-reinforced polymer composites," *Struct. J.*, vol. 100, no. 6, pp. 775–784, 2003.

[92] F. A. Fathelbab, M. S. Ramadan, and A. Al-Tantawy, "Strengthening of RC bridge slabs using CFRP sheets," *Alexandria Eng. J.*, vol. 53, no. 4, pp. 843–854, 2014.

[93] G. A. Riveros, H. Mahmoud, and C. M. Lozano, "Fatigue repair of underwater navigation steel structures using Carbon Fiber Reinforced Polymer (CFRP)," *Eng. Struct.*, vol. 173, no. July, pp. 718–728, 2018.

[94] D. Schnerch, M. Dawood, S. Rizkalla, and E. Sumner, "Proposed design guidelines for strengthening of steel bridges with FRP materials," *Constr.*

Build. Mater., vol. 21, no. 5, pp. 1001–1010, 2007.

[95] J. Brownjohn, A. Dumanoglu, and R. Severn, "Seismic analysis of the Fatih Sultan Mehmet (second Bosporus) suspension bridge," *Earthq. Eng. Struct. Dyn.*, vol. 21, no. 10, pp. 881–906, 1992.

[96] A. American, and N. Standard, "Structural Welding Code — Steel," 2011.

[97] Vishay, "Surface preparation for strain gauge bonding," 2009.

[98] ASTM E8/E8M, "Standard Test Methods for Tension Testing of Metallic Materials." American Society for Testing and Materials, West Conshohocken, PA: 194, 2009.

[99] Simulia, "ABAQUS FEA Version 6.14-5, Providence, RI., Dassault Systèmes Simulia," 2018.

[100] J. HÅKANSSON, and H. WALLERMAN, "Finite Element Design of Orthotropic Steel Bridge Decks," Chalmers University of Technology, 2015.

[101] J. Liao, "Fatigue Damage in the Orthotropic Steel Deck with respect to the Trough-to-Deck Plate Joint in between the Crossbeams," Delft University of Technology, 2011.

[102] J. M. Barsom and S. T. Rolfe, *Fracture and Fatigue Control in Structures*, Third Edition. Applications of Fracture Mechanics, 1999.

[103] Z. Fu, B. Ji, Z. Ye, and Y. Wang, "Fatigue evaluation of cable-stayed bridge steel deck based on predicted traffic flow growth," *KSCE J. Civ. Eng.*, vol. 21, no. 4, pp. 1400–1409, 2017.

[104] B. N. Kaan, F. Alemdar, C. R. Bennett, A. Matamoros, R. Barrett-Gonzalez, and S. Rolfe, "Fatigue Enhancement of Welded Details in Steel Bridges Using CFRP Overlay Elements," *J. Compos. Constr.*, vol. 16, no. 2, 2012.

[105] AASHTO, *AASHTO LRFD Bridge Design Specifications*, Fourth Edition. American Association of State Highway and Transportation Officials, Washington D.C, 2007.

[106] F. Alemdar, A. Matamoros, C. Bennett, R. Barrett-Gonzalez, and S. T. Rolfe, "Use of CFRP Overlays to Strengthen Welded Connections under Fatigue Loading," *J. Bridg. Eng.*, vol. 17, no. 3, 2012.

[107] S. Loud, and H. Kliger, "Infrastructure Composites Report." Composites Worldwide, Solana Beach, California, p. 885, 2001.

[108] G. L. Kulak, and G. Y. Grondin, "Strength of Joints that Combine Bolts and Welds." from the minutes of the AISC TC6. Connections Task Committee, 2002.

[109] K. B. Armstrong, "Carbon Fibre Fabric Repairs to Metal Aircraft Structures," in *The Third Technology Conference on Engineering with Composites, London, England, SAMPE European Chapter, 8.1-8.12*.

[110] V. M. Karbhari, and S. B. Shulley, "Use of Composites for Rehabilitation of Steel

Structures -Determination of Bond Durability," *J. Mater. Civ. Eng. ASCE*, vol. 7, pp. 239–245, 1995.

[111] R. C. Allan, J. Bird, and J. D. Clarke, "Use of Adhesives in Repair of Cracks in Ship Structures," *Mater. Sci. Technol.*, vol. 4, no. 10, pp. 853–859, 1988.

[112] S. A. Hashim, "Adhesive Bonding of Thick Steel Adherents for Marine Structures," *Mar. Struct.*, vol. 12, pp. 405–423, 1999.

[113] S. Shakir, and F. Alemdar, "Experimental Study of Fatigue Crack Behavior of Rib-To-Rib Butt Welded Connections in Orthotropic Steel Decks," *Lat. Am. J. Solids Struct.*, vol. 15, no. 10, pp. 1–19, 2018.

[114] S. T. Smith, R. Kaul, R. S. Ravindrarajah, and O. M. A. Otoom, "Durability Considerations for FRP-Strengthened RC Structures in the Australian Environment," in *Australian Structural Engineering Conference, Engineers Australia*, 2005.

[115] M. Bocciarelli, P. Colombi, G. Fava, and C. Poggi, "Fatigue performance of tensile steel members strengthened with CFRP plates," *Compos. Struct.*, vol. 87, no. 4, pp. 334–343, 2009.

[116] M. A. Youssef, "Analytical prediction of the linear and nonlinear behaviour of steel beams rehabilitated using FRP sheets," *Eng. Struct.*, vol. 28, no. 6, pp. 903–911, 2006.

[117] J. M. Dexter, R. J. and Ocel, *Manual for Repair and Retrofit of Fatigue Cracks in Steel Bridges*, 2013.

[118] R. C. on S. Connections, *Specification for Structural Joints Using ASTM A325 or A490 Bolts*, 2004.

[119] C. S. Bandara, S. C. Siriwardane, U. I. Dissanayake, and R. Dissanayake, "Full range S-N curves for fatigue life evaluation of steels using hardness measurements," *Int. J. Fatigue*, vol. 82, pp. 325–331, 2016.

[120] A. D3039/D3039M-08, *Standard Test Method for Tensile Properties of Polymer Matrix Composite Materials*. American Society for Testing and Materials', West Conshocken, PA, 2008.

[121] P. Colombi and G. Fava, "Experimental study on the fatigue behaviour of cracked steel beams repaired with CFRP plates," *Eng. Fract. Mech.*, vol. 145, pp. 128–142, 2015.

PUBLICATIONS FROM THE THESIS

Contact Information: saifaldienytu@gmail.com

Papers

1. S. Shakir, and F. Alemdar, "Experimental Study of Fatigue Crack Behavior of Rib-To-Rib Butt Welded Connections in Orthotropic Steel Decks," Lat. Am. J. Solids Struct., vol. 15, no. 10, pp. 1–19, 2018.

2. S. Shakir, Ç. Mollamahmutoğlu, and F. Alemdar, "Use of CFRP Layers and Steel Plates to Repair Fatigue Damage at the Rib-To-Rib Butt-Welded Connections of Orthotropic Steel Deck under Fatigue Loading," Steel Compos. Struct, 2020. (Under Review).

Conference Papers

1. S. Shakir, and F. Alemdar, "Estimation of the Performance of Closed Longitudinal Ribs Orthotropic Bridge deck sections on Stress Distribution," in International Conference on Advances in Science and Arts Istanbul, pp. 250–254, 2017.